Retrieval of aerosol ~~composition~~ component directly from satellite and ground-based measurements

Lei Li[1,2], Oleg Dubovik[2*], Yevgeny Derimian[2*], Gregory L Schuster[3], Tatyana Lapyonok[2], Pavel Litvinov[4], Fabrice Ducos[2], David Fuertes[4], Cheng Chen[2], Zhengqiang Li[5], Anton Lopatin[4], Benjamin Torres[2] , Huizheng Che[1]

[1]State Key Laboratory of Severe Weather (LASW) and Institute of Atmospheric Composition, Chinese Academy of Meteorological Sciences, CMA, Beijing, 100081, China
[2]Univ. Lille, CNRS, UMR 8518 - LOA - Laboratoire d'Optique Atmosphérique, F-59000 Lille, France
[3]NASA Langley Research Center, Hampton, VA, USA
[4]GRASP-SAS, Remote Sensing Developments, Cité Scientifique, Univ. Lille, Villeneuve d'Ascq, 59655, France
[5]State Environmental Protection Key Laboratory of Satellite Remote Sensing, Institute of Remote Sensing and Digital Earth, Chinese Academy of Sciences, Beijing 100101, China

Correspondence to:
O. Dubovik (oleg.dubovik@univ-lille.fr);
Y. Derimian (yevgeny.derimian@univ-lille.fr)

Abstract

This study presents a novel methodology for remote monitoring of aerosol component ~~composition~~ over large spatial and temporal domains. The concept is realized within the GRASP (Generalized Retrieval of Aerosol and Surface Properties) algorithm to directly infer aerosol component ~~composition~~ from the measured radiances. The observed aerosols are assumed as mixtures of hydrated soluble particles embedded with black carbon, brown carbon, iron oxide, and other (non-absorbing) insoluble inclusions. The complex refractive indices of the dry components are fixed a priori (although the refractive index of the soluble host is allowed to vary with hydration), and the complex refractive index of the mixture is computed using mixing rules. The volume fractions of these components are derived together with the size distribution and the fraction of spherical particles, plus the spectral surface reflectance in cases the satellite data is inverted. The retrieval is implemented as a statistically optimized fit in a continuous space of solutions. This

contrasts with most conventional approaches where the type of aerosol is either associated with a pre-assumed aerosol model that is included in a set of Look-Up-Tables, or determined from the analysis of the retrieved aerosol optical parameters (e.g., single scattering albedo, refractive index, etc. provided by the AERONET retrieval algorithm); here, we retrieve the aerosol component explicitly. The approach also bridges directly to the quantities used in the global chemical transport models. We first tested the approach with synthetic data to estimate the uncertainty, and then applied it to real ground-based AERONET and space-borne POLDER/PARASOL observations; thus, the study presents a first attempt to derive aerosol component from satellites. Our results indicate aerosol optical characteristics that are highly consistent with standard products (e.g., R of ~ 0.9 for aerosol optical thickness) and demonstrate an ability to separate intrinsic optical properties of fine- and coarse-sized aerosols. We applied our method to POLDER/PARASOL radiances on the global scale and obtained spatial and temporal patterns of the aerosol component that agree well with the knowledge on aerosol sources and transport features. Finally, we discuss limitations and perspectives of this new technique. ~~This approach is different from the conventional methods that use post-processing of the retrieved aerosol optical properties for aerosol typing. The proposed method assumes observed aerosols as mixtures of particles composed of black carbon, brown carbon, absorbing insoluble, non-absorbing insoluble embedded in a soluble host. The algorithm then derives size distribution and the fractions of these components. The complex refractive index of each component is fixed a priori and the complex refractive index of mixture is computed using mixing rules. The approach is first tested with synthetic data and the uncertainties are estimated. Then, it is applied to the real ground-based AERONET and space-borne POLDER/PARASOL observations, known to be sensitive to aerosol complex refractive index. The study presents a first attempt to derive aerosol component from satellites. The obtained aerosol optical characteristics are highly consistent with the standard products (R of ~ 0.9 for aerosol optical thickness). The approach also presented an ability to separate between aerosol properties in fine and coarse size fractions, in case of POLDER/PARASOL and AERONET. Examples of application to POLDER/PARASOL on the global scale are presented. The obtained spatial and temporal patterns of the aerosol component agree well with our knowledge on aerosol sources and transport features. Finally, limitations and perspectives are discussed.~~

1 Introduction

Information about atmospheric aerosol chemical composition has a great importance for monitoring and understanding of various aspects of climate and environment. This information can be obtained by laboratory analysis of sampled aerosol. However, the in-situ measurements require considerable effort and represent only small geographic areas without providing results on wide spatial and temporal scale. It is known that chemical transport models are able to represent chemical component concentrations with wide spatial and temporal coverage, and this

capability has been developed rapidly in the past decade. However, the models can have uncertainties because they are initialized by gridded emission inventories that presently have substantial uncertainties. For example, the carbon emissions inventories can be uncertain with a factor of two, and this uncertainty is carried forward to the model output (Bond et al., 1998; Cooke et al., 1999; Streets et al., 2001).

Aerosol components are often divided into two categories: strongly light-absorbing components and mainly scattering (non-absorbing) components. The radiative impacts of aerosols at the top of the atmosphere can change from cooling to warming as their optical properties change from highly scattering to highly absorbing (e.g. Haywood and Shine, 1995). ~~for highly scattering aerosols to warming for highly absorbing aerosols located above highly reflective surfaces like snow or clouds (Haywood and Shine, 1995).~~ There are two kinds of absorbing aerosols that are commonly found in the atmosphere: absorbing carbon and mineral dust that contains iron oxides (Sokolik and Toon, 1999).

~~Light-absorbing carbon is composed of soot carbon and brown carbon (Andreae and Gelencsér, 2006).~~ Light-absorbing carbon is produced by incomplete combustion, and it is an important component of atmospheric aerosol. The complex refractive index of light-absorbing carbon is dependent upon the type of the fuel and the conditions of combustion (Andreae and Gelencsér, 2006; Schkolnik et al., 2007). ~~Based on the origin of the material, combustion conditions, morphological characteristics, chemical component and optical properties (Andreae and Gelencsér, 2006; Schkolnik et al., 2007),~~ The term black carbon (BC) is begrudgingly (and universally) associated with soot carbon in the climate science community, and constitutes the strongest light-absorbing carbon found in the atmosphere (Andreae and Gelencsér, 2006; Bond et al., 2013). ~~The term black carbon (BC), associated with elemental carbon or soot, is used to define the strongly light-absorbing carbon in the atmosphere. Meanwhile, the term brown carbon (BrC) is used for strongly wavelength-dependent light-absorbing carbon particles whose absorption is greater at near-ultraviolet and blue wavelengths~~ Meanwhile, the term brown carbon (BrC) is used to denote organic matter that contains some absorbing organic species, and generally has much greater absorption at near-ultraviolet and blue wavelengths than at red wavelengths (Chen and Bond, 2010; Dinar et al., 2007; Hoffer et al., 2006; Jacobson, 1999; Kanakidou et al., 2005; Kirchstetter et al., 2004; Schnaiter et al., 2006; Sun et al., 2007).

Mineral dust particles can also have a strong spectral signature, with strong absorption at the UV and blue wavelengths when iron oxides are present. Hematite and goethite are different forms of free iron, and they typically appear together (Arimoto et al., 2002; Formenti et al., 2014; Lafon et al., 2006; Shi et al., 2012). The presence of iron in mineral dust particles is known to be important for its biogeochemical and radiative impacts (Jickells et al., 2005; Mahowald et al., 2005; Sokolik and Toon, 1999). Although the regional distribution of the iron concentration is important for climate studies, it is difficult to obtain since it requires in-situ aerosol sampling or simulation of complex natural processes. In addition, mineral dust

131 particles can be affected by the presence of anthropogenic aerosol particles (e.g.
132 carbonaceous particles produced from biomass burning).

133   Separating the absorption associated with light-absorbing carbon from the
134 absorption associated with mineral dust (especially iron oxides) is not an obvious
135 ~~evident~~ task (Derimian et al., 2008), and determination of the relative proportions of
136 BC, BrC and iron oxides should consider differences in absorption spectral
137 dependence. For instance, Dubovik et al. (2002a) showed that the spectral absorption
138 of carbonaceous aerosol is distinct from that of mineral dust. Schuster et al. (2005)
139 inferred the BC column content from AERONET retrievals by assuming BC is the
140 source of all significant aerosol absorption in the AERONET retrievals. Koven and
141 Fung (2006) retrieved hematite concentration at dust sites based upon ~~on~~ the spectral
142 variability of the imaginary refractive index, while Arola et al. (2011) retrieved BrC
143 from AERONET retrievals. Wang et al. (2013) have added single-scatter albedo as an
144 additional constraint to the approach using refractive index (Arola et al., 2011;
145 Schuster et al., 2005) and made it feasible to distinguish BC, BrC and dust
146 simultaneously. Similarly, Li et al. (2015, 2013) investigate the microphysical, optical
147 and chemical properties of atmospheric aerosols by fitting the AERONET complex
148 refractive indices measured at Beijing and Kanpur. Recently, Schuster et al. (2016a)
149 have used the AERONET size distributions and complex refractive indices to retrieve
150 the relative proportion of carbonaceous aerosols (BC and BrC) and free iron minerals
151 (hematite and goethite) in fine and coarse mode particles. ~~Nevertheless, all above~~
152 ~~remote sensing methods (Arola et al., 2011; Koven and Fung, 2006; Li et al., 2015,~~
153 ~~2013; Schuster et al., 2016, 2009, 2005; Wang et al., 2013) that retrieve~~ Nevertheless,
154 all of these methods for retrieving aerosol component ~~composition~~ relying upon ~~on~~ an
155 intermediate retrieval of the refractive index and/or the aerosol absorption optical
156 depth (e.g. one provided by the AERONET operational inversion). Importantly, we
157 ~~We~~ also note that these retrievals of aerosol component ~~composition~~ are only
158 conducted for ground-based remote sensing measurements.

159   Global satellite observations of aerosol properties provide an opportunity to
160 validate and constrain the model simulations at large spatial and temporal scales
161 (Collins et al., 2001; Liu et al., 2005; Yu et al., 2006, 2004, 2003; Zhang et al.,
162 2008a). The integration of observations with model results can fill gaps in satellite
163 retrievals and constrain global distributions of aerosol properties to have good
164 agreement with ground-based measurements (Liu et al., 2005; Yu et al., 2006, 2003).
165 In this regard, inverse modeling can be used to reduce large aerosol simulation
166 uncertainties. For instance, several studies (Chen et al., 2018, 2019; Dubovik et al.,
167 2008; Henze et al., 2007) showed the ability to retrieve global aerosol sources with
168 inverse models that rely upon satellite observations. Therefore, the practice of satellite
169 data fusion into models provides a possibility of improving aerosol simulations of the
170 pre- and post-satellite eras. However, besides the knowledge of amounts
171 (concentrations) and locations of aerosol emissions, ~~an~~ accurate modeling of
172 atmospheric aerosols and their effects also requires information about particle
173 composition. The lack of comprehensive datasets providing multiple constraints for
174 the key parameters employed in ~~the~~ models has hindered the improvement of model

175 simulation. Specifically, improving the ability of aerosol component ~~composition~~
176 estimation will require enhancement of remote sensing capabilities to provide the
177 aerosol component ~~composition~~ information on the global scale. The accuracy and
178 specification of the aerosol component ~~composition~~ as retrieved from satellite
179 observations should respond to the requirements of the ~~chemical~~ aerosol transport
180 models. At the same time, the information content of remote sensing is limited and
181 the main challenge is to identify the aerosol component ~~composition~~ parameters that
182 can be successfully retrieved by remote sensing measurements, given their sensitivity
183 to the aerosol optical properties and complex refractive index in particular.

184   The POLDER space instrument (Deschamps et al., 1994; Tanré et al., 2011) is an
185 example of the instrument providing satellite observations that are sensitive to aerosol
186 component ~~composition~~. The implementation of multi-wavelength, multi-angle and
187 polarization measurement capabilities has made it possible to derive particle
188 properties (size, shape and absorption; Dubovik et al., 2011; Waquet et al., 2013) that
189 are essential for characterizing and estimating aerosol component ~~composition~~. This
190 study presents a methodology for the direct retrieval of aerosol component
191 ~~composition~~ from such measurements. Our methodology is stimulated by the Schuster
192 et al. (2016a, 2009, 2005) works on deriving aerosol component ~~composition~~
193 information from ground-based Sun/sky photometers of the AERONET network.
194 Here, the idea ~~of the approach~~ has evolved and expanded to ~~for~~ retrieving the aerosol
195 component ~~composition~~ from satellite remote sensing observations as well. Namely,
196 we have incorporated an aerosol component ~~composition~~ module into the Generalized
197 Retrieval of Aerosol and Surface Properties (GRASP) algorithm (Dubovik et al.,
198 2014, 2011). It should be noted that GRASP is a versatile algorithm designed to
199 retrieve an extended set of atmospheric parameters from diverse remote sensing data,
200 including surface, airborne, and satellite observations. Here, we apply GRASP to both
201 ground- and space-based observations, with a primary objective of developing ~~to~~
202 ~~develop~~ an approach for monitoring aerosol component ~~composition~~ with extensive
203 spatial and temporal coverage.

204   The objective of our GRASP/Component ~~Composition~~ approach is to retrieve the
205 aerosol component ~~composition~~ directly from remote sensing measurements without
206 intermediate retrieval of the complex refractive index, as in previous studies (Arola et
207 al., 2011; Koven and Fung, 2006; Li et al., 2015, 2013; Schuster et al., 2016a, 2009,
208 2005; Wang et al., 2013). This new approach has a more direct link to the measured
209 radiance field than the "intermediate" approaches, and we therefore expect a
210 reduction in the retrieval uncertainties. The GRASP/Component ~~Composition~~
211 approach also incorporates ~~suggests~~ an additional constraint on the refractive index
212 spectral variability that is not employed in the conventional retrieval algorithms.
213 Specifically the spectral variability of aerosol complex refractive index is constrained
214 in the GRASP/Component ~~Composition~~ retrieval by the spectral dependences of the
215 aerosol species used in the algorithm. It is expected that such constraints can improve
216 the retrievals in various situations.

217   One of the principal difficulties, however, is the identification of an adequate
218 conversion model for linking refractive index to aerosol component ~~composition~~. An

ideal conversion model should cover the entire range of aerosol complex refractive indices and also provide a unique connection between spectral refractive index and aerosol component composition. Therefore, our primary objective focuses on identifying the optimal transformation of chemical and physical aerosol information to optical properties (e.g. refractive index). Once developed, the efficiency of the concept is verified and demonstrated by applying GRASP/Component Composition to ground-based Sun/sky photometric measurements, since this type of measurement usually presents a higher sensitivity to aerosol absorption than the satellite remote sensing. Finally, the outcome of the GRASP/Component Composition approach is demonstrated with the application of the aerosol component composition retrieval to multi-angular polarimetric POLDER/PARASOL satellite observations.

It should be noted that the retrieval of aerosol type has been clearly recognized as an important task by the scientific community and has been addressed in several studies. For example, there are a number of approaches that attempt to identify the type of aerosol through analysis of optical parameters such as single scattering albedo (SSA), Ångström Exponent (AE), AAE (absorption AE), refractive index, etc. Specifically, Russell et al. (2014) relate AERONET- and POLDER-derived optical properties to different aerosol types: urban, dust, marine, biomass burning, etc. Studies by Chung et al. (2010) and Bahadur et al. (2012) use AERONET optical properties like AE and AAE to separate BC, BrC, and dust into species-specific AAOT (absorption AOT). Schuster et al. (2005, 2009, 2016a) and Li et al. (2015) quantify the relative volume fractions of one or more aerosol species (e.g. BC, BrC, iron oxide, water) by adjusting the mixture of several components in an aerosol model to fit AERONET-retrieved refractive indices. However, our new approach differs substantially from all of these methods because it does not use a retrieval of optical parameters as an intermediate step. Thus, we expect the GRASP/Component approach to provide a stronger link to the radiation field than the previous approaches, as well as fundamentally higher retrieval accuracy.

Moreover, some of above methods have additional differences and limitations compared to our proposed approach. For example, the Russell et al. (2014) approach is rather qualitative and does not attempt to quantify the relative volume or mass fractions of different species in an aerosol mixture. Chung et al. (2012) and Bahadur et al. (2012) seem to use a technique for separating carbonaceous aerosols from dust that is not fully consistent with the AERONET retrieval assumptions, as discussed by Schuster et al. (2016b).

Also, the Look-Up Table (LUT) approaches employed in most satellite retrievals (Martonchik et al., 1998; Remer et al., 2005; Kahn and Gaitley, 2015; Popp et al., 2016; Hammer et al., 2018; etc.) are designed to search amongst a preselected set of aerosol models (or their mixtures) for a model that provides the best fit to the observations. Since the models in a LUT are usually associated with a number of aerosol types (e.g. desert dust, smoke, urban aerosol etc.), the identification of the model that provides the best fit is often considered as a retrieval of aerosol type/composition. For observations with enhanced sensitivity, such as the Multi-angle Imaging SpectroRadiometer (MISR), a large number of models can be justified in the

LUT and the differentiation of the models described by the ensembles of parameters can indeed be rather robust. However, LUT approaches are fundamentally limited to a discrete set of possible solutions, whereas the GRASP/Component approach searches through a continuous space of solutions; thus, the identification of aerosol components with our new methodology is significantly more detailed and elaborate. The proposed approach also bridges directly to the quantities of aerosol compositions used in the global chemical transport models. Specifically, our aerosol component retrievals can satisfy the requirements of chemical transport models to constrain their aerosol estimations on a large or global scale. However, we note that the GRASP/Component approach is only possible if 1) there is significant instrument sensitivity to the parameters that are related aerosol component (i.e. complex refractive index), and 2) this sensitivity is maintained while other parameters like the size distribution are adjusted.

2 Methodology

GRASP is a highly rigorous and versatile aerosol and surface reflectance retrieval algorithm that is accessible at https://www.grasp-open.com (Dubovik et al., 2014, 2011). The essence of methodological developments in this study is to integrate a new conversion model designed to link aerosol component with optical and microphysical characteristics into the standard GRASP inversion procedure. The general logistics is shown in Fig. 1 (modified from (Dubovik et al., 2011)). The algorithm is divided into several interacting but rather independent modules to enhance its flexibility. The straightforward exchange of limited parameters minimizes the interactions between the modules. The "Forward Model" and "Numerical Inversion" are the two most complex and elaborate modules in the algorithm. The "Forward Model" is developed in a quite universal way to quantitatively simulate the measured atmospheric radiation with given surface and aerosol properties. The "Numerical Inversion" module (which can be used in various applications, some not even related to atmospheric remote sensing) includes general mathematical operations unrelated to the particular physical nature of the observations. Numerical inversion is implemented as a statistically optimized fitting of observations based upon the multi-term least squares method (LSM), and combines the advantages of a variety of approaches. The module provides transparency and flexibility for developing algorithms that invert passive or active observations to derive several groups of unknown parameters (Dubovik, 2004).

As a consequence of such organization of the algorithm, it can equally be applied (with minimal changes) to invert observations from different satellite sensors or ground-based instruments (Benavent-oltra et al., 2017; Espinosa et al., 2017; Lopatin et al., 2013; Román et al., 2018, 2017; Tsekeri et al., 2017). A full description of the "Forward Model" and "Numerical Inversion" algorithm modules can be found in Dubovik et al. (2011). The following sections provide a description of the modifications conducted for realization of the GRASP/Component approach (schematically presented by red dashed frames in Fig. 1).

2.1 Forward model

The formulation of the forward radiative transfer modeling in the presented approach is generally similar to the formulation of the standard GRASP algorithm where the modeling of the aerosol scattering matrices has been implemented following the ideas described in Dubovik and King (2000) and Dubovik et al. (2006, 2002b). However, we implemented some modifications in modeling of aerosol single scattering. Namely, the real and imaginary parts of the aerosol complex refractive index are calculated using fractions of aerosol components ~~compositions~~ and fixed refractive index of these elements as assumed in the conversion model. Thus, the new component ~~composition~~ approach uses the same forward model as described in Dubovik et al. (2011), except that aerosol component fractions are iterated in the vector of the retrieved unknowns (instead of refractive index) and refractive index is computed a posteriori.

It is worth noting that the aerosol properties in the GRASP algorithm are retrieved simultaneously with the surface reflectance characteristics. The land surface Bidirectional Reflectance Distribution Function (BRDF) in GRASP is described by the kernel-driven Ross-Li model. This model uses a linear combination of three kernels f_{iso}, f_{vol}, and f_{geom} representing isotropic, volumetric, and geometric optics surface scattering, respectively (Li and Strahler, 1992; Roujean et al., 1992; Wanner et al., 1995). The semi-empirical equation by Maignan et al. (2009) is used for the Bidirectional Polarization Distribution Function (BPDF). The reflective properties of ocean surface are modeled analogously to earlier POLDER algorithm developments (Deuzé et al., 2001; Herman et al., 2005; Tanré et al., 2011). Fresnel reflection of the agitated sea surface is taken into account using the Cox and Munk model (Cox and Munk, 1954). The water leaving radiance is nearly isotropic (Voss et al., 2007) and modeling shows that its polarization is negligible (Chami et al., 2001; Chowdhary et al., 2006; Ota et al., 2010). The Fresnel term and the white cap reflection are taken into account by Lambertian unpolarized reflectance. The whitecap reflectance is driven by the wind speed at the sea surface according to the Koepke model (Koepke, 1984). The seawater reflectance at short wavelengths depends on the properties of oceanic water and can be significant. Thus, in present model, the wind speed and the magnitude of seawater reflectance at each wavelength are retrieved simultaneously with the atmospheric aerosol properties.

The aerosol and surface characteristics are determined by parameters included in the vector of unknowns and correspondingly they are inferred from observations. Table 1 shows the list of measurements and retrieved parameters from POLDER/PARASOL observations. For AERONET retrieval the list of parameters is not shown here. However, in principle, it is analogous to POLDER/PARASOL, with the difference that the set of observations is different (i.e. AERONET uses AOT and

transmitted total radiances at different wavelengths) and that surface parameters are not retrieved but fixed from the climatology.

2.2 Numerical inversion

The numerical inversion implemented in this study follows the methodology described in the paper of Dubovik et al. (2011). The only difference is that the GRASP/Component Composition approach retrieves the fractions of different aerosol components instead of the spectral dependence of the complex refractive index. Therefore, this section describes only the modifications that are needed to implement the GRASP/Component Composition approach.

GRASP retrieval is designed as a statistically optimized fitting routine and uses multiple a priori constraints. GRASP can implement two different scenarios of satellite retrievals: (i) conventional single-pixel retrieval for processing of satellite images pixel by pixel and (ii) multiple-pixel retrieval for inverting a large group of pixels simultaneously. The multi-pixel approach can be used for POLDER/PARASOL data for improving consistency of temporal and spatial variability of retrieved characteristic. The main modifications required for the component composition approach are related to the definition of a priori constraints. Correspondingly, two types of a priori constraints are reformulated in the component composition retrieval approach: constraints for single pixel and constraints limiting inter-pixel variability of derived parameters.

2.2.1 Single-pixel observation fitting

For each i-th pixel, the retrieval follows a multi-term LSM fitting of joint sets of data combining the observations with a priori constraints defined by the system of equations $\boldsymbol{f}_i^* = \boldsymbol{f}_i(\boldsymbol{a}_i) + \Delta\boldsymbol{f}_i$:

$$\begin{cases} \boldsymbol{f}_i^* = \boldsymbol{f}_i(\boldsymbol{a}) + \Delta\boldsymbol{f}_i \\ 0_i^* = \boldsymbol{S}_i\boldsymbol{a}_i + \Delta(\Delta\boldsymbol{a}_i) \Rightarrow \boldsymbol{f}_i^* = \boldsymbol{f}_i(\boldsymbol{a}_i) + \Delta\boldsymbol{f}_i \\ \boldsymbol{a}_i^* = \boldsymbol{a}_i + \Delta\boldsymbol{a}_i^* \end{cases} \tag{1}$$

Here, the term with a star represents satellite measurements. For example, $\boldsymbol{f}_i^*$ denotes a vector of the measurements, $\boldsymbol{f}_i$ denotes a vector of the estimations, $\Delta\boldsymbol{f}_i$ denotes a vector of measurement uncertainties, $\boldsymbol{a}_i$ denotes a vector of unknowns in i-th pixel. The second expression in Eq. (1) characterizes the a priori smoothness assumptions that constrain the variability of the size distributions and the spectral dependencies of the retrieved surface reflectance parameters. The matrix S includes the coefficients for calculating the m-th differences of $dV(r_j)/dlnr$, $Frac(i)$, $f_{iso}(\lambda_i)$, $f_{vol}(\lambda_i)$, and $f_{geom}(\lambda_i)$. $Frac(i)$ denotes the fraction of component, $dV(r_j)/dlnr$ $(i = 1, ..., N_r)$ denotes the values of volume size distribution in N_i size bins r_i normalized by C_v and $f_{iso}(\lambda_i)$, $f_{vol}(\lambda_i)$, $f_{geom}(\lambda_i)$ characterize the property of surface reflectance in the Ross-Li model. The m-th differences are numerical

386　equivalents of the m-th derivatives. 0_i^* represents vector of zeros and $\Delta(\Delta a)$
387　represents vector of the uncertainties that characterizes the deviations of the
388　differences from the zeros. This equation indicates that all of these m-th differences
389　are equal to zeros within the uncertainties $\Delta(\Delta a_i)$. The third expression in Eq. (1)
390　includes the vector of a priori estimates a_i^*, as well as the vector of the uncertainties
391　(Δa_i^*) in a priori estimates of the i-th pixel.

　　　The statistically optimized solution of Eq. (1) corresponds to the minimum of the
393　following quadratic form (according to multi-term LSM):

394

395
$$\Psi_i(a_i) = \Psi_f(a_i) + \Psi_\Delta(a_i) + \Psi_a(a_i)$$
396
$$= \frac{1}{2}((\Delta f^P)^T (W_f)^{-1} \Delta f^P + \gamma_\Delta(a_i)^T \Omega a_i + \gamma_a(a_i - a_i^*)^T W_a^{-1}(a_i - a_i^*)). \quad (2)$$

397

398　　　Following Dubovik et al. (2011), all equations are expressed with weighting
399　matrices W that are defined as $W = (1/\varepsilon^2)C$ (dividing the corresponding covariance
400　matrix C by its first diagonal element ε^2); the Lagrange multipliers γ_a and γ_Δ are
401　written as $\gamma_\Delta = \varepsilon_f^2/\varepsilon_\Delta^2$ and $\gamma_a = \varepsilon_f^2/\varepsilon_a^2$, where $\varepsilon_f^2, \varepsilon_\Delta^2$, and ε_a^2 represent the first
402　diagonal elements of corresponding covariance matrices C_f, C_Δ, and C_a. Thus, in this
403　general formulation the fractions ($Frac(i)$) of aerosol component ~~composition~~ are
404　presented as unknowns instead of $n(\lambda_j)$ and $k(\lambda_j)$.

405

406　**2.2.2 Multiple-pixel observation fitting**

407　　　In this retrieval regime the fitting for a group of pixels is constrained by the extra a
408　priori limitations on inter-pixel variability of aerosol and/or surface reflectance
409　properties. Since the information content of the reflected radiation from a single pixel
410　is sometimes insufficient for a unique retrieval of all unknown parameters, the
411　presented approach can improve the stability of satellite data inversions (Dubovik et
412　al., 2011). The inversion of the multi-pixel observations is a solution for a combined
413　system of equations. For example, a three-pixel system can be defined as following:

414

415
$$\begin{cases} f_1^* = f_1(a_1) + \Delta f_1 \\ f_2^* = f_2(a_2) + \Delta f_2 \\ f_3^* = f_3(a_3) + \Delta f_3 \\ \quad\quad \dots \\ 0_x^* = S_x a + \Delta(\Delta_x a) \\ 0_y^* = S_y a + \Delta(\Delta_y a) \\ 0_t^* = S_t a + \Delta(\Delta_t a) \end{cases}, \quad (3)$$

416

417　where the subscript "i" (i=1, 2, 3, …) is the pixel index. The total vector of unknowns
418　a is combined by the vectors of unknowns a_i of each i-th pixel, i.e.
419　$a^T = (a_1; a_2; a_3)^T$. The matrices S_x, S_y and S_t include the coefficients for
420　calculating the m-th differences of spatial or temporal inter-pixel variability for each
421　retrieved parameter a_k that characterizes $dV(r_j)/dlnr$, $Frac(i)$, $f_{iso}(\lambda_i)$, $f_{vol}(\lambda_i)$,

422 and $f_{geom}(\lambda_i)$. The vectors 0_x^*, 0_y^*, 0_t^* denote vectors of zeros and the vectors
423 $\Delta(\Delta_x \boldsymbol{a})$, $\Delta(\Delta_y \boldsymbol{a})$ and $\Delta(\Delta_t \boldsymbol{a})$ denote vectors of the uncertainties characterizing the
424 deviations of the differences from the zeros.
425   The statistically optimized multi-term LSM solution corresponds to the minimum
426 of the following quadratic $\Psi(\boldsymbol{a}^P)$:
427

428
$$\Psi(\boldsymbol{a}^P) = \left(\sum_{i=1}^{Npixels} \Psi_i(\boldsymbol{a}^P)\right) + \frac{1}{2}(\boldsymbol{a}^P)^T \boldsymbol{\Omega}_{inter} \boldsymbol{a}^P. \tag{4}$$

429 This is the sum of the corresponding single-pixel forms (first term) and an inter-pixel
430 smoothing component (2nd term). The smoothness matrix $\boldsymbol{\Omega}_{inter}$ in the inter-pixel
431 smoothing term is defined as:
432

433
$$\boldsymbol{\Omega}_{inter} = \gamma_x \boldsymbol{S}_x^T \boldsymbol{S}_x + \gamma_y \boldsymbol{S}_y^T \boldsymbol{S}_y + \gamma_t \boldsymbol{S}_t^T \boldsymbol{S}_t. \tag{5}$$

434

435 Hence, the solution of a multi-pixel system of N pixels is not equivalent to the
436 solution of N independent single pixel systems.
437

438 **2.2.3 A priori smoothness constraints of fitting**

439   For the framework of deriving aerosol component composition from the
440 POLDER/GRASP retrieval, the vector $\boldsymbol{a}_i$ is composed as:
441

442
$$\boldsymbol{a} = (\boldsymbol{a}_v \boldsymbol{a}_{frac} \boldsymbol{a}_{sph} \boldsymbol{a}_{Vc} \boldsymbol{a}_h \boldsymbol{a}_{brdf,1} \boldsymbol{a}_{brdf,2} \boldsymbol{a}_{brdf,3} \boldsymbol{a}_{bpdf})^T, \tag{6}$$

443

444 where $\boldsymbol{a}_v$, $\boldsymbol{a}_{frac}$, and $\boldsymbol{a}_{sph}$ represent the constituents of the vector a corresponding to
445 $dV(r_i)/dlnr$, $Frac(i)$ and C_{sph} (denotes the fraction of spherical particles). Then $\boldsymbol{a}_h$
446 characterizes the mean altitude of the aerosol layer h_a, the element $\boldsymbol{a}_{Vc}$ represents the
447 total volume concentration, and $\boldsymbol{a}_v$ are the logarithms of $dV(r)/dlnr$ which are
448 normalized by total volume concentration. The three components
449 ($\boldsymbol{a}_{brdf,1}$, $\boldsymbol{a}_{brdf,2}$, $\boldsymbol{a}_{brdf,3}$) are related to the logarithms of the spectrally dependent
450 parameters $k_{iso}(\lambda_i)$, $k_{vol}(\lambda_i)$ and $k_{geom}(\lambda_i)$ employed in Ross-Li model. The vector
451 $\boldsymbol{a}_{bpdf}$ includes the parameters of the BPDF model. Thus, this work differentiates
452 from Dubovik et al. (2011) by retrieving the volume fractions of the aerosol
453 components (i.e. $Frac(i)$) instead of the complex refractive index.
454   There is no evident connection between the retrieved fractions of aerosol
455 component composition in each single pixel, so no smoothness constraints are used
456 for $\boldsymbol{a}_{frac}$. The matrix S for each i-th pixel is the same and has the following array
457 structure (Dubovik et al., 2011):
458

459

$$\boldsymbol{Sa} = \begin{pmatrix} S_v & 0000 & 0 & 0 & 0 & 0 \\ 0 & 0000 & 0 & 0 & 0 & 0 \\ 0 & 0000 & 0 & 0 & 0 & 0 \\ 0 & 0000 & 0 & 0 & 0 & 0 \\ 0 & 0000 & 0 & 0 & 0 & 0 \\ 0 & 0000 & S_{brdf,1} & 0 & 0 & 0 \\ 0 & 0000 & 0 & S_{brdf,2} & 0 & 0 \\ 0 & 0000 & 0 & 0 & S_{brdf,3} & 0 \\ 0 & 0000 & 0 & 0 & 0 & S_{bpdf} \end{pmatrix} \begin{pmatrix} \boldsymbol{a}_v \\ a_{frac} \\ a_{sph} \\ a_{Vc} \\ a_h \\ \boldsymbol{a}_{brdf,1} \\ \boldsymbol{a}_{brdf,2} \\ \boldsymbol{a}_{brdf,3} \\ \boldsymbol{a}_{bpdf} \end{pmatrix}, \qquad (7)$$

460

461 where the corresponding matrices S$_{...}$ have different dimensions and describe
462 differences of different order. The vectors in Eq. (7) corresponding to $\boldsymbol{a}_{frac}$, $\boldsymbol{a}_{sph}$,
463 $\boldsymbol{a}_{Vc}$, $\boldsymbol{a}_h$ contain only zeros because no smoothness constraint can be applied to these
464 parameters. The errors $\Delta(\Delta\boldsymbol{a})$ are assumed independent for different components of
465 the vector $(\Delta\boldsymbol{a})^*$ and the smoothness matrix for each i-th pixel can be written as:

466

467

$$\gamma_\Delta\Omega = \begin{pmatrix} \gamma_{\Delta,1}\Omega_1 & 0000 & 0 & 0 & 0 & 0 \\ 0 & 0000 & 0 & 0 & 0 & 0 \\ 0 & 0000 & 0 & 0 & 0 & 0 \\ 0 & 0000 & 0 & 0 & 0 & 0 \\ 0 & 0000 & 0 & 0 & 0 & 0 \\ 0 & 0000 & \gamma_{\Delta,2}\Omega_2 & 0 & 0 & 0 \\ 0 & 0000 & 0 & \gamma_{\Delta,3}\Omega_3 & 0 & 0 \\ 0 & 0000 & 0 & 0 & \gamma_{\Delta,4}\Omega_4 & 0 \\ 0 & 0000 & 0 & 0 & 0 & \gamma_{\Delta,5}\Omega_5 \end{pmatrix}, \qquad (8)$$

468

469 where $\boldsymbol{\Omega}_i = \boldsymbol{S}_i^T \boldsymbol{W}_i^{-1} \boldsymbol{S}_i$ uses the derivative matrices $\boldsymbol{S}_i$ (i=1, …, 5), $\boldsymbol{S}_v$, $\boldsymbol{S}_{brdf,1}$, $\boldsymbol{S}_{brdf,2}$,
470 $\boldsymbol{S}_{brdf,3}$, $\boldsymbol{S}_{bpdf}$.

471 The inter-pixel smoothing term given by Eq. (5) is defined in a very similar way as
472 described by Dubovik et al. (2011), and therefore it is not written here explicitly.
473 Indeed, the spatial and temporal variability of component ~~composition~~ is very similar
474 to the variability of refractive index, since both depend only upon the variability of
475 aerosol type.

476 We note that the above equations apply to the POLDER/GRASP retrievals, but
477 corresponding equations are trivially obtained for the AERONET/GRASP retrievals
478 by excluding parameters describing surface reflectance and aerosol height.

479
480

2.3 Model of optical properties of aerosol component ~~composition~~

2.3.1 Definition and assumptions

483 The aerosol refractive index required for the forward calculations (see Fig. 1) is
484 derived by assuming a mixing model and employing fractions of aerosol species;
485 therefore, the retrieval of aerosol component ~~composition~~ requires the selection of a
486 mixing rule. In our work, we decided to use a simple and widely tested Maxwell-

487 Garnett effective medium approximation. Indeed, the choice of the mixing rule is of
488 importance since it can ~~significantly~~ affect the retrieval results. For example, the
489 study of Xie et al. (2014) showed that the Bruggeman approximation was found as
490 more suitable for the dust case, the Maxwell-Garnett for the haze case, and volume
491 average for the clean case. Thus, in order to get an idea about the influence of the
492 mixing rule choice, in our study the retrievals were produced also using the volume
493 weighted mixing rule. ~~and the results are inter-compared.~~ We have not identified a
494 significant influence of the mixing rule choice on the quality of the retrievals in our
495 approach. Moreover, the aerosol optical properties were rather well comparable in
496 both cases. The fractions of the elements evidently present some differences due to
497 the differences in the formulation, but are still in a reasonable agreement.
498   The Maxwell-Garnett mixing rule has been extensively applied in many studies for
499 retrieval of aerosol component ~~composition~~ from ground-based remote sensing
500 measurements (Li et al., 2015, 2013; Schuster et al., 2016a, 2009, 2005; Wang et al.,
501 2013). As Fig. 2 illustrates, the first step in the Maxwell-Garnett conversion model is
502 the designation of a "host" and calculation of the refractive index of the host. In
503 general, the host can be formed by water and soluble inorganic species (e.g.
504 ammonium nitrite, ammonium sulfate, sea salt). It is well known that inorganic salt
505 particles are mostly hygroscopic and deliquescence in humid air. The phase transition
506 from a solid particle to a saline droplet (host) usually occurs when the relative
507 humidity reaches a specific value, known as the deliquescence point, that is specific to
508 the chemical composition of the aerosol particle (Orr et al., 1958; Tang, 1976; Tang
509 and Munkelwitz, 1993). The refractive indices of hygroscopic aerosols change with
510 the additional amount of water that is absorbed in response to changing relative
511 humidity. These changes in refractive index, including also the changes in specific
512 density, size and mass fraction, have been accurately measured as functions of
513 relative humidity (Tang, 1996; Tang and Munkelwitz, 1994, 1991). Schuster et al.
514 (2009) illustrated that the soluble aerosol components (sea salt, ammonium sulfate,
515 ammonium nitrate, etc.) indicate similar refractive indices for similar mixing ratios,
516 even though the dry refractive indices can be quite different. Hence, the aerosol water
517 fraction can be derived from the mixture real refractive index if the aerosols are
518 known to be one of the common soluble aerosols.
519   In the presented approach, the host is assumed to depend upon the properties and
520 proportions of ammonium nitrate and water (uncertainties due to selection of
521 ammonium nitrate are evaluated further on). The real refractive index (at the 0.6328
522 μm wavelength) for a host mixture of ammonium nitrate and water can be expressed
523 as
524
525 $$n = 1.33 + (1.22 \times 10^{-3})X + (8.997 \times 10^{-7})X^2 + (1.666 \times 10^{-8})X^3, \quad (9)$$
526
527 where X is the weight percent of ammonium nitrate (Tang and Munkelwitz, 1991).
528   Refractive indices at other wavelengths are spectrally interpolated utilizing
529 measured data (Downing and Williams, 1975; Gosse et al., 1997; Hale and Querry,
530 1973; Kou et al., 1993; Palmer and Williams, 1974; Tang, 1996; Tang and

531 Munkelwitz, 1991). A detailed description and FORTRAN subroutines for calculating
532 the host complex refractive index is accessible at the website of GACP (Global
533 Aerosol Climatology Project, https://gacp.giss.nasa.gov/data_sets/).

534 Once the refractive index of the host is determined, the refractive index of the
535 mixture is computed using the Maxwell-Garnett equations. The Maxwell-Garnett
536 effective medium approximation allows computation of the average dielectric
537 function based upon the average electric fields and polarizations of a host matrix with
538 embedded inclusions, and can model insoluble particles suspended in a solution
539 (Bohren and Huffman, 1983; Lesins et al., 2002).

540 The dielectric functions of aerosols are not typically tabulated in the literature, so
541 they must be computed from the refractive index. Once the dielectric functions are
542 known for the host and its constituents, the Maxwell-Garnett dielectric function for a
543 mixture can be calculated. For example, for two types of inclusions in a host, the
544 dielectric function of the mixture can be expressed as (Schuster et al., 2005):

545

$$546 \quad \varepsilon_{MG} = \varepsilon_m \left[1 + \frac{3\left(f_1 \frac{\varepsilon_1 - \varepsilon_m}{\varepsilon_1 + 2\varepsilon_m} + f_2 \frac{\varepsilon_2 - \varepsilon_m}{\varepsilon_2 + 2\varepsilon_m}\right)}{1 - f_1 \frac{\varepsilon_1 - \varepsilon_m}{\varepsilon_1 + 2\varepsilon_m} - f_2 \frac{\varepsilon_2 - \varepsilon_m}{\varepsilon_2 + 2\varepsilon_m}} \right], \tag{10}$$

547

548 where ϵ_m, ϵ_1, and ϵ_2 are the complex dielectric functions of the host matrix and
549 inclusions, and f_1, f_2 are the volume fractions of the inclusions. If we use the case of
550 $f_2 = 0$, the corresponding complex refractive index of the mixture can be obtained by
551 Eqs. (11) and (12):

$$552 \quad m_r = \sqrt{\frac{\sqrt{\varepsilon_r^2 + \varepsilon_i^2} + \varepsilon_r}{2}}, \tag{11}$$

553

$$554 \quad m_i = \sqrt{\frac{\sqrt{\varepsilon_r^2 + \varepsilon_i^2} - \varepsilon_r}{2}}, \tag{12}$$

555

556 where ε_r and ε_i denote the real and imaginary components of the mixture dielectric
557 function, ε_{MG}.

558 The selected refractive indices of inclusions in the Maxwell-Garnett effective
559 medium approximation model in this study are shown in Fig. 3. Figure 3 also
560 illustrates the assumption on the size resolved aerosol component composition
561 presented as an additional constraint. Table 2 shows the description of aerosol
562 components and the complex refractive indices at 0.440 μm and 0.865 μm of each
563 component employed in the GRASP/Component approach, as well as those used in
564 the uncertainty tests. Our selection of aerosol elements and the size resolved
565 component composition results from the examination of a series of sensitivity tests
566 and stability of the inversion results. The size resolved component composition
567 formulation was chosen because a similarity in spectral signatures of some aerosol
568 species induced a difficulty of their distinguishing in the considered in this study

569   observational configurations. For instance, brown carbon (BrC) and iron oxides
570   (hematite and goethite) have similar tendency in spectral absorption; that is,
571   increasing the imaginary refractive index towards ultraviolet wavelengths (Chen and
572   Cahan, 1981; Chen and Bond, 2010; Kerker et al., 1979; Schuster et al., 2016a). At
573   the same time, it is known that carbonaceous absorbing aerosol particles dominate in
574   the fine mode and mineral dust absorption dominates in the coarse mode. Hence,
575   black carbon (BC) and brown carbon (BrC) are assumed to be the only absorbing
576   insolubles in the fine mode and iron oxides are assumed to be the only absorbing
577   insolubles in the coarse mode. In addition, the fine mode includes non-absorbing
578   insoluble species (FNAI) that represent fine dust or non-absorbing organic carbon
579   (OC), non-absorbing soluble species (FNAS) representing anthropogenic salts and
580   aerosol water content (FAWC). The coarse mode includes absorbing insoluble species
581   (CAI), which are mainly iron oxides, but can also include all other absorbing
582   elements. The coarse mode also includes non-absorbing insoluble (CNAI) species that
583   mainly represent the bulk dust material, but can be also non-absorbing insoluble
584   organic carbon particles, non-absorbing soluble species (CNAS) representing
585   anthropogenic or natural salts (e.g. sea salts) and aerosol water content (CAWC). It
586   should be clarified that refractive index of only one element is used for each species;
587   however, our tests confirmed that some elements are indistinguishable from the
588   optical point of view, at least for the measurement configurations expected in the
589   scope of the presented algorithm applications. Thus, several of the assumed species in
590   the mixing model elements can be associated with different elements. It should be
591   also mentioned that the maximal fractions for BC and CAI (mainly representing iron
592   oxides) are limited in the algorithm due to possible range of complex refractive
593   indices in the pre-computed kernels of aerosol optical characteristics. That is, the
594   volume fractions of these two highly absorbing species are limited in the algorithm to
595   10% for BC and 3% for CAI. The limitation criteria are based on previous in-situ
596   studies (Ganor and Foner, 1996; Guieu et al., 2002; Lafon et al., 2004, 2006, Alfaro et
597   al., 2004; Wagner et al., 2012; Formenti et al., 2014) demonstrating that the volume
598   fraction of free iron in dust particles approximately accounts for $1.4 - 3.25\%$ $(2.8 -$
599   6.5% by mass as the density is 4.28 g cm^{-3} for goethite, 5.25 g cm^{-3} for hematite, and
600   2.65 g cm^{-3} for illite, kaolinite, quartz, and calcite; Formenti et al., 2014). The fraction
601   of BC in atmospheric aerosol was generally reported not exceeding 10% (Bond et al.,
602   2013). Analysis of our results showed that the introduced maximal values were never
603   reached in the inversion procedure and therefore the presented limitations should not
604   introduce artificially limited concentrations. It is also to note that the retrievals of
605   aerosol component derived from AERONET measurements by Schuster et al. (2016a)
606   demonstrated that the volume fraction of free iron remains relatively constant in West
607   Africa throughout the year (1.4−1.7%) and the volume fraction of black carbon
608   reaches a peak of 1.0% for the fine mode during West African biomass burning
609   season and a peak of 3.0% for the fine mode in southern Africa biomass burning.

610

611   **2.3.2 Sensitivity tests**

612   Using the above modifications to the GRASP algorithm described in Dubovik et
613   al. (2011), the aerosol component composition retrieval approach was tested for
614   inversion of ground-based AERONET and POLDER/PARASOL satellite
615   observations. For verification of the proposed concept and the algorithm performance,
616   a series of sensitivity tests were conducted using synthetic data. A comprehensive
617   series of sensitivity tests were mainly conducted with the POLDER/PARASOL
618   observations because, unlike the AERONET retrievals, sensitivity of
619   POLDER/PARASOL observations to aerosol complex refractive index has not been
620   systematically explored. Thus, first, the POLDER/PARASOL radiances and
621   polarization measurements were simulated using forward calculations. Then, the
622   synthetic measurements were inverted using the GRASP algorithm with the size-
623   dependent aerosol component composition approach and the Maxwell-Garnett mixing
624   model. The tests were conducted for a range of aerosol component composition
625   fractions for the species described above and a variety of observational configurations
626   such as spectral channels, viewing geometry etc. Figure 4 presents an example of the
627   assumed and retrieved fractions of aerosol species in fine and coarse modes. The
628   statistics of the sensitivity test results are presented in Table 23, where we compare
629   assumed and retrieved aerosol parameters (fractions of aerosol elements, aerosol
630   optical thickness (AOT), Single Scattering Albedo (SSA) and complex refractive
631   index at 675 nm). The results for other wavelengths are very similar to that presented
632   at 675 nm. In all the conducted tests, the results demonstrated that in frame of the
633   designed model the use of the size-dependent Maxwell-Garnett conversion model
634   allows the algorithm to distinguish amongst the assumed aerosol species, including
635   ammonium nitrate and water in the host.

636

2.3.3 Uncertainty assessment

638   An important range of variability exists in the literature-reported refractive indices
639   of the aerosol species. Different assumptions on the refractive index of an aerosol
640   species can result in different retrieved fractions of the species proposed in this study.
641   To evaluate a possible range of the retrieved fractions due to uncertain knowledge of
642   the refractive indexes and difficulty to select one representative value, a series of
643   supplementary calculations were conducted using a range of refractive indices found
644   in the literature. Figure 5 shows the refractive indices employed in the algorithm and
645   those used for the assessment of the uncertainties in the retrieved aerosol fractions.
646   The uncertainty is defined in percentage as the retrieved fraction minus the assumed
647   fraction and divided by the assumed fraction. The tests are conducted as follows: first,
648   synthetic measurements are created by forward calculations while employing the
649   complex refractive index assumed in the algorithm; second, another complex
650   refractive index is used in the inversion procedure while retrieving the fractions of the
651   aerosol species from the synthetic measurements. Thus, the comparison of the
652   assumed in the forward calculations and the retrieved in the inversion procedure
653   aerosol species fractions provides an error assessment due to possible variability of

their complex refractive index. The calculations were conducted for all aerosol species that are assumed be embedded in the host of the Maxwell-Garnett effective medium approximation. In addition, the tests are also conducted for different fractions of the elements and for different values of AOT, reflecting sensitivity of the retrievals to varying aerosol loading.

An extensive review of BC refractive indices can be found in Bond and Bergstrom (2006) where the recommended imaginary part is in range from 0.63 to 0.79 at visible wavelengths. The spectrally invariant value of 0.79 was adopted in the previous studies (Bond et al., 2013; Bond and Bergstrom, 2006). Based on this literature, we use the spectrally invariant complex refractive index for BC of 1.95 + 0.79i for our current aerosol component ~~composition~~ retrievals. We estimate then the uncertainty in the retrieved BC fraction using a BC refractive index of 1.75 + 0.63i. The results of the uncertainty test for retrieving BC from POLDER/PARASOL are presented in Fig. 6a. As can be seen, the uncertainty strongly depends on the BC fraction and increases when the BC fractions are low. We note that the uncertainty can be large (over 100 %) when the BC fraction is below 0.01 and aerosol loading is weak. However, the uncertainty decreases rapidly and can be 50 % or better for moderate and high aerosol loading (AOT at 440 nm equal or more than 0.4) and when the BC fraction is above 0.01. Therefore, the estimates should be quite reasonable in the cases of large pollution loading. ~~in cases of elevated pollution.~~

The reported in the literature refractive index of BrC is variable. For the forward model we employed the BrC refractive index derived from Sun et al. (2007), which was used to retrieve aerosol component ~~composition~~ from ground-based remote sensing measurements (e.g. Arola et al., 2011; Schuster et al., 2016a). The BrC refractive index, representing carbonaceous particles with light absorption in the blue and ultraviolet spectral regions emitted from biomass combustion (Kirchstetter et al., 2004), was used for the uncertainty estimate. The tests show (Fig. 6b) that the uncertainty in BrC fraction is more than 100 % when the fractions are below 0.1 and decreases to below 100 % when the BrC fractions are above 0.1 and the aerosol loading is elevated. Note that the uncertainty in BrC fraction is within 50 % when the fractions are above 0.1 even for very low aerosol loading (AOT = 0.05).

Hematite and goethite are the dominant absorbers in the coarse mode particles. The hematite refractive index was selected for the employed aerosol component ~~composition~~ mixing model. The literature shows that the hematite refractive indices can also exhibit quite a large range of variability (e.g. see Fig. 5b). Figure 6c thus shows the uncertainties in the retrieved CAI fraction from POLDER/PARASOL associated with the hematite refractive given by Longtin et al. (1988) in the forward calculations and of Triaud (2005) in the inversion. Except the very low fraction of CAI (below 0.005), the uncertainty in CAI fraction is within 50 %.

The insoluble organic carbon and the non-absorbing dust present very similar spectral dependence of complex refractive index (Ghosh, 1999; Koepke et al., 1997) and it is practically impossible to distinguish between these species in the considered in this work measurement configurations and the retrieval approach. Thus, the non-absorbing insoluble organic carbon and non-absorbing mineral dust are expressed by

17

a non-absorbing insoluble species (NAI). The refractive index for the NAI in the presented algorithm was taken as the dust refractive index in Ghosh (1999). The uncertainty tests for the NAI fraction retrievals are presented for fine and coarse fractions by replacing the dust refractive index with the refractive indices of dust composed of quartz (Ghosh, 1999), kaolinite (Sokolik and Toon, 1999) and illite (Sokolik and Toon, 1999) with the proportions of 48%, 26%, and 26%, respectively (the proportions are recalculated from (Journet et al., 2014)) (see legend of Fig. 5). The estimated uncertainties for fine and coarse NAI fractions (FNAI and CNAI) decrease significantly (from 100 % to below 50 % and varying about the zero) when the NAI fraction is above 0.1 (see Fig. 7a and 7b).

~~The non-absorbing insoluble can stand also for the insoluble organic carbon,~~ The non-absorbing insoluble component can represent not only non-absorbing dust, but also non-absorbing organic carbon, as was mentioned above. Thus, an additional test was conducted when the dust refractive index (Ghosh, 1999) used in the forward calculations was replaced at the retrievals stage by refractive index of insoluble organic carbon from Koepke et al. (1997). The corresponding results of the retrieved in this case fine and coarse fractions of NAI for POLDER/PARASOL observations are presented in Fig. 7c and 7d. The variability for each fraction indicates that the choice of NAI refractive index can cause an uncertainty in the retrieved NAI fraction less than 100% for FNAI and less than 50% for CNAI when the fractions are above 0.1.

Figure 8 shows the uncertainties for the host species fraction (FNAS, CNAS, FAWC, and CAWC), which are attributed to the differences between the refractive indices and hygroscopic properties of ammonium nitrate and ammonium sulfate. The uncertainties are small for FNAS, CNAS, FAWC, and CAWC, particularly when the fractions are more than 0.2.

3 Application to real remote sensing data

3.1 Component ~~Composition~~ retrieval from AERONET

AERONET provides measurements that are among the most sensitive data to the aerosol refractive index. In addition, the AOT in AERONET is result of direct measurements and not retrieved as in the case of satellite observations. The GRASP aerosol component ~~composition~~ retrieval concept was therefore first tested with the real AERONET data to check if the retrieved optical characteristics are consistent with the results of standard AERONET product.

Figure 9 presents the AERONET measured AOT and Ångström Exponent (870 nm/440 nm) and retrieved Single-Scattering Albedo (SSA) at 675 nm versus those retrieved using the GRASP/Component ~~Composition~~ approach. Namely, the operational AERONET product is presented versus the derived from GRASP/Component ~~Composition~~ for 3 sites in the African continent: Banizoumbou (data for April 2007), Skukuza (data for September 2007), and Ilorin (data for January

2007), representing according to the sites location and the considered seasons the dust, the biomass burning and the mixture of dust and biomass burning cases, respectively. It can be seen that the aerosol optical properties are reproduced very well by GRASP/Component Composition approach not only for the recalculated AOT and its spectral behavior, but also for the SSA. The mean difference in AOT is about 0.01, which is on the level of the AERONET calibration uncertainty, the difference in SSA is also well within the expected retrieval uncertainty of 0.03 (Dubovik et al., 2002a). There is no biases observed and the correlation coefficient is nearly 1.0 for AOT and Ångström Exponent.

It should be mentioned here that the fine mode in the presented retrievals is described by 10 bins and the coarse mode by 15 bins, which is different than the 22 bins that are used for the entire size distribution in the standard AERONET algorithm (Fig. 9). The component composition retrieval has the ability to infer different refractive indices for the fine and coarse modes. This is a significant improvement over the standard AERONET and POLDER/PARASOL algorithms, which allow refractive indices to vary with wavelength but not with size. Indeed, the use of fixed spectral dependences of the refractive indices in the GRASP/Component Composition algorithm provides an additional constraint and reduces the number of the unknown parameters. Thus, this approach makes the inversion more stable. Nevertheless, the inter-comparison of retrievals by the component composition approach shows full consistency with the operational AERONET product, mainly thanks to an additional physical constraint on the spectral dependence of refractive index.

In addition to the better characterization of aerosol fine and coarse modes and preserving consistency in retrievals of optical characteristics, the new approach can also provide insights on aerosol component composition. For example, Fig. 10 shows the volume fractions of aerosol species retrieved in fine and coarse modes (panels a-f), and fractions of the species in the total volume (panels g-i) for the mentioned above African sites. The Banizoumbou site is located near Niamey (Niger) north of the Sahel, the Ilorin site (Nigeria) is located in the Sahel, and the Skukuza site is located in southern Africa. The retrieved aerosol components compositions for Banizoumbou and Ilorin present similarity in terms of abundant dust aerosol. However, contributions of BrC and BC are strong in Ilorin, and the contribution of coarse absorbing insoluble aerosol fraction is strong in Banizoumbou. The southern Africa site presents a different picture: a strong contribution of coarse mode soluble and of fine mode non-absorbing insoluble aerosol fractions attributed to water soluble organic carbon and water insoluble organic carbon in the biomass burning region, and almost twice more important than in the Sahel site contribution of BC. The BrC contribution, however, is about two times smaller in southern Africa than that in Sahel, which is consistent with AERONET's low spectral dependence for the imaginary index. The SSA in Banizoumbou is highest (0.97 at 675 nm) and in Skukuza is lowest (0.82) because dust and biomass burning aerosols dominate respectively in these two regions.

3.2 POLDER/PARASOL satellite observations

After testing the aerosol component ~~composition~~ retrieval approach with the AERONET measurements, the algorithm was applied to the POLDER/PARASOL satellite observations. Figures 11, 12 and Table 3~~4~~ summarize an inter-comparison of aerosol optical characteristics derived by the GRASP/Component ~~Composition~~ approach applied for POLDER/PARASOL and those of the operational AERONET product. The inter-comparison is presented for six sites in Africa and Middle East (Fig. 11) and for all available AERONET data (Fig. 12) representing performance for different aerosol types and on the global scale. Because of a limited sensitivity to absorption when the aerosol loading is low, the SSA product is filtered for AOT at 0.440 μm equal or higher than 0.4 (Dubovik et al., 2002a; Dubovik and King, 2000). The SSA and the Ångström Exponent in Fig. 11 are presented for all six sites together because the dynamic range of the values for each single site is limited by a dominant aerosol type. It should also be noted that in the inter-comparison on the global scale (Fig. 12) the correlation for Ångström Exponent was notably better for higher AOT (R of ~ 0.6 for all AOTs and of ~ 0.8 for AOT equal or more than 0.2). The better SSA and Ångström Exponent retrievals for higher AOT is, however, known also for standard retrievals and other satellite products (de Leeuw et al., 2015; Popp et al., 2016). Nevertheless, the good agreements for AOT (R is generally of ~ 0.9 or better), and for Ångström Exponent and SSA (R of ~ 0.70 - 0.80) show that the inversion of POLDER/PARASOL satellite measurements using the component ~~composition~~ approach is consistent with the ground-based AERONET reference in terms of aerosol optical properties. Analysis of the per site aerosol optical properties retrievals for different aerosol types (Fig. 11) also does not reveal any evident problem. In addition, the GRASP/Component approach produces almost the same average residual (2.4±0.9% for MG and 2.4±1.0% for VW) as that of the standard GRASP algorithm (2.3±0.9%) while the maximum residual for GRASP/Component (5.0% for MG and 5.7% for VW) is smaller than that for standard GRASP (6.6%); ± denotes standard deviation.

The selected mixing model influence on the retrievals is assessed by comparison of the results from Maxwell-Garnett effective medium approximation with performance using a simplified volume-weighted (VW) aerosol mixture. Definition of the species constituting the VW mixing model is quite similar to Maxwell-Garnett, it employs BC, BrC in fine mode, absorbing insoluble in coarse mode, non-absorbing insoluble and aerosol water content in both fine and coarse modes. The tests were conducted in the same manner as for the Maxwell-Garnett effective medium approximation. The sensitivity tests revealed that implementation of the volume-weighted mixing rule yields stable results and this model can indeed be used for the retrievals. Moreover, the VW model can be preferable in some applications due to its simplicity. Figure 11 and Table 3~~4~~ illustrate that the GRASP/Component ~~Composition~~ retrievals using the MG and VW mixing models almost equally well reproduce the aerosol optical properties. The inter-comparison of the standard GRASP/PARASOL retrievals

827 (without retrieval of aerosol component ~~composition~~) with AERONET is also
828 presented in Fig. 11 and Table ~~3~~4. It should noted that in all three shown cases the
829 results obtained for AOT and Ångström Exponent (AE) from PARASOL using the
830 component ~~composition~~ approach show comparable and even better correlations with
831 AERONET than the standard GRASP/PARASOL retrieval that derives directly the
832 spectral refractive indices instead of fractions of the aerosol species with fixed
833 refractive indices. This can be considered as confirmation that the constraints adapted
834 in the component ~~composition~~ approach adequate provide realistic and practically
835 useful additional constraints that help to improve satellite retrievals. At the same
836 time, it can be seen that the SSA obtained by standard GRASP/PARASOL correlates
837 better with AERONET than those obtained by GRASP/PARASOL component
838 ~~composition~~ approach. Specifically, this GRASP/PARASOL component ~~composition~~
839 shows systematically lower absorption than standard GRASP/PARASOL retrieval.
840 This can be explained by the fact that the complex refractive index in
841 GRASP/Component ~~Composition~~ are constrained by the information (on both
842 magnitudes and spectral tendencies) adapted from the literature while in case of
843 standard GRASP/PARASOL and operational AERONET products there are no such
844 constraints. As discussed by Dubovik and King (2000) and Dubovik et al. (2011) the
845 standard retrieval approach uses only smoothness constraints on spectral variability of
846 complex refractive index. In these regards, tests by Dubovik et al. (2000)
847 demonstrated that in presence of measurements noise the standard approach tends to
848 generate retrievals with higher values of absorption in the situation with lower aerosol
849 loading (lower AOT). This happens simply due to increased spread of SSAs for
850 situation with lower aerosol signal. Indeed, due to physical constraints SSA can not
851 higher than 1, as a result appearance of any spread caused by presence of the noise
852 generates lower SSA bias. Such bias has been often discussed by modelers
853 community as rather unfortunate feature of AERONET retrievals. Therefore, the
854 slightly higher SSA in case of GRASP/Component ~~Composition~~ can be considered
855 rather a positive effect of the additional constrain. Probably, additional focused
856 analysis should be done in future, but it can be expected that the slightly higher values
857 in case of GRASP/Component ~~Composition~~ may also on average be closer to what is
858 expected from models because tied to similar physical assumptions.
859
860

4 Illustration of global scale satellite aerosol component ~~composition~~ retrieval

863 We processed the POLDER/PARASOL observations globally using the aerosol
864 component ~~composition~~ retrieval algorithm. The results of this processing present the
865 first attempt to assess the measurement-based global distribution and seasonal
866 variability of aerosol component ~~composition~~. The data were processed for the year
867 2008, which provides a notable variety of different aerosol types, including volcanic
868 aerosols from a Hawaiian eruption.

The results are further presented as seasonal means. It should be mentioned however that any interpretation of the statistical values should take into account also the number of available observations. Therefore, it is worth presenting the global maps of the number of available cloud-free pixels. Figure 13 shows that the number of the cloud free pixels over land is significantly higher than over ocean, which can produce a difference in the mean values and create some artificial spatial patterns. In addition, the sensitivity tests and experience of remote sensing observations treatment show that the accuracy of the retrievals is low and the sensitivity to absorbing aerosol and refractive index variability is particularly limited when the aerosol loading is low. Therefore, it is also worth presenting the global maps of the aerosol optical thickness (Fig. 14), prior to analyzing the aerosol component composition retrievals. It should also be outlined that despite the fractions of the elements are the initial retrieval parameters, direct interpretation of the maps of these fractions can be confusing because do not always correspond to a significant aerosol concentration. For instance, a large fraction of an element retrieved for a size mode where aerosol volume concentration is very low, can have no significant meaning as not having contribution to the optical signal. Therefore, the columnar volume concentrations of the retrieved elements and not the fractions will be further presented. Figures 15 to 20 thus show seasonal variabilities of the retrieved columnar aerosol volume concentrations (mm^3/m^2, which denotes the volume concentration in total atmospheric column with unit surface area) for different aerosol species.

4.1 Black Carbon

The retrieved aerosol component composition shows patterns of biomass burning in the Sahel and southern Africa regions, expressed by elevated concentrations of BC (Fig. 15). The derived BC concentrations show a pronounced seasonal and spatial variability. The largest concentrations can be observed over the African continent, another noticeable region is Asia, namely India and China. The most intensive BC emissions appear during DJF, which is constituted from contributions of the Sahel region, India and China. Somewhat lower concentrations during SON and JJA are attributed to biomass burning regions in southern African. A global minimum of the BC concentrations is during MAM. The obtained spatial and seasonal patterns of BC are consistent with the knowledge that DJF is the season of intense agricultural burning across the sub-Sahelian region of Africa. BC generated from such agricultural burning can extend for thousands of kilometers from east to west across the continent, as can be seen in Fig. 15. The BC concentration in northern Africa appears mainly over land near the west coast, especially from Senegal south to Gabon on the equator, and over the Gulf of Guinea, which is attributed to the biomass burning during DJF (e.g. Haywood et al., 2008). The BC observed over the ocean is generally transported from biomass burning areas by prevailing trade winds. The retrievals show that the BC concentration in India and China, which can be rather attributed to anthropogenic activity, is maximal during DJF. This result is consistent with a previous study by Li

911 et al. (2015) that also found a maximal BC mass concentration during DJF. The work
912 by Li et al. (2015) is based on retrieval of aerosol component ~~composition~~ from
913 AERONET measurements in Beijing and Kanpur sites and presents twelve years'
914 climatology for the period 2002 - 2013.

915   During JJA and SON, the elevated BC concentrations are mostly over southern
916 Africa, which is in line with the known African monsoon cycle. The variations of the
917 retrieved BC are consistent with the biomass burning activity progressing from north
918 to south Africa, starting from June, peaking in July - August and then decreasing in
919 intensity until late October with the end of the dry season (Cahoon et al., 1992;
920 Liousse et al., 1996; Maenhaut et al., 1996; Swap et al., 1996).

921   It should be reminded, however, that sensitivity to the absorption and therefore to
922 the BC signal is limited when the AOT is low. In addition, for very low AOT values
923 the aerosol volume concentrations are also low and therefore the retrieved fractions of
924 the aerosol species are more uncertain. Very low aerosol loading is typical for over
925 ocean observations (Fig. 14) and thus appearance of some BC concentrations over
926 ocean should be interpreted with caution.
927

928 4.2 Brown Carbon

929   Similar to BC, the observed patterns of BrC (Fig. 16) show seasonal variations,
930 primarily association with the biomass burning in Africa and the contribution of
931 Asian anthropogenic activities. A closer comparison of BrC and BC concentrations
932 reveals, however, that their maximal concentrations are not always collocated. This
933 observation reflects that fresh biomass burning aerosols have higher BC content than
934 aged aerosols (Abel et al., 2003; Haywood et al., 2003; Reid et al., 1998). During
935 SAFARI-2000, for example, the single scattering albedo has an increase from 0.84 to
936 0.90 between smoke close to the source and aged haze 5 h downwind from a large fire
937 (Abel et al., 2003), which is attributed to changes in aerosol component ~~composition~~.
938 There can be some rapid changes occurring in the relative concentration of particle
939 types with the aging of smoke and the BC particles become gradually more
940 aggregated with organic and sulfate particles during the aging of smoke (Pósfai et al.,
941 2003). Therefore, the more abundant presence of particles with the spectral absorption
942 signature of BC is reasonable for the areas near the biomass burning emissions,
943 whereas particles with a spectrally dependent absorption signature of BrC are
944 generally enriched in downwind region, which can explain appearance of BrC
945 concentrations in aerosol particles transported over ocean in northern hemisphere.

946

947 4.3 Fine mode Non-Absorbing Soluble

948   The NAS component is represented by the real part of the refractive index of
949 ammonium nitrate; however, sulfates, sea salt or aged hydroscopic particles are also
950 included in the NAS component. Figure 17 presents seasonal means of the NAS
951 retrieved for the fine mode (FNAS). The FNAS volume concentration dominates over

23

952 China and India, especially during DJF and SON, which can correspond to industrial
953 aerosol and heating activity in megacities with high population density. The spatial
954 patterns of FNAS also coincide with the patterns of BC in southern Africa that
955 indicates presence of non-absorbing particles fraction in the biomass burning
956 emissions (e.g. water soluble organic carbon). Indeed, the carbonaceous organic
957 particles can provide a favorable surface for aging processes and sulfate nucleation
958 (Li et al., 2003). Pronounced FNAS particles concentrations are retrieved during JJA
959 over the Mediterranean Sea region, which is in line with the knowledge on abundant
960 presence of anthropogenic and biogenic sulfate particles in the Mediterranean region
961 (Ganor et al., 2000; Lelieveld et al., 2002; Levin, 2005; Levin et al., 1996). The
962 FNAS particles are also retrieved south from the Mediterranean Sea, deep inland over
963 Libya and Egypt. This FNAS component can be possible in this area considering
964 persistent north-south, north-east air mass transport in the eastern Mediterranean
965 region governed by semi-permanent low-pressure trough extending in JJA from the
966 Persian Gulf (Bitan and Sa'Aroni, 1992).
967

4.4 Coarse mode Non-Absorbing Insoluble

969 In the northern and western Africa, the coarse mode non-absorbing insoluble
970 component appears all year long with the pronounced maximum concentrations
971 during MAM to JJA (Fig. 18), representing the non-absorbing part of mineral dust.
972 Notable is a shift in the maximum of this component towards higher latitudes in JJA
973 that corresponds to the northern shift of the inter-tropical convergence zone. The
974 retrievals also clearly show a "hot spot" of coarse mode non-absorbing dust over the
975 Bodélé depression, located between the Tibesti Mountains and Lake Chad, and known
976 as the most active dust source in the Sahara desert (Gasse, 2002; Prospero et al., 2002;
977 Washington et al., 2003). This dust source is caused by the coincidence of an
978 extensive source of diatomite sediment and high velocity winds associated with the
979 Bodélé Low Level Jet (Todd et al., 2007; Washington et al., 2006; Washington and
980 Todd, 2005) with the emission peaks during DJF and MAM (Herrmann et al., 1999;
981 Koren and Kaufman, 2004; Todd et al., 2007; Washington and Todd, 2005) that are
982 also distinguishable in the presented retrievals. This CNAI aerosol type also appears
983 over the Middle East, the Arabian Peninsula and extends over Asia, which is known
984 as the global dust belt. The coarse mode non-absorbing dust concentration is
985 particularly high over the Arabian Peninsula, central to southern Pakistan, as well as
986 over the Oman and Arabian seas. Over this region, the maximum dust concentration is
987 observed during MAM and JJA, while dust concentration substantially decreases
988 during SON and DJF. Higher dust concentration during MAM and JJA is primarily
989 caused by the strong northwesterly winds known as "Shamal Wind" and dry
990 conditions. The JJA peak is caused by several major sources of dust that have
991 maximum dust activity during JJA, including desert areas in Syria and Iraq where a
992 strong northwesterly Shamal Wind is blowing (Choobari et al., 2014). The Sistan
993 region can also be distinguished among the high dust concentrations. This region is
994 considered as a major dust source in southwest Asia (Ginoux et al., 2012; Goudie,

24

995 2014; Léon and Legrand, 2003; Middleton, 1986a) attributed to the strong persistent
996 northeasterly winds (Alizadeh Choobari et al., 2013; Middleton, 1986b; Miri et al.,
997 2007). This source can cause frequent dust and sand storms, especially during the
998 period of June to August contributing to the deterioration of air quality (Rashki et al.,
999 2013). In addition, during DJF and SON some elevated CNAI concentrations are
1000 observed in Australia (area of Lake Eyre and The Great Artesian Basin). It should be
1001 also noted that some CNAI concentrations are retrieved during the seasons and over
1002 the regions in Africa known for biomass burning and over south-east of USA. These
1003 concentrations indicate presence of some coarse mode non-absorbing particles
1004 possibly of organic origin.

1005

1006 4.5 Coarse mode Absorbing Insoluble

1007 The Coarse mode Absorbing Insoluble (CAI) particles, which mainly represent the
1008 iron oxides contained in mineral dust, are generally associated with the desert regions
1009 and with the elevated concentrations of CNAI. The high CAI concentrations are
1010 observed during MAM and JJA over western Africa and the Arabian Peninsula (Fig.
1011 19). High CAI concentrations are also retrieved over Asia during the same MAM and
1012 JJA seasons and are quite clearly attributed to the region of the Taklimakan desert
1013 located in northwest China. It is worth noting that the maximum of CAI and CNAI do
1014 not always coincide, reflecting different percentage of iron oxides in desert dust that
1015 is varying depending on the soil mineralogy of the source region. Calculations of the
1016 ratio of CAI to CNAI concentrations over African continent provided values of up to
1017 about 0.05, which is consistent with up to 3 to 5 % iron oxides in desert dust (e.g.
1018 Ganor and Foner, 1996; Guieu et al., 2002; Zhang et al., 2003; Lafon et al., 2004).

1019 The high CAI concentrations over western Africa are mainly present over Niger,
1020 Mauritania and near the west coast. This is in line with a study by Formenti et al.
1021 (2008) that demonstrates the higher iron oxide content in Sahelian dust originated
1022 from the Sahel belt, while a lower content is in the Chad basin. Lázaro et al. (2008)
1023 also reported that the iron oxide content of dust transported to the Canary Islands,
1024 near the west coast, tends to have higher values for source areas between 0°N - 20°N.
1025 In addition, high CAI concentrations are also derived over the Arabian Peninsula and
1026 the Arabian Sea, which may be attributed to the dust originated from Saudi Arabia,
1027 known for presence of an important iron content (Krueger et al., 2004). It should be
1028 mentioned here that a discontinuity in the retrieved concentrations can be noted
1029 between over land and over water in the regions of the Red Sea and Arabian Sea.
1030 Given that such discontinuity does not appear in all coastal regions, but only in
1031 particular circumstances, we suppose that there are some physical explanations. For
1032 instance, the observed discontinuity corresponds well to the land topography, i.e.
1033 presence of surrounding mountains and the observed in other work accumulation of
1034 aerosol over the Red Sea (Brindley et al., 2015). It is also interesting to admit that
1035 some coarse mode absorbing aerosol appear in the regions and seasons associated
1036 with biomass burning and elevated concentrations of BrC and BC in the fine mode,

e.g. in Africa during DJF and SON seasons. This fact can reflect presence of absorbing carbonaceous material in the coarse mode, which was fitted by refractive index of iron oxide assumed as only the absorbing component of the coarse mode.

4.6 Fine mode Non-Absorbing Insoluble

Because the fine mode non-absorbing insoluble component (Fig. 20) can stand for both OC and non-absorbing dust, the Ångström Exponent can be used as an additional post retrieval criteria for a better interpretation of this component. For instance, the joint FNAI and Ångström Exponent (maps are presented in supplementary material) analysis shows that the particles concentrations derived over western Africa, Middle East, Central Asia and northwest China mainly reflect presence of fine mode non-absorbing dust because are associated with the values of Ångström Exponent generally well below one. Specific examples are the concentrations derived over the Bodélé depression during DJF, the Taklimakan desert in China during MAM and Arabian Peninsula during JJA. However, the elevated FNAI particles concentrations retrieved over southern Africa and South America during JJA and SON, over eastern part of China and Siberia during JJA, and generally over India, are associated with high values of Ångström Exponent, thus should rather be classified as organic carbon. For example, high OC in southern China (Sichuan Basin and the Pearl River Delta region) and urban south Asia is confirmed in several previous studies (Decesari et al., 2010; Stone et al., 2010; Zhang et al., 2008b; Zhang et al., 2012). The OC of urban origin in China is enhanced around May to June and October (Zhang et al., 2012), which may be an explanation of the retrieved high OC concentration during JJA in southern China. Secondary OC (SOC) can also contribute to the total concentrations of OC (Miyazaki et al., 2006; Weber et al., 2007; Zhang et al., 2008b; Zhang et al., 2005) and be retrieved here as FNAI. Additionally, the elevated OC concentration over South America during SON correspond well to the known season of biomass burning that starts in July and peaks generally in August and September (Duncan et al., 2003).

A plume structure of elevated fine non-absorbing insoluble (Fig. 20) and soluble (Fig. 17) components originated from Hawaiian Islands in the North Pacific Ocean is also notable. This structure is visible during three seasons from MAM to SON and corresponds to a Hawaiian volcano emission. The material emitted into the atmosphere in this case was not the coarse volcanic ash, but continuous gaseous emissions that can form secondary aerosol during downwind transport (Craddock and Greeley, 2009; Edmonds et al., 2013). Identification of this material by the suggested approach as a mixture of components equivalent to ammonium sulfate and fine non-absorbing dust is therefore quite plausible.

4.7 Aerosol Water Content and Coarse mode Non-Absorbing Soluble

The algorithm also provides aerosol water content that is required to create the host by mixture with non-absorbing soluble component. As result, the retrieved spatial and temporal patterns of aerosol water content and non-absorbing soluble are very similar. That is, the fine mode aerosol water content is mainly retrieved in the regions with high loading of anthropogenic aerosol, similarly to the fine mode non-absorbing soluble. For instance, the fine mode aerosol water content can be seen over India and China during SON and DJF, at high latitudes of northern hemisphere and over Eurasia during SON. Some notable water concentrations are also retrieved over southern Africa during the biomass burning season (JJA), but mainly over ocean that correspond to visibly transported and likely aged aerosol. The maps of FAWC are presented in the supplementary material as they are very similar to already presented FNAS (Fig. 17).

The retrieved coarse mode aerosol water content and coarse non-absorbing soluble also present very similar spatial and temporal patterns. However, they are different from the patterns of fine mode. The concentrations are very low everywhere, except over ocean in the regions associated with high concentrations of the coarse non-absorbing insoluble (dust) component. This feature is associated with dust transported from western Africa and Arabian Peninsula. These coarse mode AWC and NAS retrievals require a careful interpretation. First, it should be realized that even relatively small aerosol water fraction retrieved in the regions of very high aerosol concentration can result in a pronounced volume concentration. In addition, aerosols with low real refractive index, which cannot be fully explained by the assumed dust aerosol model, will be interpreted as a water fraction. For instance, some low water aerosol concentration erroneously appears over the Bodélé depression during DJF. The Bodélé dust, however, is known to contain much fossil diatom (Formenti et al., 2008), which would have a different real part of refractive index then assumed in this study mixture of quartz, kaolinite and illite. At the same time, possible hygroscopicity of mineral dust, its coating by organics and internal mixture with sea salt, were found in several laboratory and field studies (e.g. Usher et al., 2003; Falkovich et al., 2004; Laskin et al., 2005; Derimian et al., 2017). The fact that the notable aerosol water content is observed in the retrievals only over ocean and not over land, except for retrievals over Bodélé, also agrees with hypothesis of the dust hygroscopicity. We therefore conclude that despite this pronounced water aerosol content in the coarse mode should be questioned and interpreted with caution, a physical significance of this result should not be excluded. Indeed, this retrieval result may not be fully understood at present but it was not enforced by any specific assumption or measurement artifact, and therefore it is likely to represent a manifestation of specific physical or chemical transformation of aerosol or properties of dust. In addition to the described above main feature of CAWC and CNAS, the derived maps are presented in supplements, together with the maps of FAWC, which are similar to already presented FNAS.

5 Conclusions

We present a new approach for monitoring atmospheric aerosol component composition with remote sensing observations. Unlike existing aerosol component composition retrieval algorithms that interpret an intermediate retrieval of the refractive index, this study utilizes a direct fit of measurements. We demonstrate retrievals of several aerosol components in fine and coarse size modes under assumption of an internal aerosol mixing rule. The tests using a volume weighted mixing rule were also conducted and the results compared.

The approach is implemented in a state of the art GRASP algorithm (Dubovik et al., 2014, 2011) designed to process space-borne and ground-based remote sensing observations. The component composition module is incorporated in GRASP thus the new GRASP/Component Composition version of the code employs mixtures of aerosol components with known refractive indices. This approach serves also as an additional physical constraint on spectral dependences of complex refractive index. The component composition module uses the Maxwell-Garnett effective medium approximation (EMA) and is based on the Schuster et al. (2016a, 2009) approach, but assumes independent aerosol mixtures in the fine and coarse modes and the direct fit of radiances instead of an intermedia step of fitting the retrieved refractive indices.

A series of numerical sensitivity tests with synthetic data were conducted to evaluate the component composition retrieval. Results of the tests showed that the new conversion module allows the retrieval to distinguish amongst several assumed aerosol components. The tests with the new module also show consistency with GRASP tests that are traditionally configured for ground-based AERONET measurements.

We also tested the algorithm with real measurements. Application of the GRASP/Component Composition algorithm to the AERONET Sun/sky photometric measurements retrievals of AOT, Ångström Exponent and SSA presented good agreement with the standard operational AERONET product for sites dominated by dust, biomass burning, and mixtures of dust and biomass burning aerosol. In addition, because of the reduced number of parameters (instead of 8 parameters for complex refractive index retrievals using 6 parameters for component composition retrievals) and an additional physical constrain on spectral dependence of refractive index in the component composition retrieval, the GRASP/Component Composition approach applied for AERONET can split the characteristics of fine and coarse mode aerosol. The GRASP/Component Composition algorithm was also applied for the POLDER/PARASOL satellite observations. An inter-comparison of aerosol optical characteristics derived from POLDER/PARASOL using the component composition approach and those of the AERONET operational product demonstrated a high reliability of the results.

The performance of the aerosol component composition algorithm has been demonstrated by the application to POLDER/PARASOL observations on the global

scale for year 2008. The obtained spatial and temporal patterns of aerosol component composition distribution seem to agree well with known physical expectations. For a proper interpretation of the obtained results it should be also realized that the retrieved aerosol species and their concentrations compose a set of parameters that reproduces well the measured radiation field and provides adequate retrieved optical properties of aerosol. At the same time, the direct interpretation from the chemical point of view is not always evident and even possible. For instance, as mentioned in the methodology part, the distinguishing of some chemical species is not possible for the given configuration of remote sensing measurements. However, the retrieved component composition still reflects the aerosol microphysics and chemistry, and their variability. One should also remember that, based on the sensitivity tests and experience of aerosol characterization by remote sensing, the accuracy of the retrievals depends on the aerosol loading (AOT). Accuracy of the absorbing components retrieval can be primary affected. Thus, interpretation of all the obtained patters requires a more detailed analysis and it is realized that some erroneous component composition features can be possible. The principle limitations of the presented approach are: (i) lack of sensitivity to absorption species in case of low AOT; (ii) difficulty to distinguish between iron oxide and absorbing carbonaceous species (BrC and BC), which is mainly related to the limited number of spectral channels in shortwave solar spectrum; (iii) non-absorbing insoluble component can include organic material, but also non-absorbing dust. These assumptions can lead to some misinterpretation; for instance, the analysis of the BrC retrievals at some locations reveals that the aerosol absorbing properties attributed to BrC should be attributed to the iron oxides that are present in the fine size fraction. A post-retrieval classification is helpful to resolve the shortcomings. For example, analysis of Ångström Exponent can indicate dominance of coarse particles of mineral dust origin or fine particles of combustion origin, which can provide more information about the non-absorbing insoluble component.

Nevertheless, the results are encouraging. For example, the derived BC and BrC exhibit a seasonal and spatial variability that is attributed to the known biomass burning season cycle in Africa and the anthropogenic pollution patterns in Asia, in particular India and China. Coarse mode absorbing (mainly iron oxides) and non-absorbing (mainly dust) insoluble components show a similar seasonal and spatial variability, reaching a peak during MAM and a minimum during SON. It is also noted that the maximums of iron oxide concentration are not co-located with those of dust, because the elemental and mineralogical components compositions of mineral dust vary depending on the source region. The global dust belt extending from western Africa, through the Middle East to Central Asia is also observed in the component composition retrieval. GRASP/Component Composition indicates high concentrations of non-absorbing insoluble appear over the Sahara, Arabian Peninsula, Caspian Sea and Aral Sea regions in Central Asia, and the Gobi and Taklimakan desert in China. In addition, dust was also detected over some regions in Australia during DJF and SON.

The component ~~composition~~ retrieval algorithm demonstrated here using AERONET and POLDER/PARASOL data can also be used for interpreting other observations. That is, the component ~~composition~~ approach is now incorporated in the GRASP algorithm, which has a generalized input and can be easily modified and adapted to other both passive and active remote sensing instruments, for example, the Directional Polarimetric Camera (DPC) launched onboard the GaoFen-5 Satellite in Chinese High-resolution Earth Observation Program, which is the first Chinese multi-angle polarized earth observation satellite sensor (Dubovik et al., 2019; Li et al., 2018). Moreover, the proposed aerosol parameterization using components can be helpful not only for retrieving additional information about aerosol component ~~composition~~, but also for optimizing retrieval stability.

Additionally, we tested the volume-weighted mixing model, in addition to the Maxwell-Garnett EMA, to evaluate the sensitivity of our approach to the assumed aerosol EMA. We tested both approaches using our suite of aerosol species (i.e. BC, BrC, coarse mode absorbing insoluble, fine and coarse mode non-absorbing insoluble). The sensitivity tests revealed that implementation of the volume-weighted mixing rule also presents stable results that are consistent with the Maxwell-Garnett EMA. Thus, the volume-weighted model can also be employed in GRASP/Component ~~Composition~~ retrieval, and may be preferable in some applications due to its simplicity.

The results of the aerosol component ~~composition~~ retrieval from AERONET and POLDER/PARASOL satellite measurements demonstrate a potential for constraining global and regional aerosol modeling that can be particularly valuable because no other aerosol component ~~composition~~ data are often available on a large spatial and temporal scale.

Data availability: The retrievals can be requested directly from the corresponding author (oleg.dubovik@univ-lille.fr or yevgeny.derimian@univ-lille.fr)

Author contributions: LL, OD, YD and GLS developed the retrieval algorithm, designed and realized the sensitivity and uncertainty tests and applied the algorithm to the real data. OD with contributions of YD and GLS suggested the aerosol component retrieval conception. TL, PL, AL, FD, DF and CC contributed to the modifications of the GRASP code and application to the satellite data. BT and AL contributed in application to the AERONET data. ZL and HC supported the work and provided expertise on Asian aerosol observations. LL, YD and OD wrote the paper with input from all the authors.

Competing interests: The authors declare that they have no conflict of interest.

Reference:

Abel, S.J., Haywood, J.M., Highwood, E.J., Li, J., Buseck, P.R.: Evolution of biomass burning aerosol properties from an agricultural fire in southern Africa, Geophys. Res. Lett., 30, 10–13, https://doi.org/10.1029/2003GL017342, 2003.

Alfaro, S., Lafon, S., Rajot, J., Formenti, P., Gaudichet, A., and Maille, M.: Iron oxides and light absorption by pure desert dust: an experimental study, J. Geophys. Res., 109, D08208, doi:10.1029/2003JD004374, 2004.

Alizadeh Choobari, O., Zawar-Reza, P., Sturman, A.: Low level jet intensification by mineral dust aerosols, Ann. Geophys., 31, 625–632, https://doi.org/10.5194/angeo-31-625-2013, 2013.

Andreae, M.O. and Gelencsér, A.: Black carbon or brown carbon? the nature of light-absorbing carbonaceous aerosols, Atmos. Chem. Phys., 6, 3131–3148, https://doi.org/10.5194/acp-6-3131-2006, 2006.

Arimoto, R., Balsam, W., Schloesslin, C.: Visible spectroscopy of aerosol particles collected on filters: Iron-oxide minerals, Atmos. Environ., 36, 89–96, https://doi.org/10.1016/S1352-2310(01)00465-4, 2002.

Arola, A., Schuster, G., Myhre, G., Kazadzis, S., Dey, S., Tripathi, S.N.: Inferring absorbing organic carbon content from AERONET data, Atmos. Chem. Phys., 11, 215–225, https://doi.org/10.5194/acp-11-215-2011, 2011.

Bahadur, R., Praveen, P., Xu, Y., and Ramanathan, V.: Solar absorption by elemental and brown carbon determined from spectral observations, P. Natl. Acad. Sci. USA, 109, 17366–17371, https://doi.org/10.1073/pnas.1205910109, 2012.

Benavent-oltra, J.A., Román, R., Granados-muñoz, M.J., Pérez-ramírez, D.: Comparative assessment of GRASP algorithm for a dust event over Granada (Spain) during ChArMEx-ADRIMED 2013 campaign, Atmos. Meas. Tech., 10, 4439–4457, https://doi.org/10.5194/amt-10-4439-2017, 2017.

Bitan, A. and Sa'Aroni, H.: The horizontal and vertical extension of the Persian Gulf pressure trough, Int. J. Climatol., 12, 733–747, https://doi.org/10.1002/joc.3370120706, 1992.

Bohren, C.F. and Huffman, D.R.: Scattering Coefficients, in: Absorption and Scattering of Light by Small Particles, 1983.

Bond, T.C. and Bergstrom, R.W.: Light Absorption by Carbonaceous Particles: An Investigative Review, Aerosol Sci. Technol., 40, 27–67, https://doi.org/10.1080/02786820500421521, 2006.

Bond, T.C., Charlson, R.J., Heintzenberg, J.: Quantifying the emission of light-absorbing particles: Measurements tailored to climate studies, Geophys. Res. Lett., 25, 337–340, https://doi.org/10.1029/98GL00039, 1998.

Bond, T.C., Doherty, S.J., Fahey, D.W., Forster, P.M., Berntsen, T., Deangelo, B.J., Flanner, M.G., Ghan, S., Kärcher, B., Koch, D., Kinne, S., Kondo, Y., Quinn, P.K., Sarofim, M.C., Schultz, M.G., Schulz, M., Venkataraman, C., Zhang, H., Zhang, S., Bellouin, N., Guttikunda, S.K., Hopke, P.K., Jacobson, M.Z., Kaiser, J.W., Klimont, Z., Lohmann, U., Schwarz, J.P., Shindell, D., Storelvmo, T., Warren, S.G., Zender, C.S.: Bounding the role of black carbon in the climate system: A scientific assessment, J. Geophys. Res. Atmos., 118, 5380–5552, https://doi.org/10.1002/jgrd.50171, 2013.

Brindley, H., Osipov, S., Bantges, R., Smirnov, A., Banks, J., Levy, R., Jish Prakash, P., Stenchikov, G.: An assessment of the quality of aerosol retrievals over the Red Sea and evaluation of the climatological cloud-free dust direct radiative effect in the region, J. Geophys. Res. Atmos., 120, 10862-10878, https://doi.org/10.1002/2015JD023282, 2015.

Cahoon, D.R., Stocks, B.J., Levine, J.S., Cofer, W.R., O'Neill, K.P.: Seasonal distribution of African savanna fires, Nature, 359, 812–815, https://doi.org/10.1038/359812a0, 1992.

Chakrabarty, R.K., Moosmüller, H., Chen, L.W.A., Lewis, K., Arnott, W.P., Mazzoleni, C., Dubey, M.K., Wold, C.E., Hao, W.M., Kreidenweis, S.M.: Brown carbon in tar balls from smoldering biomass combustion, Atmos. Chem. Phys., 10, 6363–6370, https://doi.org/10.5194/acp-10-6363-2010, 2010.

Chami, M., Santer, R., Dilligeard, E.: Radiative transfer model for the computation of radiance and polarization in an ocean–atmosphere system: polarization properties of suspended matter for remote sensing, Appl. Opt., 40, 2398, https://doi.org/10.1038/laban1011-313, 2001.

Chen, C., Dubovik, O., Henze, D.K., Lapyonak, T., Chin, M., Ducos, F., Litvinov, P., Huang, X., Li, L.: Retrieval of desert dust and carbonaceous aerosol emissions over Africa from POLDER/PARASOL products generated by the GRASP algorithm, Atmos. Chem. Phys., 18, 12551–12580, https://doi.org/10.5194/acp-18-12551-2018, 2018.

Chen, C., Dubovik, O., Henze, D. K., Chin, M., Lapyonok, T., Schuster, G. L., Ducos, F., Fuertes, D., Litvinov, P., Li, L., Lopatin, A., Hu, Q., and Torres, B.: Constraining global aerosol emissions using POLDER/PARASOL satellite remote sensing observations, Atmos. Chem. Phys. Discuss., https://doi.org/10.5194/acp-2019-623, in review, 2019.

Chen, C.T. and Cahan, B.D.: Visible and ultraviolet optical properties of single-crystal and polycrystalline hematite measured by spectroscopic ellipsometry, J. Opt. Soc. Am., 71, 932–934, 1981.

Chen, Y. and Bond, T.C.: Light absorption by organic carbon from wood combustion, Atmos. Chem. Phys., 10, 1773–1787, 2010.

Choobari, O.A., Zawar-Reza, P., Sturman, A.: The global distribution of mineral dust and its impacts on the climate system: A review, Atmos. Res., 138, 152–165, https://doi.org/10.1016/j.atmosres.2013.11.007, 2014.

Chowdhary, J., Cairns, B., Travis, L.D.: Contribution of water-leaving radiances to multiangle, multispectral polarimetric observations over the open ocean: bio-optical model results for case 1 waters, Appl. Opt., 45, 5542–67, https://doi.org/10.1364/AO.45.005542, 2006.

Chung, C., Ramanathan, V., and Decremer, D.: Observationally constrained estimates of carbonaceous aerosol radiative forcing, P. Natl. Acad. Sci. USA, 109, 11624–11629, https://doi.org/10.1073/pnas.1203707109, 2012.

Collins, W.D., Rasch, P.J., Eaton, B.E., Khattatov, B. V, Lamarque, J.-F., Zender, C.S.: Simulating aerosols using a chemical transport model with assimilation of satellite aerosol retrievals: Methodology for INDOEX, J. Geophys. Res. Atmos., 106, 7313–7336, https://doi.org/10.1029/2000JD900507, 2001.

Cooke, W.F., Liousse, C., Cachier, H., Feichter, J.: Construction of a 1° × 1° fossil fuel emission data set for carbonaceous aerosol and implementation and radiative impact in the ECHAM4 model, J. Geophys. Res. Atmos., 104, 22137–22162, https://doi.org/10.1029/1999JD900187, 1999.

Cox, C. and Munk, W.: Measurement of the Roughness of the Sea Surface from Photographs of the Sun's Glitter, J. Opt. Soc. Am., 44, 838, https://doi.org/10.1364/JOSA.44.000838,

1954.

Craddock, R.A. and Greeley, R.: Minimum estimates of the amount and timing of gases released into the martian atmosphere from volcanic eruptions, Icarus, 204, 512–526, https://doi.org/10.1016/j.icarus.2009.07.026, 2009.

de Leeuw, G., Holzer-Popp, T., Bevan, S., Davies, W.H., Descloitres, J., Grainger, R.G., Griesfeller, J., Heckel, A., Kinne, S., Klüser, L., Kolmonen, P., Litvinov, P., Martynenko, D., North, P., Ovigneur, B., Pascal, N., Poulsen, C., Ramon, D., Schulz, M., Siddans, R., Sogacheva, L., Tanré, D., Thomas, G.E., Virtanen, T.H., von Hoyningen Huene, W., Vountas, M., Pinnock, S.: Evaluation of seven European aerosol optical depth retrieval algorithms for climate analysis, Remote Sens. Environ., 162, 295–315, https://doi.org/10.1016/j.rse.2013.04.023, 2015.

Decesari, S., Facchini, M.C., Carbone, C., Giulianelli, L., Rinaldi, M., Finessi, E., Fuzzi, S., Marinoni, A., Cristofanelli, P., Duchi, R., Bonasoni, P., Vuillermoz, E., Cozic, J., Jaffrezo, J.L., Laj, P.: Chemical composition of PM10 and PM1 at the high-altitude Himalayan station Nepal Climate Observatory-Pyramid (NCO-P) (5079 m a.s.l.), Atmos. Chem. Phys., 10, 4583–4596, https://doi.org/10.5194/acp-10-4583-2010, 2010.

Derimian, Y., Choel, M., Rudich, Y., Deboudt, K., Dubovik, O., Laskin, A., Legrand, M., Damiri, B., Koren, I., Unga, F., Moreau, M., Andreae, M. O., Karnieli, A.: Effect of sea breeze circulation on aerosol mixing state and radiative properties in a desert setting, Atmos. Chem. Phys., 17, 11331-11353, https://doi.org/10.5194/acp-17-11331-2017, 2017.

Derimian, Y., Karnieli, A., Kaufman, Y.J., Andreae, M.O., Andreae, T.W., Dubovik, O., Maenhaut, W., Koren, I.: The role of iron and black carbon in aerosol light absorption, Atmos. Chem. Phys., 8, 3632–3637, 2008.

Deschamps, P.Y., Buriez, J.C., Bréon, F.M., Leroy, M., Podaire, A., Bricaud, A., Sèze, G. : The POLDER Mission: Instrument Characteristics and Scientific Objectives, IEEE Trans. Geosci. Remote Sens., 32, 598–615, https://doi.org/10.1109/36.297978, 1994.

Deuzé, J.L., Bréon, F.M., Devaux, C., Goloub, P., Herman, M., Lafrance, B., Maignan, F., Marchand, A., Nadal, F., Perry, G., Tanré, D.: Remote sensing of aerosols over land surfaces from POLDER-ADEOS-1 polarized measurements, J. Geophys. Res. Atmos., 106, 4913–4926, https://doi.org/10.1029/2000JD900364, 2001.

Dinar, E., Abo Riziq, A., Spindler, C., Erlick, C., Kiss, G., Rudich, Y., The complex refractive index of atmospheric and model humic-like substances (HULIS) retrieved by a cavity ring down aerosol spectrometer (CRD-AS), Faraday Discuss., 137, 279–295, https://doi.org/10.1039/b703111d, 2007.

Downing, H.D. and Williams, D.: Optical constants of water in the infrared, J. Geophys. Res., 80, 1656–1661, https://doi.org/10.1029/JC080i012p01656, 1975.

Dubovik, O.: Optimization of Numerical Inversion in Photopolarimetric Remote Sensing, in: Photopolarimetry in Remote Sensing, Kluwer Academic Publishers, Dordrecht, pp. 65–106, https://doi.org/10.1007/1-4020-2368-5_3, 2004.

Dubovik, O., Herman, M., Holdak, A., Lapyonok, T., Tanré, D., Deuzé, J.L., Ducos, F., Sinyuk, A., Lopatin, A.: Statistically optimized inversion algorithm for enhanced retrieval of aerosol properties from spectral multi-angle polarimetric satellite observations, Atmos. Meas. Tech., 4, 975–1018, https://doi.org/10.5194/amt-4-975-2011, 2011.

Dubovik, O., Holben, B., Eck, T.F., Smirnov, A., Kaufman, Y.J., King, M.D., Tanré, D., Slutsker, I.: Variability of Absorption and Optical Properties of Key Aerosol Types Observed in Worldwide Locations, J. Atmos. Sci., 59, 590–608, 2002a.

Dubovik, O., Holben, B.N., Lapyonok, T., Sinyuk, A., Mishchenko, M.I., Yang, P., Slutsker, I.: Non-spherical aerosol retrieval method employing light scattering by spheroids, Geophys. Res. Lett., 29, 541-544, https://doi.org/10.1029/2001GL014506, 2002b.

Dubovik, O. and King, M.D.: A flexible inversion algorithm for retrieval of aerosol optical properties from Sun and sky radiance measurements, J. Geophys. Res. Atmos., 105, 20673–20696, https://doi.org/10.1029/2000JD900282, 2000.

Dubovik, O., Lapyonok, T., Kaufman, Y.J., Chin, M., Ginoux, P., Kahn, R.A., Sinyuk, A.:

Retrieving global aerosol sources from satellites using inverse modeling, Atmos. Chem. Phys., 8, 209–250, https://doi.org/10.5194/acp-8-209-2008, 2008.

Dubovik, O., Lapyonok, T., Litvinov, P., Herman, M., Fuertes, D., Ducos, F., Torres, B., Derimian, Y., Huang, X., Lopatin, A., Chaikovsky, A., Aspetsberger, M., Federspiel, C.: GRASP: a versatile algorithm for characterizing the atmosphere, SPIE Newsroom 2–5, https://doi.org/10.1117/2.1201408.005558, 2014.

Dubovik, O., Li, Z., Mishchenko, M.I., Tanré, D., Karol, Y., Bojkov, B., Cairns, B., Diner, D.J., Espinosa, W.R., Goloub, P., Gu, X., Hasekamp, O., Hong, J., Hou, W., Knobelspiesse, K.D., Landgraf, J., Li, L., Litvinov, P., Liu, Y., Lopatin, A., Marbach, T., Maring, H., Martins, V., Meijer, Y., Milinevsky, G., Mukai, S., Parol, F., Qiao, Y., Remer, L., Rietjens, J., Sano, I., Stammes, P., Stamnes, S., Sun, X., Tabary, P., Travis, L.D., Waquet, F., Xu, F., Yan, C., Yin, D.: Polarimetric remote sensing of atmospheric aerosols: Instruments, methodologies, results, and perspectives, J. Quant. Spectrosc. Radiat. Transf., 224, 474–511, https://doi.org/10.1016/j.jqsrt.2018.11.024, 2019.

Dubovik, O., Sinyuk, A., Lapyonok, T., Holben, B.N., Mishchenko, M., Yang, P., Eck, T.F., Volten, H., Muñoz, O., Veihelmann, B., van der Zande, W.J., Leon, J.F., Sorokin, M., Slutsker, I. : Application of spheroid models to account for aerosol particle nonsphericity in remote sensing of desert dust, J. Geophys. Res. Atmos., 111, 1–34, https://doi.org/10.1029/2005JD006619, 2006.

Duncan, B.N., Martin, R. V., Staudt, A.C., Yevich, R., Logan, J.A.: Interannual and seasonal variability of biomass burning emissions constrained by satellite observations, J. Geophys. Res., 108, 4100, https://doi.org/10.1029/2002JD002378, 2003.

Edmonds, M., Sides, I.R., Swanson, D.A., Werner, C., Martin, R.S., Mather, T.A., Herd, R.A., Jones, R.L., Mead, M.I., Sawyer, G., Roberts, T.J., Sutton, A.J., Elias, T.: Magma storage, transport and degassing during the 2008-10 summit eruption at Kilauea Volcano, Hawaii, Geochim. Cosmochim. Acta., 123, 284–301, https://doi.org/10.1016/j.gca.2013.05.038, 2013.

Espinosa, W.R., Remer, L.A., Dubovik, O., Ziemba, L., Beyersdorf, A., Orozco, D., Schuster, G., Lapyonok, T., Fuertes, D., Martins, J.V.: Retrievals of aerosol optical and microphysical properties from Imaging Polar Nephelometer scattering measurements, Atmos. Meas. Tech., 10, 811–824, https://doi.org/10.5194/amt-10-811-2017, 2017.

Falkovich, A. H., Schkolnik, G., Ganor, E., Rudich, Y.: Adsorption of organic compounds pertinent to urban environments onto mineral dust particles, J. Geophys. Res. Atmos., 109, https://doi.org/10.1029/2003jd003919, 2004.

Formenti, P., Caquineau, S., Chevaillier, S., Klaver, A., Desboeufs, K., Rajot, J.L., Belin, S., Briois, V.: Dominance of goethite over hematite in iron oxides of mineral dust from Western Africa: Quantitative partitioning by X-ray absorption spectroscopy, J. Geophys. Res. Atmos., 119, 12740-12754, https://doi.org/10.1002/2014JD021668, 2014.

Formenti, P., Rajot, J.L., Desboeufs, K., Caquineau, S., Chevaillier, S., Nava, S., Gaudichet, A., Journet, E., Triquet, S., Alfaro, S., Chiari, M., Haywood, J., Coe, H., Highwood, E.: Regional variability of the composition of mineral dust from western Africa: Results from the AMMA SOP0/DABEX and DODO field campaigns, J. Geophys. Res. Atmos., 113, 1–12, https://doi.org/10.1029/2008JD009903, 2008.

Ganor, E. and Foner, H. A.: The mineralogical and chemical properties and the behavior of aeolian Saharan dust over Israel, in: The Impact of Desert Dust Across the Mediterranean, edited by: Guerzoni, S., and Chester, R., Kluwer Academic Publishers, Printed in the Netherlands, 163-172, 1996.

Ganor, E., Foner, H.A., Bingemer, H.G., Udisti, R., Setter, I.: Biogenic sulphate generation in the Mediterranean Sea and its contribution to the sulphate anomaly in the aerosol over Israel and the Eastern Mediterranean, Atmos. Environ., 34, 3453–3462, https://doi.org/10.1016/S1352-2310(00)00077-7, 2000.

Gasse, F.: Diatom-inferred salinity and carbonate oxygen isotopes in Holocene waterbodies of the western Sahara and Sahel (Africa), Quat. Sci. Rev., 21, 737–767, https://doi.org/10.1016/S0277-3791(01)00125-1, 2002.

Ghosh, G.: Dispersion-equation coefficients for the refractive index and birefringence of

calcite and quartz crystals, Opt. Commun., 163, 95–102, https://doi.org/10.1016/S0030-4018(99)00091-7, 1999.

Ginoux, P., Prospero, J.M., Gill, T.E., Hsu, N.C., Zhao, M.: Global-scale attribution of anthropogenic and natural dust sources and their emission rates based on MODIS Deep Blue aerosol products, Rev. Geophys., 50, 1–36, https://doi.org/10.1029/2012RG000388, 2012.

Gosse, S.F., Wang, M., Labrie, D., Chylek, P.: Imaginary part of the refractive index of sulfates and nitrates in the 0.7-2.6-micron spectral region, Appl. Opt., 36, 3622–3634, 1997.

Goudie, A.S.: Desert dust and human health disorders, Environ. Int., 63, 101–113, https://doi.org/10.1016/j.envint.2013.10.011, 2014.

Guieu, C., Loye-Pilot, M. D., Ridame, C., Thomas, C.: Chemical characterization of the Saharan dust end-member: Some biogeochemical implications for the western Mediterranean Sea, J. Geophys. Res., 107 (D15), 4258, https://doi.org/4210.1029/2001JD000582, 2002.

Hammer, M.S., Martin, R.V., Li, C., Torres, O., Manning, M., Boys, B.L.: Insight into global trends in aerosol composition from 2005 to 2015 inferred from the OMI Ultraviolet Aerosol Index, Atmos. Chem. Phys., 18, 8097–8112, https://doi.org/10.5194/acp-18-8097-2018, 2018.

Hale, G.M. and Querry, M.R.: Optical Constants of Water in the 200-nm to 200-microm Wavelength Region, Appl. Opt., 12, 555–563, https://doi.org/10.1364/AO.12.000555, 1973.

Haywood, J.M., Osborne, S.R., Francis, P.N., Keil, A., Formenti, P., Andreae, M.O., Kaye, P.H.: The mean physical and optical properties of regional haze dominated by biomass burning aerosol measured from the C-130 aircraft during SAFARI 2000, J. Geophys. Res. Atmos., 108, 1–9, https://doi.org/10.1029/2002JD002226, 2003.

Haywood, J. M., Pelon, J., Formenti, P., Bharmal, N., Brooks, M., Capes, G., Chazette, P., Chou, C., Christopher, S., Coe, H., Cuesta, J., Derimian, Y., Desboeufs, K., Greed, G., Harrison, M., Heese, B., Highwood, E. J., Johnson, B., Mallet, M., Marticorena, B., Marsham, J., Milton, S., Myhre, G., Osborne, S. R., Parker, D. J., Rajot, J. L., Schulz, M., Slingo, A., Tanre, D., Tulet, P.: Overview of the Dust and Biomass-burning Experiment and African Monsoon Multidisciplinary Analysis Special Observing Period-0, J. Geophys. Res. Atmos., 113, https://doi.org/10.1029/2008jd010077, 2008.

Haywood, J.M. and Shine, K.P.: The effect of anthropogenic sulfate and soot aerosol on the clear sky planetary radiation budget, Geophys. Res. Lett., 22, 603–606, https://doi.org/10.1029/95GL00075, 1995.

Henze, D.K., Hakami, A., Seinfeld, J.H.: Development of the adjoint of GEOS-Chem, Atmos. Chem. Phys., 7, 2413–2433, https://doi.org/10.5194/acp-7-2413-2007, 2007.

Herman, M., Deuzé, J.L., Marchand, A., Roger, B., Lallart, P.: Aerosol remote sensing from POLDER/ADEOS over the ocean: Improved retrieval using a nonspherical particle model, J. Geophys. Res. D Atmos., 110, 1–11, https://doi.org/10.1029/2004JD004798, 2005.

Herrmann, L., Stahr, K., Jahn, R.: The importance of source region identification and their properties for soil-derived dust: The case of Harmattan dust sources for eastern West Africa, Contrib. to Atmos. Phys., 72, 141–150, 1999.

Hoffer, A., Gelencsér, A., Guyon, P., Kiss, G., Schmid, O., Frank, G.P., Artaxo, P., Andreae, M.O.: Optical properties of humic-like substances (HULIS) in biomass-burning aerosols, Atmos. Chem. Phys., 6, 3563–3570, https://doi.org/10.5194/acp-6-3563-2006, 2006.

Jacobson, M.Z.: Isolating nitrated and aromatic aerosols and nitrated aromatic gases as sources of ultraviolet light absorption, J. Geophys. Res. Atmos., 104, 3527–3542, https://doi.org/10.1029/1998JD100054, 1999.

Jickells, T.D., An, Z.S., Andersen, K.K., Baker, A.R., Bergametti, C., Brooks, N., Cao, J.J., Boyd, P.W., Duce, R.A., Hunter, K.A., Kawahata, H., Kubilay, N., LaRoche, J., Liss, P.S., Mahowald, N., Prospero, J.M., Ridgwell, A.J., Tegen, I., Torres, R.: Global iron

connections between desert dust, ocean biogeochemistry, and climate, Science, 308, 67–71, https://doi.org/10.1126/science.1105959, 2005.

Journet, E., Balkanski, Y., Harrison, S.P.: A new data set of soil mineralogy for dust-cycle modeling, Atmos. Chem. Phys., 14, 3801–3816, https://doi.org/10.5194/acp-14-3801-2014, 2014.

Kahn, R.A. and Gaitley, B.J.: An analysis of global aerosol type as retrieved by MISR, J. Geophys. Res. Atmos., 120, 4248–4281, https://doi.org/10.1002/2015JD023322, 2015.

Kanakidou, M., Seinfeld, J.H., Pandis, S.N., Barnes, I., Dentener, F.J., Facchini, M.C., Van Dingenen, R., Ervens, B., Nenes, A., Nielsen, C.J., Swietlicki, E., Putaud, J.P., Balkanski, Y., Fuzzi, S., Horth, J., Moortgat, G.K., Winterhalter, R., Myhre, C.E.L., Tsigaridis, K., Vignati, E., Stephanou, E.G., Wilson, J.: Organic aerosol and global climate modelling: a review, Atmos. Chem. Phys., 5, 1053–1123, https://doi.org/10.5194/acp-5-1053-2005, 2005.

Kerker, M., Scheiner, P., Cooke, D.D., Kratohvil, J.P.: Absorption index and color of colloidal hematite, J. Colloid Interface Sci., 71, 176–187, https://doi.org/10.1016/0021-9797(79)90231-5, 1979.

Kirchstetter, T.W., Novakov, T., Hobbs, P. V.: Evidence that the spectral dependence of light absorption by aerosols is affected by organic carbon, J. Geophys. Res. Atmos., 109. https://doi.org/10.1029/2004JD004999, 2004.

Koepke, P.: Effective reflectance of oceanic whitecaps, Appl. Opt., 23, 1816, https://doi.org/10.1364/AO.23.001816, 1984.

Koepke, P., Hess, M., Schult, I., Shettle, E.P.: Global Aerosol Data Set, Max-Planck-Institut fur Meteorologie, https://doi.org/ISSN: 0937-1060, 1997.

Koren, I., Kaufman, Y.J.: Direct wind measurements of Saharan dust events from Terra and Aqua satellites, Geophys. Res. Lett., 31, 1–4, https://doi.org/10.1029/2003GL019338, 2004.

Kou, L., Labrie, D., Chylek, P.: Refractive indices of water and ice in the 0.65 to 2.5 μm spectral range, Appl. Opt., 32, 3531, https://doi.org/10.1364/AO.32.003531, 1993.

Koven, C.D. and Fung, I.: Inferring dust composition from wavelength-dependent absorption in Aerosol Robotic Network (AERONET) data, J. Geophys. Res. Atmos., 111, https://doi.org/10.1029/2005JD006678, 2006.

Krueger, B.J., Grassian, V.H., Cowin, J.P., Laskin, A.: Heterogeneous chemistry of individual mineral dust particles from different dust source regions: The importance of particle mineralogy, Atmos. Environ., 38, 6253–6261, https://doi.org/10.1016/j.atmosenv.2004.07.010, 2004.

Lafon, S., Rajot, J. L., Alfaro, S. C., Gaudichet, A.: Quantification of iron oxides in desert aerosol, Atmos. Environ., 38, 1211-1218, 2004.

Lafon, S., Sokolik, I.N., Rajot, J.L., Caquincau, S., Gaudichet, A.: Characterization of iron oxides in mineral dust aerosols: Implications for light absorption, J. Geophys. Res. Atmos., 111, 1–19, https://doi.org/10.1029/2005JD007016, 2006.

Laskin, A., Iedema, M. J., Ichkovich, A., Graber, E. R., Taraniuk, I., Rudich, Y.: Direct observation of completely processed calcium carbonate dust particles, Faraday Discuss., 130, 453-468, https://doi.org/10.1039/b417366j, 2005.

Lázaro, F.J., Gutiérrez, L., Barrón, V., Gelado, M.D.: The speciation of iron in desert dust collected in Gran Canaria (Canary Islands): Combined chemical, magnetic and optical analysis, Atmos. Environ., 42, 8987–8996, https://doi.org/10.1016/j.atmosenv.2008.09.035, 2008.

Lelieveld, J., Berresheim, H., Borrmann, S., Crutzen, P.J., Dentener, F.J., Fischer, H., Feichter, J., Flatau, P.J., Heland, J., Holzinger, R., Korrmann, R., Lawrence, M.G., Levin, Z., Markowicz, K.M., Mihalopoulos, N., Minikin, A., Ramanathan, V., De Reus, M., Roelofs, G.J., Scheeren, H.A., Sciare, J., Schlager, H., Schultz, M., Siegmund, P., Steil, B., Stephanou, E.G., Stier, P., Traub, M., Warneke, C., Williams, J., Ziereis, H.: Global air pollution crossroads over the Mediterranean, Science, 298, 794–799, https://doi.org/10.1126/science.1075457, 2002.

Léon, J.F. and Legrand, M.: Mineral dust sources in the surroundings of the North Indian

Ocean, Geophys. Res. Lett., 30, https://doi.org/10.1029/2002GL016690, 2003.

Lesins, G., Chylek, P., Lohmann, U.: A study of internal and external mixing scenarios and its effect on aerosol optical properties and direct radiative forcing, J. Geophys. Res. Atmos., 107, https://doi.org/10.1029/2001JD000973, 2002.

Levin, Z.: On the interactions of mineral dust, sea-salt particles, and clouds: A measurement and modeling study from the Mediterranean Israeli Dust Experiment campaign, J. Geophys. Res., 110, D20202, https://doi.org/10.1029/2005JD005810, 2005.

Levin, Z., Ganor, E., Gladstein, V.: The effects of desert particles coated with sulfate on rain formation in the Eastern Mediterranean, J. Appl. Meteorol., 35, 1511–1523, 1996.

Li, J., Pósfai, M., Hobbs, P. V., Buseck, P.R.: Individual aerosol particles from biomass burning in southern Africa: 2, Compositions and aging of inorganic particles, J. Geophys. Res. Atmos., 108, https://doi.org/10.1029/2002JD002310, 2003.

Li, X. and Strahler, A.H.: Geometric-Optical Bidirectional Reflectance Modeling of the Discrete Crown Vegetation Canopy: Effect of Crown Shape and Mutual Shadowing, IEEE Trans. Geosci. Remote Sens., 30, 276–292, https://doi.org/10.1109/36.134078, 1992.

Li, Z., Gu, X., Wang, L., Li, D., Xie, Y., Li, K., Dubovik, O., Schuster, G., Goloub, P., Zhang, Y., Li, L., Ma, Y., Xu, H.: Aerosol physical and chemical properties retrieved from ground-based remote sensing measurements during heavy haze days in Beijing winter, Atmos. Chem. Phys., 13, 10171–10183, https://doi.org/10.5194/acp-13-10171-2013, 2013.

Li, Z., Hou, W., Hong, J., Zheng, F., Luo, D., Wang, J., Gu, X., Qiao, Y.: Directional Polarimetric Camera (DPC): Monitoring aerosol spectral optical properties over land from satellite observation, J. Quant. Spectrosc. Radiat. Transf., 218, 21–37, https://doi.org/10.1016/j.jqsrt.2018.07.003, 2018.

Li, Z., Li, L., Zhang, F., Li, D., Xie, Y., Xu, H. : Comparison of aerosol properties over Beijing and Kanpur: Optical, physical properties and aerosol component composition retrieved from 12 years ground-based Sun-sky radiometer remote sensing data, J. Geophys. Res. Atmos., 120, 1520–1535, https://doi.org/10.1002/2014JD022593, 2015.

Liousse, C., Penner, J.E., Chuang, C., Walton, J.J., Eddleman, H., Cachier, H.: A global three-dimensional model study of carbonaceous aerosols, J. Geophys. Res., 101, 19411–19432, https://doi.org/10.1029/95JD03426, 1996.

Liu, H., Pinker, R.T., Holben, B.N.: A global view of aerosols from merged transport models, satellite, and ground observations, J. Geophys. Res. Atmos., 110, 1–16, https://doi.org/10.1029/2004JD004695, 2005.

Longtin, D.R., Shettle, E.P., Hummel, J.R., Pryce, J.D.: A Wind Dependent Desert Aerosol Dust Model: Radiative Properties, Scientific Report No.6, 1988.

Lopatin, A., Dubovik, O., Chaikovsky, A., Goloub, P., Lapyonok, T., Tanré, D., Litvinov, P.: Enhancement of aerosol characterization using synergy of lidar and Sun- photometer coincident observations : the GARRLiC algorithm, Atmos. Meas. Tech., 6, 2065–2088, https://doi.org/10.5194/amt-6-2065-2013, 2013.

Maenhaut, W., Salma, I., Cafmeyer, J., Annegarn, H.J., Andreae, M.O.: Regional atmospheric aerosol composition and sources in the eastern Transvaal, South Africa, and impact of biomass burning, J. Geophys. Res., 101, 23631, https://doi.org/10.1029/95JD02930, 1996.

Mahowald, N.M., Baker, A.R., Bergametti, G., Brooks, N., Duce, R.A., Jickells, T.D., Kubilay, N., Prospero, J.M., Tegen, I.: Atmospheric global dust cycle and iron inputs to the ocean. Global Biogeochem, Cycles, 19, https://doi.org/10.1029/2004GB002402, 2005.

Maignan, F., Bréon, F.M., Fédèle, E., Bouvier, M.: Polarized reflectances of natural surfaces: Spaceborne measurements and analytical modeling, Remote Sens. Environ., 113, 2642–2650, https://doi.org/10.1016/j.rse.2009.07.022, 2009.

Martonchik, J., Diner, D., Kahn, R., Verstraete, M., Pinty, B., Gordon, H., Ackerman, T.: Techniques for the retrieval of aerosol properties over land and ocean using multiangle data, IEEE Transactions on Geoscience and Remote Sensing, 36, 1212-1227, 1998.

Middleton, N.J.: A geography of dust storms in South–West Asia, J. Climatol., 6, 183–196, https://doi.org/10.1002/joc.3370060207, 1986a.

Middleton, N.J.: Dust storms in the Middle East, J. Arid Environ., 10, 83–96, https://doi.org/10.1016/S0140-1963(18)31249-7, 1986b.

Miri, A., Ahmadi, H., Ghanbari, A., Moghaddamnia, A.: Dust Storms Impacts on Air Pollution and Public Health under Hot and Dry Climate, Int. J. Energy Environ., 2, 101–105, 2007.

Miyazaki, Y., Kondo, Y., Takegawa, N., Komazaki, Y., Fukuda, M., Kawamura, K., Mochida, M., Okuzawa, K., Weber, R.J.: Time-resolved measurements of water-soluble organic carbon in Tokyo, J. Geophys. Res. Atmos., 111, 1–12, https://doi.org/10.1029/2006JD007125, 2006.

Orr, C., Hurd, F.K., Corbett, W.J.: Aerosol size and relative humidity, J. Colloid Sci., 13, 472–482, https://doi.org/10.1016/0095-8522(58)90055-2, 1958.

Ota, Y., Higurashi, A., Nakajima, T., Yokota, T.: Matrix formulations of radiative transfer including the polarization effect in a coupled atmosphere-ocean system, J. Quant. Spectrosc. Radiat. Transf., 111, 878–894, https://doi.org/10.1016/j.jqsrt.2009.11.021, 2010.

Palmer, K.F. and Williams, D.: Optical properties of water in the near infrared, J. Opt. Soc. Am., 64, 1107, https://doi.org/10.1364/JOSA.64.001107, 1974.

Popp, T., De Leeuw, G., Bingen, C., Brühl, C., Capelle, V., Chedin, A., Clarisse, L., Dubovik, O., Grainger, R., Griesfeller, J., Heckel, A., Kinne, S., Klüser, L., Kosmale, M., Kolmonen, P., Lelli, L., Litvinov, P., Mei, L., North, P., Pinnock, S., Povey, A., Robert, C., Schulz, M., Sogacheva, L., Stebel, K., Zweers, D.S., Thomas, G., Tilstra, L.G., Vandenbussche, S., Veefkind, P., Vountas, M., Xue, Y.: Development, production and evaluation of aerosol climate data records from European satellite observations (Aerosol_cci), Remote Sens., 8, https://doi.org/10.3390/rs8050421, 2016.

Pósfai, M., Simonics, R., Li, J., Hobbs, P. V., Buseck, P.R.: Individual aerosol particles from biomass burning in southern Africa1: Compositions and size distributions of carbonaceous particles, J. Geophys. Res. Atmos., 108, https://doi.org/10.1029/2002JD002291, 2003.

Prospero, J.M., Ginoux, P., Torres, O., Nicholson, S.E., Gill, T.E.: Environmental characterization of global sources of atmospheric soil dust identified with the Nimbus 7 Total Ozone Mapping Spectrometer (TOMS) absorbing aerosol product, Rev. Geophys., 40, 1–31, https://doi.org/10.1029/2000RG000095, 2002.

Rashki, A., Rautenbach, C.J. d. W., Eriksson, P.G., Kaskaoutis, D.G., Gupta, P.: Temporal changes of particulate concentration in the ambient air over the city of Zahedan, Iran, Air Qual. Atmos. Heal., 6, 123–135, https://doi.org/10.1007/s11869-011-0152-5, 2013.

Reid, J.S., Hobbs, P. V., Ferek, R.J., Blake, D.R., Martins, J.V., Dunlap, M.R., Liousse, C.: Physical, chemical, and optical properties of regional hazes dominated by smoke in Brazil, J. Geophys. Res. Atmos., 103, 32059–32080, https://doi.org/10.1029/98JD00458, 1998.

Remer, L., Kaufman, Y., Tanré, D., Mattoo, S., Chu, D., Martins, J., Li, R., Ichoku, C., Levy, R., Kleidman, R., Eck, T., Vermote, E., and Holben, B.: The MODIS aerosol algorithm, products and validation, Journal of the Atmospheric Sciences, 62, 947-973, 2005.

Román, R., Benavent-oltra, J.A., Casquero-vera, J.A., Lopatin, A., Cazorla, A., Lyamani, H., Denjean, C., Fuertes, D., Perez-Ramirez, D., Torres, B., Toledano, C., Dubovik, O., Cachorro, V.E., de Frutos, A.M., Olmo, F.J., Alados-Arboledas, L.: Retrieval of aerosol profiles combining sunphotometer and ceilometer measurements in GRASP code, Atmos. Res., 204, 161–177, https://doi.org/10.1016/j.atmosres.2018.01.021, 2018.

Román, R., Torres, B., Fuertes, D., Cachorro, V.E., Dubovik, O., Toledano, C., Cazorla, A., Barreto, A., Frutos, A. De, Alados-arboledas, L.: Remote sensing of lunar aureole with a sky camera : Adding information in the nocturnal retrieval of aerosol properties with GRASP code, Remote Sens. Environ., 196, 238–252, https://doi.org/10.1016/j.rse.2017.05.013, 2017.

Roujean, J.-L., Leroy, M., Deschamps, P.-Y. : A bidirectional reflectance model of the

Earth's surface for the correction of remote sensing data, J. Geophys. Res., 97, 20455, https://doi.org/10.1029/92JD01411, 1992.

Russell, P., Kacenelenbogen, M., Livingston, J., Hasekamp, O., Burton, S., Schuster, G., Johnson, M., Knobelspiesse, K., Redemann, J., Ramachandran, S., and Holben, B.: A multiparameter aerosol classification method and its application to retrievals from spaceborne polarimetry, J. Geophys. Res., 119, https://doi.org/10.1002/2013JD021411, 2014.

Schkolnik, G., Chand, D., Hoffer, A., Andreae, M.O., Erlick, C., Swietlicki, E., Rudich, Y.: Constraining the density and complex refractive index of elemental and organic carbon in biomass burning aerosol using optical and chemical measurements, Atmos. Environ., 41, 1107–1118, https://doi.org/10.1016/j.atmosenv.2006.09.035, 2007.

Schnaiter, M., Gimmler, M., Llamas, I., Linke, C., Jäger, C., Mutschke, H.: Strong spectral dependence of light absorption by organic carbon particles formed by propane combustion, Atmos. Chem. Phys., 6, 2981–2990, https://doi.org/10.5194/acp-6-2981-2006, 2006.

Schuster, G.L., Dubovik, O., Arola, A.: Remote sensing of soot carbon – Part 1: Distinguishing different absorbing aerosol species, Atmos. Chem. Phys., 16, 1565–1585, https://doi.org/10.5194/acp-16-1565-2016, 2016a.

Schuster, G.L., Dubovik, O., Arola, A., Eck, T.F., Holben, B.N.: Remote sensing of soot carbon – Part 2: Understanding the absorption Ångström exponent, Atmos. Chem. Phys., 16, 1587–1602, https://doi.org/10.5194/acp-16-1587-2016, 2016b.

Schuster, G.L., Dubovik, O., Holben, B.N., Clothiaux, E.E.: Inferring black carbon content and specific absorption from Aerosol Robotic Network (AERONET) aerosol retrievals, J. Geophys. Res., 110, D10S17, https://doi.org/10.1029/2004JD004548, 2005.

Schuster, G.L., Lin, B., Dubovik, O.: Remote sensing of aerosol water uptake, Geophys. Res. Lett., 36, https://doi.org/10.1029/2008GL036576, 2009.

Shi, Z., Krom, M.D., Jickells, T.D., Bonneville, S., Carslaw, K.S., Mihalopoulos, N., Baker, A.R., Benning, L.G.: Impacts on iron solubility in the mineral dust by processes in the source region and the atmosphere: A review, Aeolian Res., 5, 21–42, https://doi.org/10.1016/j.aeolia.2012.03.001, 2012.

Sokolik, I.N. and Toon, O.B.: Incorporation of mineralogical composition into models of the radiative properties of mineral aerosol from UV to IR wavelengths, J. Geophys. Res. Atmos., 104, 9423–9444, https://doi.org/10.1029/1998JD200048, 1999.

Stone, E., Schauer, J., Quraishi, T.A., Mahmood, A. : Chemical characterization and source apportionment of fine and coarse particulate matter in Lahore, Pakistan, Atmos. Environ., 44, 1062–1070, https://doi.org/10.1016/j.atmosenv.2009.12.015, 2010.

Streets, D.G., Gupta, S., Waldhoff, S.T., Wang, M.Q., Bond, T.C., Yiyun, B.: Black carbon emissions in China, Atmos. Environ., 35, 4281–4296, https://doi.org/10.1016/S1352-2310(01)00179-0, 2001.

Sun, H., Biedermann, L., Bond, T.C.: Color of brown carbon: A model for ultraviolet and visible light absorption by organic carbon aerosol, Geophys. Res. Lett., 34, https://doi.org/10.1029/2007GL029797, 2007.

Swap, R., Garstang, M., Macko, S.A., Tyson, P.D., Maenhaut, W., Artaxo, P., Kållberg, P., Talbot, R.: The long-range transport of southern African aerosols to the tropical South Atlantic, J. Geophys. Res. Atmos., 101, 23777–23791, https://doi.org/10.1029/95JD01049, 1996.

Tang, I.N.: Chemical and size effects of hygroscopic aerosols on light scattering coefficients, J. Geophys. Res. Atmos., 101, 19245–19250, https://doi.org/10.1029/96JD03003, 1996.

Tang, I.N.: Phase transformation and growth of aerosol particles composed of mixed salts, J. Aerosol Sci., 7361–7371, https://doi.org/10.1016/0021-8502(76)90022-7, 1976.

Tang, I.N. and Munkelwitz, H.R.: Water activities, densities, and refractive indices of aqueous sulfates and sodium nitrate droplets of atmospheric importance 99, 18801–18808, 1994.

Tang, I.N. and Munkelwitz, H.R.: Composition and temperature dependence of the deliquescence properties of hygroscopic aerosols, Atmos. Environ., 27, 467–473,

https://doi.org/10.1016/0960-1686(93)90204-C, 1993.

Tang, I.N. and Munkelwitz, H.R.: Simultaneous determination of refractive index and density of an evaporating aqueous solution droplet, Aerosol Sci. Technol., 15, 201–207, https://doi.org/10.1080/02786829108959527, 1991.

Tang, I. N., Wong, W.T., Munkelwitz, H.R.: The relative importance of atmospheric sulfates and nitrates in visibility reduction, Atmos. Environ., 15, 2463–2471, 1981.

Tanré, D., Bräon, F.M., Deuzä, J.L., Dubovik, O., Ducos, F., Franäois, P., Goloub, P., Herman, M., Lifermann, A., Waquet, F.: Remote sensing of aerosols by using polarized, directional and spectral measurements within the A-Train: The PARASOL mission, Atmos. Meas. Tech., 4, 1383–1395, https://doi.org/10.5194/amt-4-1383-2011, 2011.

Todd, M.C., Washington, R., Martins, J.V., Dubovik, O., Lizcano, G., M'Bainayel, S., Engelstaedter, S.: Mineral dust emission from the Bodélé Depression nothern Chad, during BoDEx 2005, J. Geophys. Res. Atmos., 112, 1–12, https://doi.org/10.1029/2006JD007170, 2007.

Toon, O.B., Pollack, J.B., Khare, B.N.: The optical constants of several atmospheric aerosol species: atmmonium sulfate, aluminum oxide, and sodium chloride, J. Geophys. Res., 81, 5733–5748, 1976.

Triaud, A.H.M.J.: Earth observation data group: aerosol refractive index archive. http://eodg.atm.ox.ac.uk/ARIA/data?Minerals/Hematite/(Triaud_2005)/hematite_Triaud _2005.ri, 2005.

Tsekeri, A., Lopatin, A., Amiridis, V., Marinou, E., Igloffstein, J., Siomos, N., Solomos, S., Kokkalis, P., Engelmann, R., Baars, H., Gratsea, M., Raptis, P.I.: GARRLiC and LIRIC : strengths and limitations for the characterization of dust and marine particles along with their mixtures, Atmos. Meas. Tech., 10, 4995–5016, https://doi.org/10.5194/amt-10-4995-2017, 2017.

Usher, C. R., Michel, A. E., Grassian, V. H.: Reactions on mineral dust, Chem. Rev., 103, 4883-4939, https://doi.org/10.1021/cr020657y, 2003.

Voss, K.J., Morel, A., Antoine, D.: Detailed validation of the bidirectional effect in various Case 1 waters for application to ocean color imagery, Biogeosciences, 4, 781–789, https://doi.org/10.5194/bg-4-781-2007, 2007

Wagner, R., Ajtai, T., Kandler, K., Lieke, K., Linke, C., Müller, T., Schnaiter, M., and Vragel, M.: Complex refractive indices of Saharan dust samples at visible and near UV wavelengths: a laboratory study, Atmos. Chem. Phys., 12, 2491–2512, doi:10.5194/acp-12-2491-2012, 2012.

Wang, L., Li, Z., Tian, Q., Ma, Y., Zhang, F., Zhang, Y., Li, D., Li, K., Li, L. : Estimate of aerosol absorbing components of black carbon, brown carbon, and dust from ground-based remote sensing data of sun-sky radiometers, J. Geophys. Res. Atmos., 118, 6534–6543, https://doi.org/10.1002/jgrd.50356, 2013.

Wanner, W., Li, X., Strahler, A. : On the derivation of kernels for kernel-driven models of bidirectional reflectance, J. Geophys. Res., 100, 21077–21089, 1995.

Waquet, F., Cornet, C., Deuzé, J.L., Dubovik, O., Ducos, F., Goloub, P., Herman, M., Lapyonok, T., Labonnote, L.C., Riedi, J., Tanré, D., Thieuleux, F., Vanbauce, C.: Retrieval of aerosol microphysical and optical properties above liquid clouds from POLDER/PARASOL polarization measurements, Atmos. Meas. Tech., 6, 991–1016, https://doi.org/10.5194/amt-6-991-2013, 2013.

Washington, R., Todd, M., Middleton, N.J., Goudie, A.S.: Dust-storm source areas determined by the total ozone monitoring spectrometer and surface observations, Ann. Assoc. Am. Geogr., 93, 297–313, https://doi.org/10.1111/1467-8306.9302003, 2003.

Washington, R. and Todd, M.C.: Atmospheric controls on mineral dust emission from the Bodélé Depression, Chad: The role of the low level jet, Geophys. Res. Lett., 32, 1–5. https://doi.org/10.1029/2005GL023597, 2005.

Washington, R., Todd, M.C., Engelstaedter, S., Mbainayel, S., Mitchell, F.: Dust and the low-level circulation over the Bodélé Depression, Chad: Observations from BoDEx 2005, J. Geophys. Res. Atmos., 111, 1–15, https://doi.org/10.1029/2005JD006502, 2006.

Weber, R.J., Sullivan, A.P., Peltier, R.E., Russell, A., Yan, B., Zheng, M., de Grouw, J., Warneke, C., Brock, C., Holloway, J.S., Atlas, E.L., Edgerton, E.: A study of secondary organic aerosol formation in the anthropogenic-influenced southeastern United States, J. Geophys. Res. Atmos., 112, 1–13, https://doi.org/10.1029/2007JD008408, 2007.

Xie Y., Li Z., Li L. et al.: Study on influence of different mixing rules on the aerosol components retrieval from ground-based remote sensing measurements. Atmospheric Research, 145: 267-278, 2014.

Yu, H., Dickinson, R.E., Chin, M., Kaufman, Y.J., Holben, B.N., Geogdzhayev, I. V., Mishchenko, M.I.: Annual cycle of global distributions of aerosol optical depth from integration of MODIS retrievals and GOCART model simulations, J. Geophys. Res. Atmos., 108, 1–14, https://doi.org/10.1029/2002JD002717, 2003

Yu, H., Dickinson, R.E., Chin, M., Kaufman, Y.J., Zhou, M., Zhou, L., Tian, Y., Dubovik, O., Holben, B.N.: Direct radiative effect of aerosols as determined from a combination of MODIS retrievals and GOCART simulations, J. Geophys. Res. Atmos., 109, 1–13, https://doi.org/10.1029/2003JD003914, 2004.

Yu, H., Kaufman, Y.J., Chin, M., Feingold, G., Remer, L.A., Anderson, T.L., Balkanski, Y., Bellouin, N., Boucher, O., Christopher, S., DeCola, P., Kahn, R., Koch, D., Loeb, N., Reddy, M.S., Schulz, M., Takemura, T., Zhou, M.: A review of measurement-based assessments of the aerosol direct radiative effect and forcing, Atmos. Chem. Phys., 6, 613–666, https://doi.org/10.5194/acp-6-613-2006, 2006.

Zhang, X. Y., Gong, S. L., Shen, Z. X., Mei, F. M., Xi, X. X., Liu, L. C., Zhou, Z. J., Wang, D., Wang, Y. Q., Cheng, Y.: Characterization of soil dust aerosol in China and its transport and distribution during 2001 ACE-Asia: 1. Network observations, J. Geophys. Res., 108 (D9), 4261, https://doi.org/4210.1029/2002JD002632, 2003.

Zhang, J., Reid, J.S., Westphal, D.L., Baker, N.L., Hyer, E.J.: A system for operational aerosol optical depth data assimilation over global oceans, J. Geophys. Res. Atmos., 113, 1–13, https://doi.org/10.1029/2007JD009065, 2008a.

Zhang, X.Y., Wang, Y.Q., Niu, T., Zhang, X.C., Gong, S.L., Zhang, Y.M., Sun, J.Y.: Atmospheric aerosol compositions in China: Spatial/temporal variability, chemical signature, regional haze distribution and comparisons with global aerosols, Atmos. Chem. Phys., 12, 779–799, https://doi.org/10.5194/acp-12-779-2012, 2012.

Zhang, X.Y., Wang, Y.Q., Wang, D., Gong, S.L., Arimoto, R., Mao, L.J., Li, J.: Characterization and sources of regional-scale transported carbonaceous and dust aerosols from different pathways in coastal and sandy land areas of China, J. Geophys. Res. Atmos., 110, 1–13, https://doi.org/10.1029/2004JD005457, 2005.

Zhang, X.Y., Wang, Y.Q., Zhang, X.C., Guo, W., Gong, S.L.: Carbonaceous aerosol composition over various regions of China during 2006, J. Geophys. Res. Atmos., 113, 1–10, https://doi.org/10.1029/2007JD009525, 2008b.

1843 **Tables**
1844
1845 **Table 1**. List of measured and retrieved characteristic considered in POLDER/GRASP with
1846 aerosol component ~~composition~~ mixing model. $\mu_0 = cos(\vartheta_0)$ depends on the solar zenith
1847 angle ϑ_0, $\mu_1 = cos(\vartheta_1)$ depends on the observation zenith angle ϑ_1. φ_0 and φ_1 represent the
1848 solar and observation azimuth angles.
1849

POLDER/PARASOL measurements	
Measurements type:	
$I(\mu_0; \mu_1; \varphi_0; \varphi_1; \lambda_i) = I(\Theta_j; \lambda_i)$	– I reflected total radiances
$Q(\mu_0; \mu_1; \varphi_0; \varphi_1; \lambda_i) = Q(\Theta_j; \lambda_i)$	– Q component of the Stokes vector
$U(\mu_0; \mu_1; \varphi_0; \varphi_1; \lambda_i) = U(\Theta_j; \lambda_i)$	– U component of the Stokes vector
Observation specifications:	
Angular:	
$I(\Theta_j; \lambda_i)$, $Q(\Theta_j; \lambda_i)$ and $U(\Theta_j; \lambda_i)$ measured in up to 16 viewing directions, that may cover the range of scattering angle Θ from $\sim 80°$ to $180°$	
Spectral:	
$I(\Theta_j; \lambda_i)$ measured in 6 window channels λ_i = 0.440, 0.490, 0.565, 0.670, 0.865 and 1.02 μm	
$Q(\Theta_j; \lambda_i)$ and $U(\Theta_j; \lambda_i)$ measured in 3 window channels λ_i = 0.490, 0.670, and 0.865 μm	
Retrieved characteristic	
Aerosol parameters:	
C_v	– total volume concentration of aerosol ($\mu m^3/\mu m^2$)
$dV(r_i)/dlnr$	– ($i = 1, ..., N_r$) values of volume size distribution in N_i size bins r_i normalized by C_v
C_{sph}	– fraction of spherical particles
h_0	– mean height of aerosol layer
$Frac(F_i)$	– ($i = 1, ..., N_f$) the fraction of component ~~composition~~ in fine mode
$Frac(C_i)$	– ($i = 1, ..., N_c$) the fraction of component ~~composition~~ in coarse mode
Surface reflection parameters:	
Ross-Li model parameters:	
$k_{iso}(\lambda_i)$	– ($i = 1, ..., N_\lambda = 6$) first Ross-Li model parameter (isotropic parameter characterizing isotropic surface reflectance)
$k_{vol}(\lambda_i)$	– ($i = 1, ..., N_\lambda = 6$) second Ross-Li model parameter (volumetric parameter characterizing anisotropy of reflectance)
$k_{geom}(\lambda_i)$	– ($i = 1, ..., N_\lambda = 6$) third Ross-Li model parameter (geometric parameter characterizing anisotropy of reflectance)
Maignan et al. (2009) model:	
$B(\lambda_i)$	– ($i = 1, ..., N_\lambda = 6$) free parameter

1850
1851
1852
1853

1854 **Table 2.** Description of aerosol components and complex refractive indices at 0.440

1855 μm and 0.865 μm employed in the GRASP components retrieval approach, as well as

1856 those used in the uncertainty tests.

Abb.	Component	Complex refractive index		Reference
		0.440 μm	0.865 μm	
BC	Black carbon representing wavelength-independent strong absorption	1.95+0.79i	1.95+0.79i	Bond & Bergstrom (2006)
		1.75+0.63i	1.75+0.63i	Bond & Bergstrom (2006)
BrC	Brown carbon representing wavelength-dependent absorption	1.54+0.07i	1.54+0.003i	Sun et al. (2007)
		1.54+0.06i	1.54+0.0005i	Kirchstetter et al. (2004)
FNAI	Fine mode non-absorbing insoluble representing fine non-absorbing dust and organic carbon	1.54+0.0005i	1.52+0.0005i	Ghosh (1999)
		1.53+0.005i	1.53+0.005i	"GKI"[1]
		1.52+0.0006i	1.50+0.0006i	Koepke et al. (1997)
FNAS	Fine mode non-absorbing soluble representing inorganic salts	$1.337+10^{-9}$i	$1.339+10^{-8}$i	Tang et al. (1981); Gosse et al. (1997) for "AN"[2]
		$1.537+10^{-7}$i	$1.517+10^{-7}$i	Toon et al. (1976) for "AS"[3]
FAWC	Fine mode aerosol water content	$1.337+10^{-9}$i	$1.329+10^{-6.5}$i	Hale & Querry (1973)
CAI	Coarse mode absorbing insoluble representing iron oxides	2.90+0.345i	2.75+0.003i	Longtin et al. (1988)
		2.88+0.987i	2.72+0.140i	Triaud (2005)
CNAI	Coarse mode non-absorbing insoluble represented by non-absorbing dust	1.54+0.0005i	1.52+0.0005i	Ghosh (1999)
		1.53+0.005i	1.53+0.005i	"GKI"[1]
CNAI	by Organic Carbon	1.52+0.0006i	1.50+0.0006i	Koepke et al. (1997)
CNAS	Coarse mode non-absorbing soluble represented by an inorganic salt - AN[2]	$1.337+10^{-9}$i	$1.339+10^{-8}$i	Tang et al. (1981); Gosse et al. (1997)
CNAS	by AS[3]	$1.537+10^{-7}$i	$1.517+10^{-7}$i	Toon et al. (1976)
CAWC	Coarse mode aerosol water content	$1.337+10^{-9}$i	$1.329+10^{-6.5}$i	Hale & Querry (1973)

1857 "GKI"[1] denotes dust composed of a mixture of quartz (Ghosh, 1999), kaolinite (Sokolik and

1858 Toon, 1999) and illite (Sokolik and Toon, 1999) with the proportions recalculated from

1859 Journet et al. (2014).

1860 "AN"[2] denotes ammonium nitrate, which can be used to create a host in aerosols.

1861 "AS"[3] denotes ammonium sulfate, which is an alternative species for the host estimation in

1862 aerosols.

1863
1864
1865
1866
1867
1868
1869
1870
1871
1872
1873
1874
1875
1876
1877
1878
1879
1880

1881

1882

1883 **Table 23**. List of statistics for parameters between assumed and retrieved in the sensitivity

1884 tests of GRASP component ~~composition~~ retrieval using Maxwell-Garnett mixing model. The

1885 values of slope (A), intercept (B), correlation coefficient (R), root-mean-square error

1886 (RMSE), mean absolute error (MEA), mean relative error (MRE) and standard error deviation

1887 (STD) are presented for aerosol components ~~compositions~~, aerosol optical thickness (AOT),

1888 Single-scattering albedo (SSA), real (n) and imaginary (k) parts of complex refractive index

1889 in fine mode (FM) and coarse mode (CM) at 675 nm.

1890

	A	B	R	RMSE	MAE	MRE	STD
BC	1.00	0.00	1.00	0.00	0.00	0.4%	0.00
BrC	1.00	0.00	1.00	0.00	0.00	2.7%	0.00
FNAI	1.02	-0.02	0.99	0.03	-0.01	-1.0%	0.03
FNAS	1.03	-0.03	1.00	0.01	-0.02	-6.0%	0.01
FAWC	0.99	0.00	1.00	0.02	0.00	-0.2%	0.02
RH	0.94	0.04	0.97	0.03	0.00	0.3%	0.03
CAI	1.00	0.00	1.00	0.00	0.00	-1.1%	0.00
CNAI	0.95	0.01	0.99	0.02	0.00	8.2%	0.02
CNAS	0.95	0.00	1.00	0.01	-0.02	-4.5%	0.01
CAWC	1.01	0.00	1.00	0.02	0.00	0.9%	0.02
AOT	1.00	0.00	1.00	0.00	0.00	0.0%	0.00
SSA	1.00	0.00	1.00	0.00	0.00	0.0%	0.00
FM(n)	0.98	0.03	1.00	0.00	0.00	0.1%	0.00
FM(k)	1.00	0.00	1.00	0.0003	0.0001	0.5%	0.00
CM(n)	1.00	0.00	1.00	0.00	0.00	0.0%	0.00
CM(k)	0.96	0.00	1.00	0.0000	0.0000	5.8%	0.00

1891
1892
1893
1894
1895
1896
1897
1898
1899
1900
1901
1902
1903
1904
1905
1906
1907
1908
1909
1910
1911
1912
1913

1914

1915 **Table 34.** The statistics of aerosol parameters in Fig. 10: number of measurements (N), slope
1916 (A), intercept (B), correlation coefficient (R), root-mean-square error (RMSE), mean absolute
1917 error (MAE), standard error deviation (STD). GRASP approach (GA): Maxwell-Garnett
1918 (MG) mixing model, volume-weighted (VW) mixing model; standard (ST)
1919 GRASP/PARASOL retrievals without aerosol component composition mixing model.
1920

	Banizoumbou AOT (675 nm)			Tamanrasset AOT (675 nm)			Mongu AOT (675 nm)		
N	78			76			118		
GA	MG	VW	ST	MG	VW	ST	MG	VW	ST
A	0.75	0.96	0.68	0.68	0.88	0.49	0.90	0.96	0.96
B	-0.02	-0.05	0.08	0.03	0.06	0.13	-0.01	0.00	0.00
R	0.97	0.96	0.91	0.89	0.88	0.51	0.96	0.95	0.94
RMSE	0.08	0.11	0.13	0.05	0.07	0.12	0.04	0.05	0.06
MAE	-0.15	-0.07	-0.08	-0.02	0.04	0.05	-0.04	-0.01	-0.01
STD	0.13	0.11	0.19	0.07	0.07	0.14	0.05	0.05	0.06

	Skukuza AOT (675 nm)			Solar village AOT (675 nm)			Agoufou AOT (675 nm)		
N	92			98			117		
GA	MG	VW	ST	MG	VW	ST	MG	VW	ST
A	0.83	0.96	0.89	0.75	0.83	0.67	0.83	0.98	0.72
B	-0.01	0.00	0.01	0.00	0.02	0.10	0.00	0.00	0.20
R	0.79	0.76	0.84	0.91	0.91	0.79	0.94	0.94	0.84
RMSE	0.05	0.06	0.04	0.09	0.10	0.13	0.14	0.16	0.21
MAE	-0.03	-0.01	-0.01	-0.11	-0.06	-0.05	-0.10	-0.01	0.04
STD	0.05	0.06	0.04	0.11	0.11	0.16	0.16	0.16	0.25

	All sites AOT (675 nm)			All sites AE (870/440)			All sites SSA (675 nm)		
N	579			429			101		
GA	MG	VW	ST	MG	VW	ST	MG	VW	ST
A	0.79	0.93	0.77	0.86	0.79	0.88	0.57	0.59	0.65
B	0.00	0.00	0.07	0.20	0.17	0.16	0.44	0.42	0.32
R	0.95	0.95	0.88	0.93	0.92	0.94	0.83	0.84	0.77
RMSE	0.09	0.11	0.15	0.24	0.24	0.24	0.02	0.02	0.03
MAE	-0.07	-0.02	-0.01	0.08	0.00	0.06	0.04	0.04	0.00
STD	0.11	0.11	0.17	0.26	0.29	0.25	0.03	0.03	0.04

1921
1922
1923
1924
1925
1926
1927
1928
1929

1930
1931
Figures

1933
1934
1935
1936
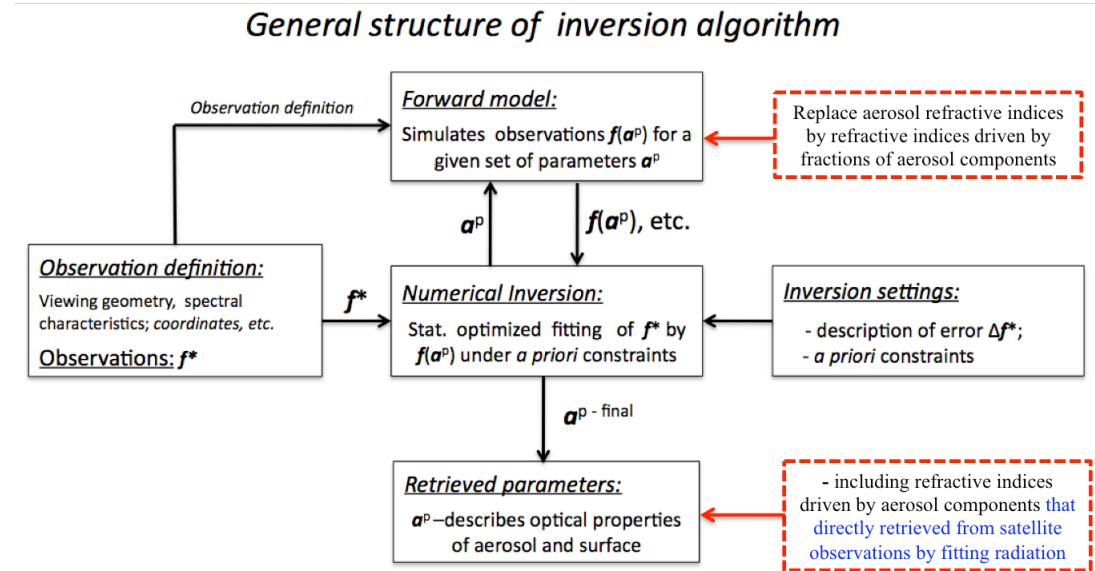
1937
Figure 1. The general structure of GRASP algorithm with aerosol component ~~composition~~ conversion model, courtesy of (Dubovik et al., 2011). The red dashed frames represent modifications for the component ~~composition~~ inversion approach. f^* represents vector of inverted measurements, a^P represents vector of unknowns at the p-th iteration, $f(a^P)$ represents vector of measurement fit at the p-th iteration.
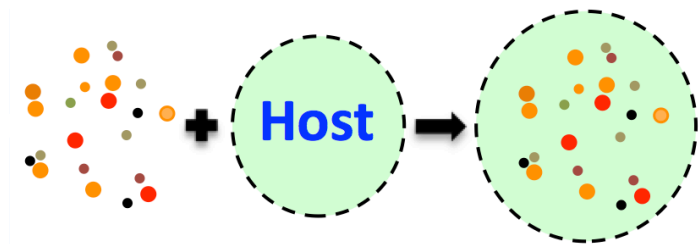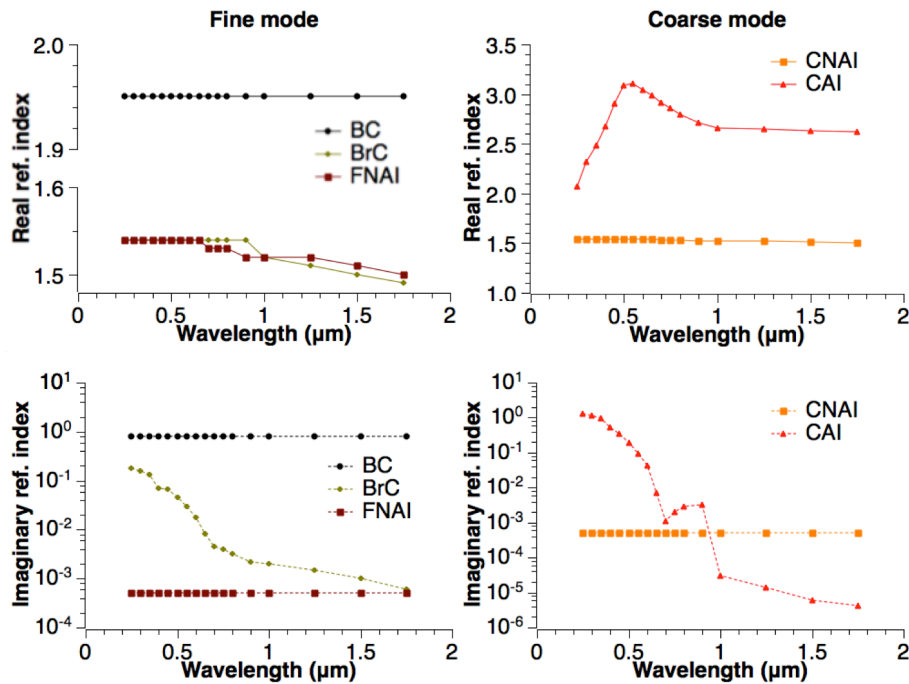
1943
1944
1945
1946
1947
1948

1949
1950 **Figure 2.** Illustrates a general logistics of an effective refractive index calculation using a
1951 conversion model that is based upon the Maxwell-Garnett effective medium approximation.
1952
1953

1954
1955

1956
1957 **Figure 3.** The refractive indices of assumed aerosol components ~~compositions~~ embedded in
1958 the host of the size-dependent Maxwell-Garnett conversion model. The parameters of BC
1959 refer to Bond and Bergstrom (2006). The parameters of BrC refer to Sun et al. (2007) and
1960 Schuster et al. (2016a). The parameters of fine non-absorbing insoluble (FNAI) and coarse
1961 non-absorbing insoluble (CNAI) refer to Ghosh (1999). FNAI represents dust and OC in fine
1962 mode particles, while CNAI represents dust in coarse mode particles. The parameters of
1963 coarse absorbing insoluble (CAI) refer to Longtin et al. (1988) representing hematite.

1964
1965
1966
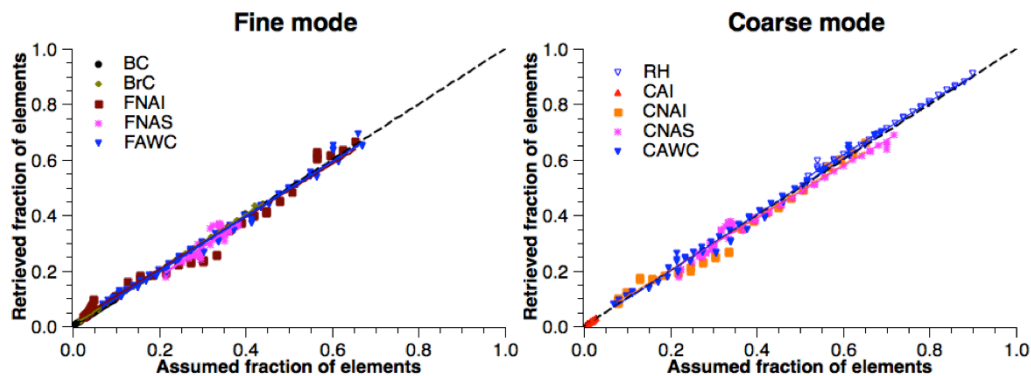
1967
1968 **Figure 4**. Assumed and retrieved fractions of aerosol ~~composition~~ species resulting from the
1969 sensitivity tests of GRASP/Component ~~Composition~~ retrieval using Maxwell-Garnett mixing
1970 model.

1971
1972
1973
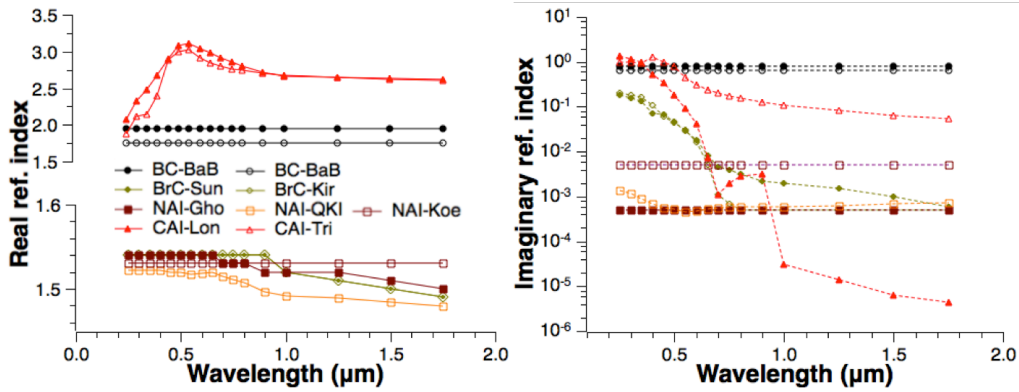
Figure 5. Complex refractive index of several aerosol species (BC, BrC, CAI, and NAI) in the host. The values with filled symbols are used in the presented size-dependent Maxwell-Garnett conversion model. The values with open symbols are used to replace the corresponding values to test the uncertainties in the aerosol component ~~composition~~ retrievals. "BaB" for Bond and Bergstrom (2006); "Sun" for Sun et al. (2007); "Kir" for Kirchstetter et al. (2004); "Gho" for Ghosh (1999); "QKI" for dust composed of a mixture of quartz (Ghosh, 1999), kaolinite (Sokolik and Toon, 1999) and illite (Sokolik and Toon, 1999) with the proportions of 48%, 26%, and 26%, respectively (Journet et al., 2014); "Koe" for Koepke et al. (1997); "Lon" for Longtin et al. (1988); and "Tri" for Triaud (2005).
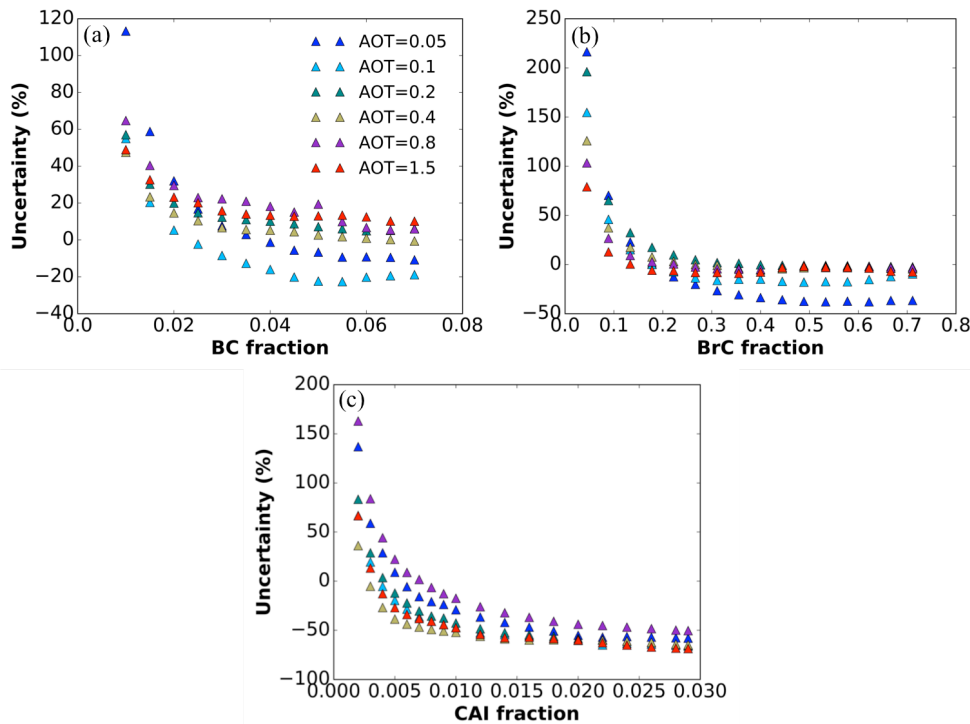
Figure 6. Uncertainty in absorbing species retrievals from POLDER/PARASOL attributed to the refractive index variability; uncertainties in (a) BC, (b) BrC, and (c) CAI fractions.
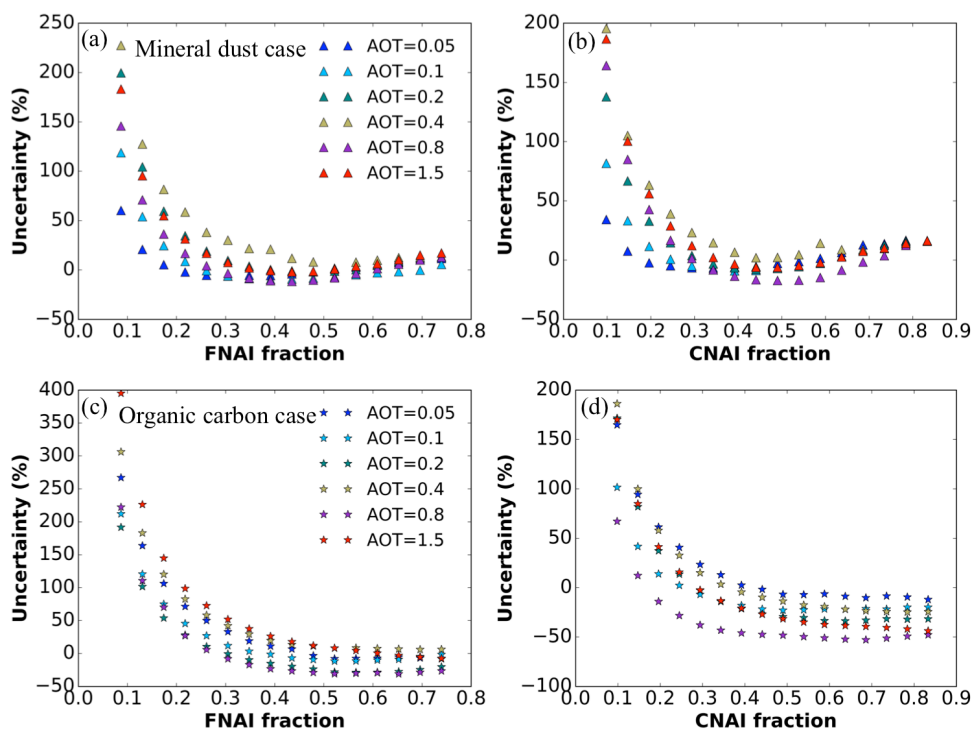
1994
1995
1996 **Figure 7.** Uncertainty in Non-Absorbing Insoluble particles fraction in Fine (FNAI) and
1997 Coarse (CNAI) modes attributed to the refractive index variability: (a), (b) for the case of
1998 mineral dust and (c), (d) for organic carbon.
1999
2000
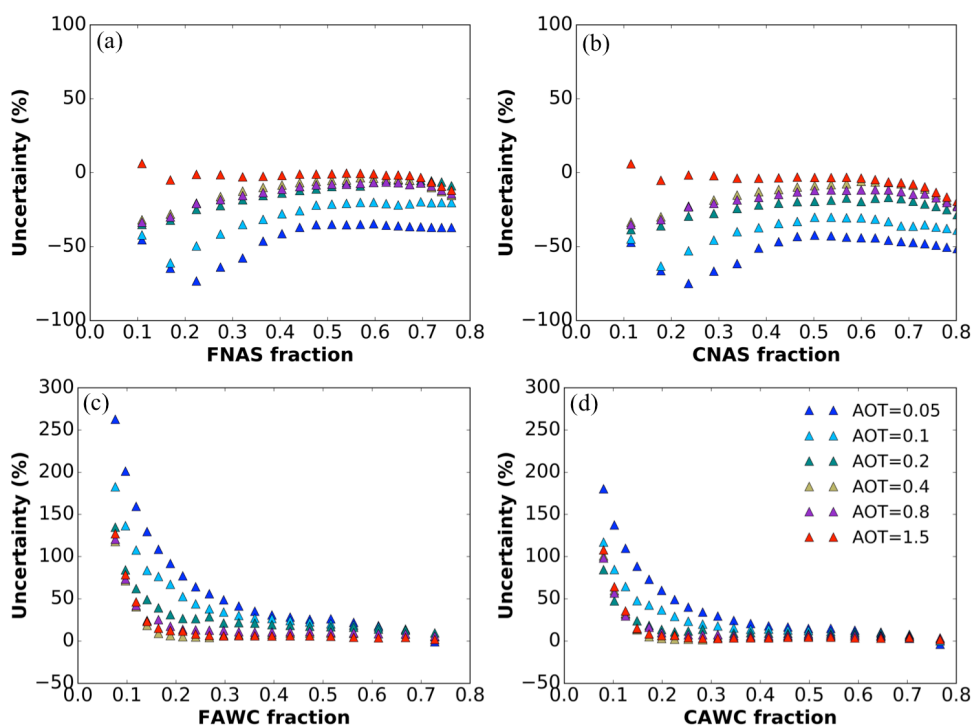
2001
2002 **Figure 8.** Uncertainty in Non-Absorbing Soluble particles and aerosol water content fraction
2003 in Fine (FNAS, FAWC) and Coarse (CNAS, CAWC) modes attributed to the refractive index
2004 and hygroscopic properties of ammonium nitrate and ammonium sulfate.

2005
2006
2007
2008

2009
2010
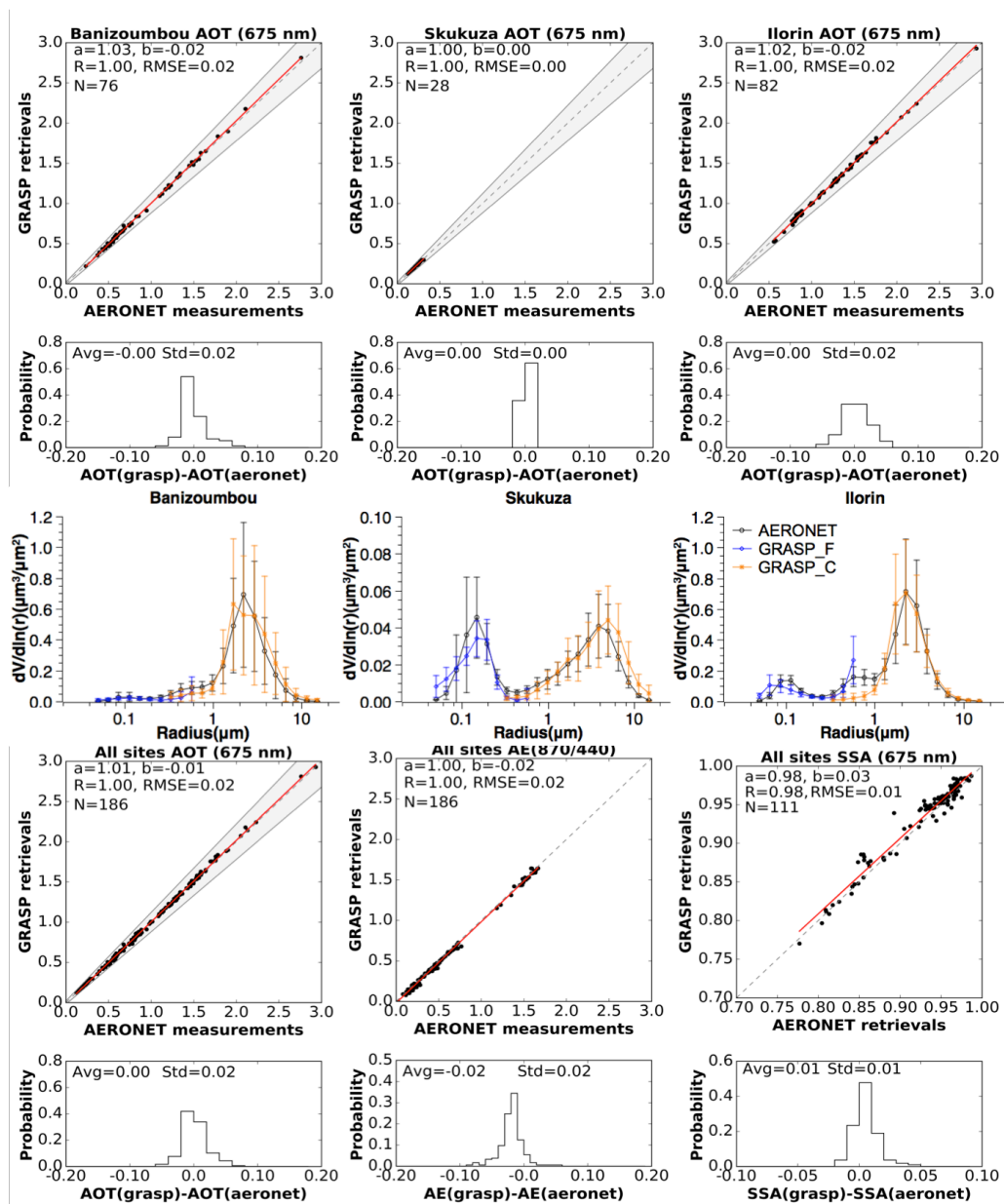
2011 **Figure 9.** The inter-comparison of aerosol optical properties derived from Sun/sky
2012 photometer measurements using the GRASP/Component Composition approach with the
2013 corresponding values of the AERONET operational product. The data presented for the
2014 Banizoumbou site in April 2007 represent mineral dust aerosol, for the Skukuza site in
2015 September 2007 represent the biomass burning aerosol, and for the Ilorin site in January 2007
2016 represent the mixture of dust and biomass burning.

2017
2018
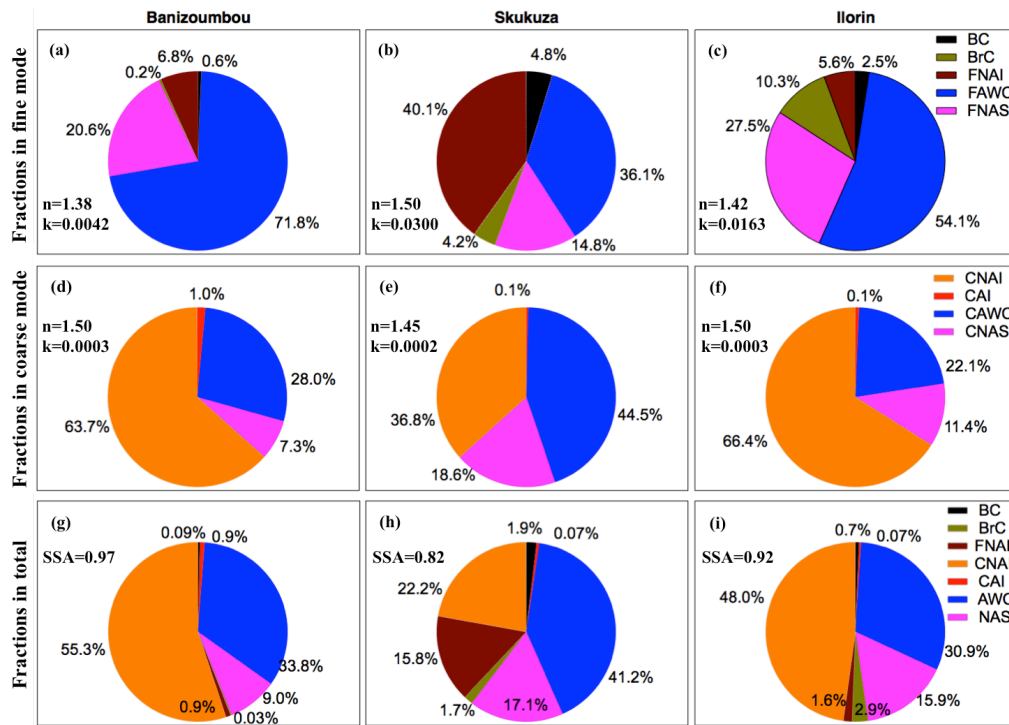
Figure 10. Examples of aerosol component ~~composition~~ retrievals derived from AERONET Sun/sky photometer measurements using the GRASP/Component ~~Composition~~ approach. Panels: (a, d, g) the mineral dust case at the Banizoumbou site (April 8th, 2007); (b, e, h) the biomass burning case at the Skukuza site (September 2nd, 2007); and (c, f, i) the mixture of dust and biomass burning at the Ilorin site (January 25th, 2007). In the panes are also indicated the values of complex refractive index (n, k) at 675 nm retrieved for the fine and coarse modes, and of SSA at 675 nm derived for ensemble of aerosol.
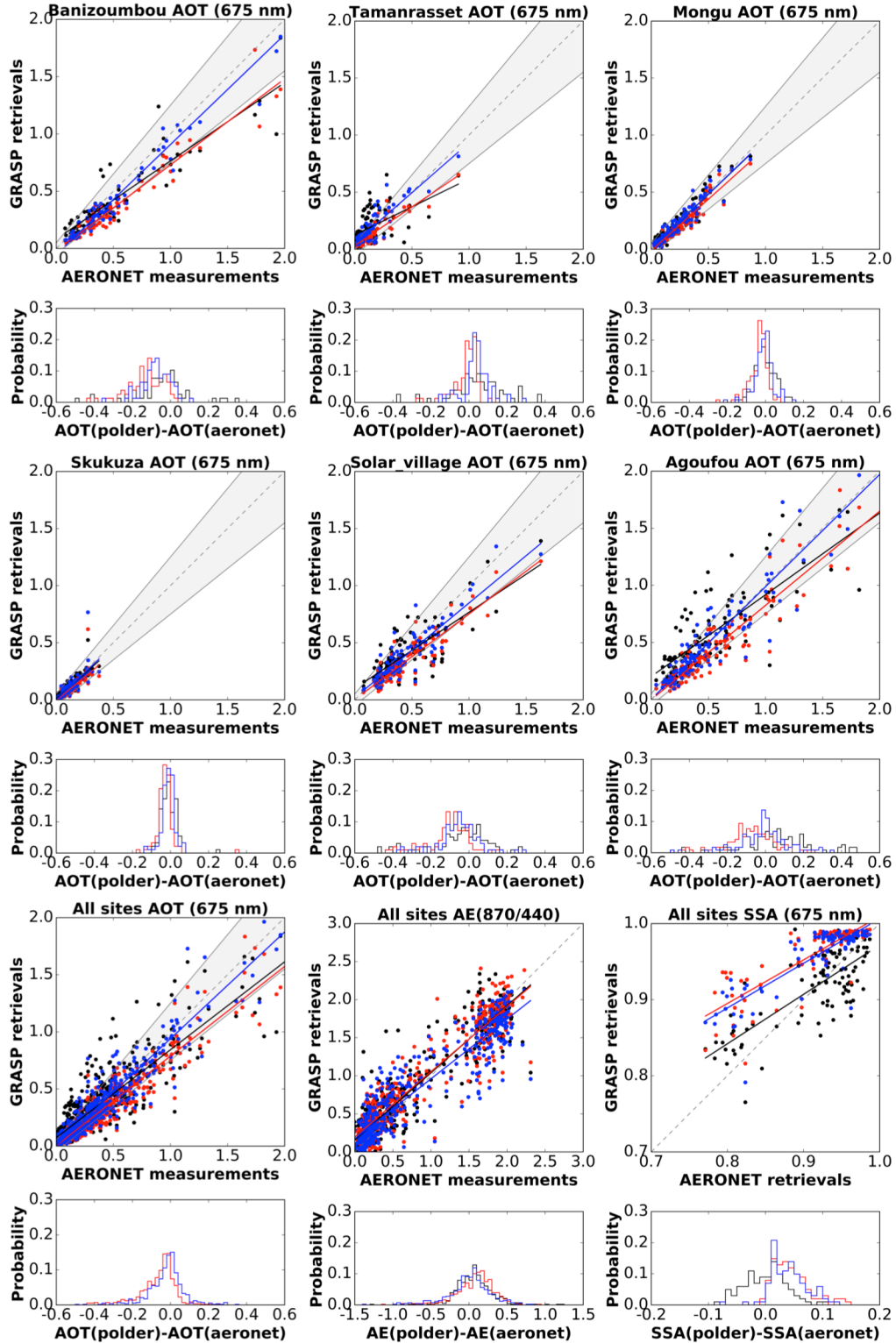
Figure 11. Inter-comparison of aerosol optical properties retrieved from POLDER/PARASOL and provided by AERONET operational product in six AERONET sites located in Africa and Middle East during the period 2006 to 2008. Red color represents the Maxwell-Garnett (MG) mixing model; blue color represents the volume-weighted (VW) mixing model; and black color represents the standard (ST) GRASP/PARASOL product that do not employ the aerosol component composition retrievals.

52

2037
2038
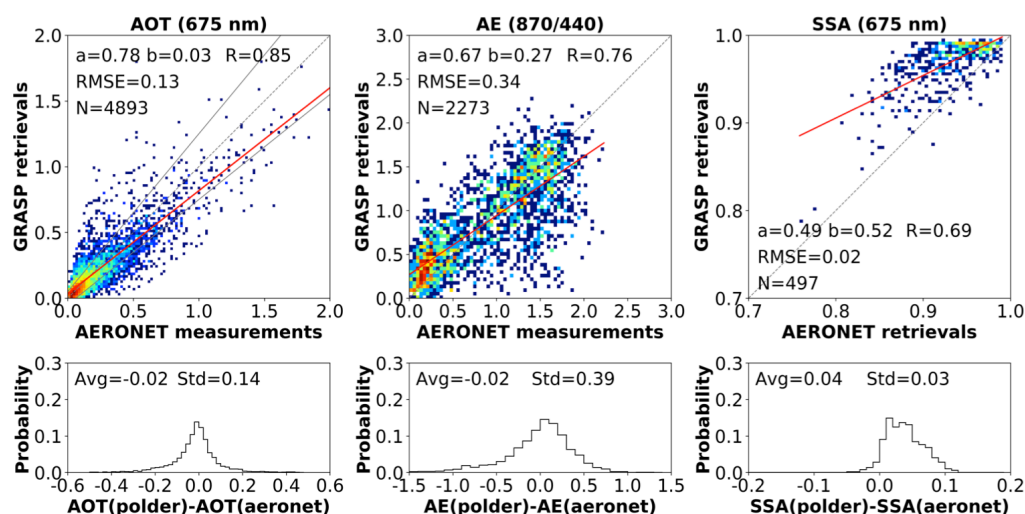
2039
2040 **Figure 12.** Inter-comparison of aerosol optical properties retrieved using the
2041 POLDER/PARASOL component composition (MG mixing model) approach and the
2042 corresponding operational AERONET products from all globally available sites in 2008.
2043

2044

2045
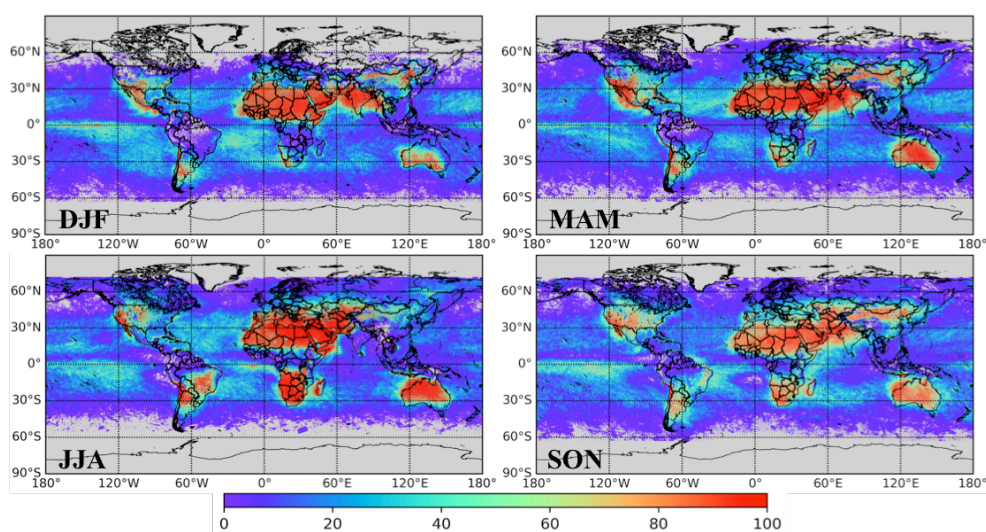
2046
2047 **Figure 13**. Seasonal variability of number of pixels in 0.1×0.1 degree resolution observed by
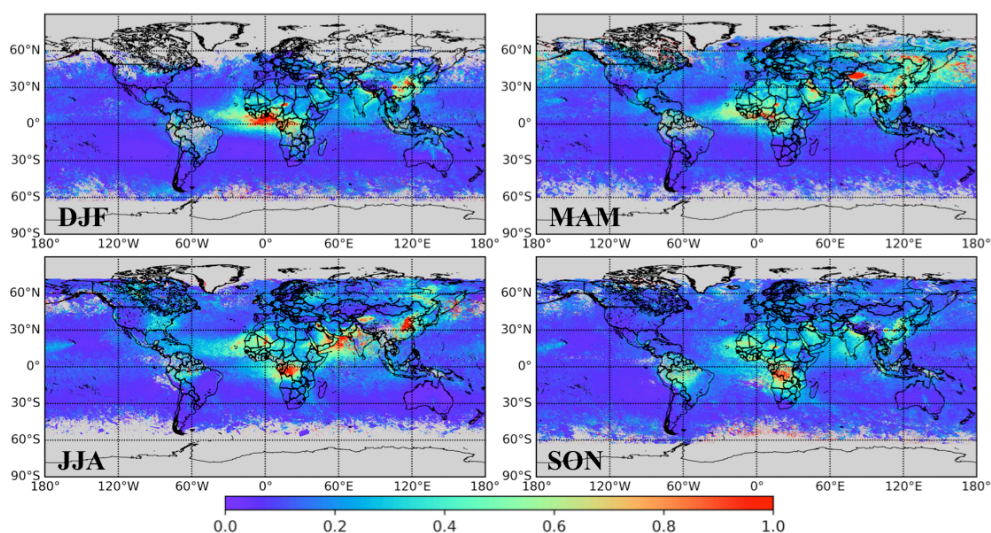2048 POLDER/PARASOL satellite over the globe in 2008.
2049
2050
2051
2052
2053

Figure 14. Seasonal variability of AOT at 565 nm in 2008 as retrieved by GRASP/Component Composition algorithm from POLDER/PARASOL satellite observations.
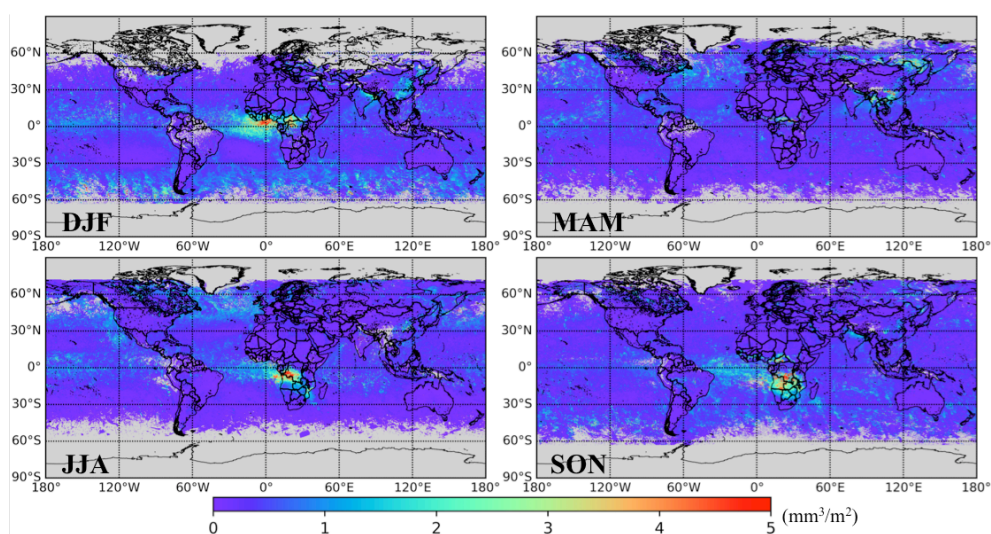
Figure 15. Seasonal variability of BC column volume concentration (mm^3/m^2) over the globe in 2008 as retrieved by GRASP/Component Composition algorithm from POLDER/PARASOL satellite observations.
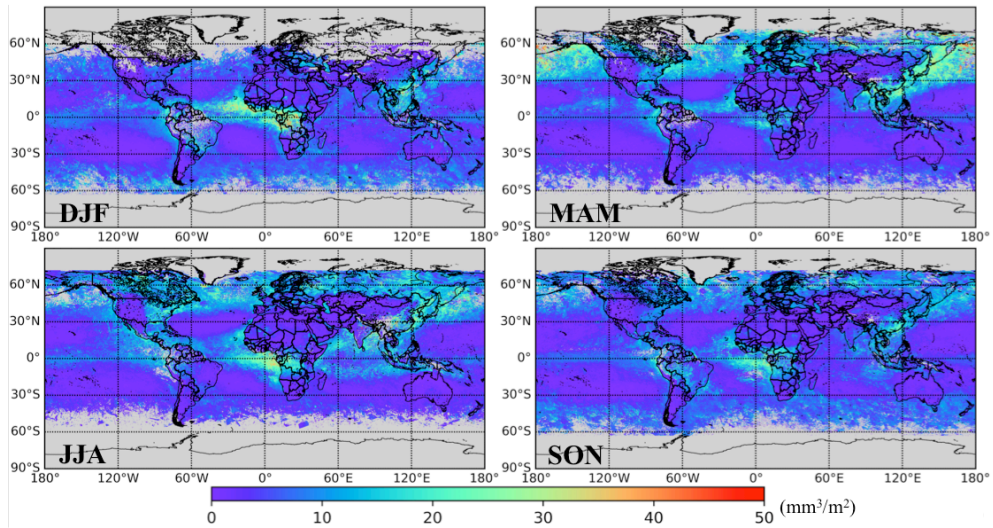
2074
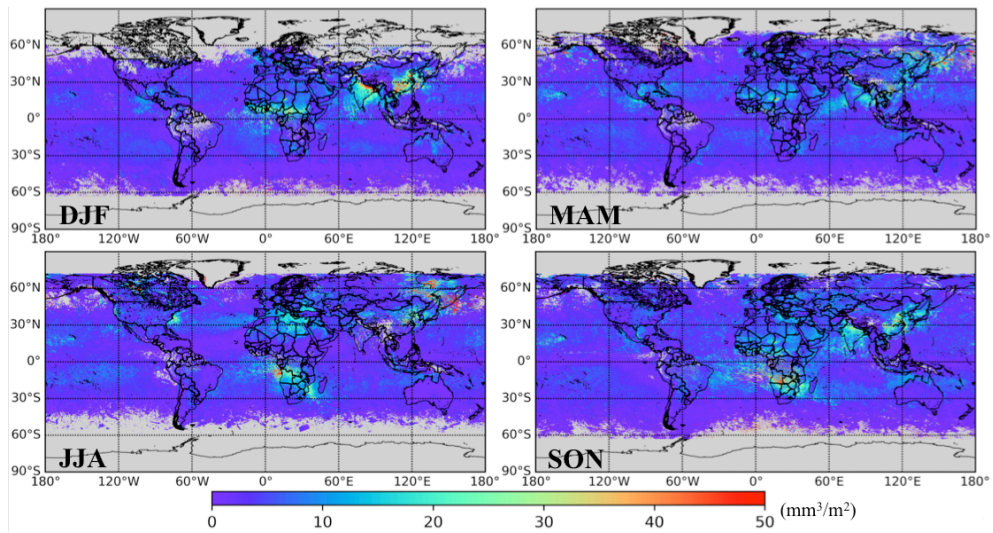2075 **Figure 16.** Same as Fig. 15, but for BrC
2076
2077
2078
2079

2080
2081
2082 **Figure 17**. Same as Fig. 15, but for fine mode non-absorbing soluble (FNAS)
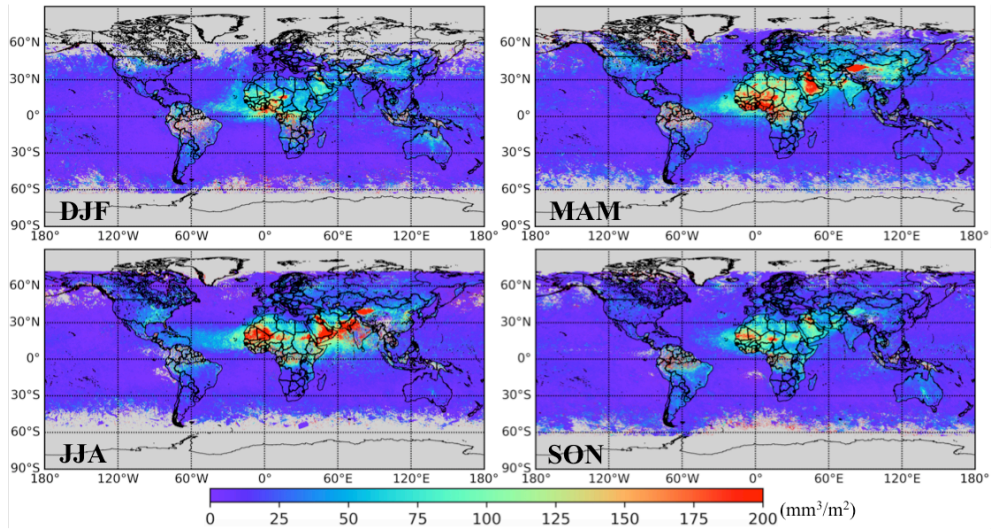2083
2084
2085
2086

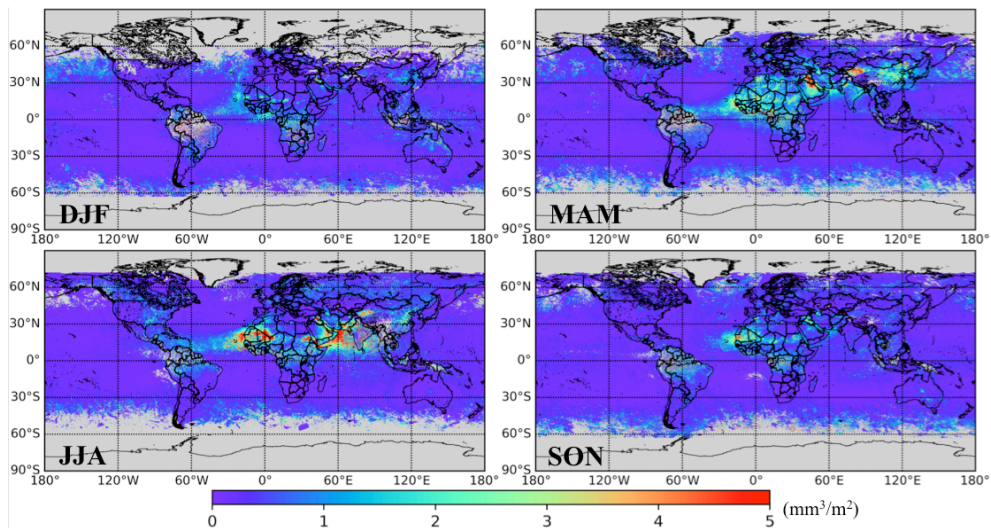**Figure 18**. Same as Fig. 15, but for coarse mode non-absorbing insoluble (CNAI, dust)

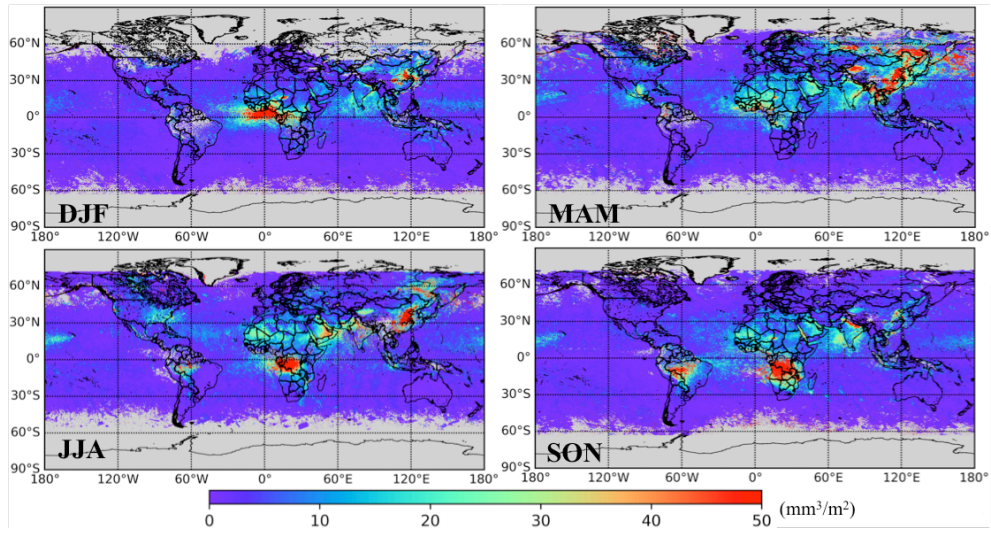**Figure 19**. Same as Fig. 15, but for coarse mode absorbing insoluble (CAI, FeOx and Carbonaceous particles)

Figure 20. Same as Fig. 15, but for fine mode non-absorbing insoluble (FNAI, dust and OC)

Response to comments of referee #1 on "Retrieval of aerosol composition directly from satellite and ground-based measurements" by Lei Li et al.

We appreciate the referee's thoughtful reading, valuable suggestions and time that we hope helped us to improve the manuscript. Our point-to-point replies are presented below in blue.

Anonymous Referee #1

This paper presents an interesting strategy for using polarized/multiangular satellite measurements to infer aerosol composition. The method uses the Generalized Retrieval of Aerosol and Surface Properties (GRASP) along with assuming that aerosols are mixtures of non-soluble particles embedded within a soluble host. GRASP then derives size distribution, loading and light absorption characteristics based on determining the fractions of each aerosol type. The algorithm is applied first on synthetic data, then on ground-based AERONET, then on historic POLDER data.

General comments:

Although quite long, I find this paper to be well-organized, well-written and worthy of publication. I really like the idea that the GRASP retrieval can combine specific aerosol types (size + shape + absorption) to retrieve the aggregate. This makes it possible to compare directly with models (that also assume these types). I think the authors should highlight this even more than they have already. Finally, this is probably well beyond the scope of the paper, But I would like to see some sort of graphic (even for a single panels from Figs 15-19), to compare how your global maps (of species type) compare with other maps, such as from AeroCom models, and/or MISR size/shape/absorption climatology. Right now, they look reasonable, but I would be curious whether they might "change" our way of thinking about aerosol types distribution.

Response: We appreciate the referee's suggestion. The direct bridging to the models is highlighted now in the abstract and the discussion is extended in the manuscript. Also, in fact, a comparison of our GRASP retrievals with GEOS-5/GOCART model estimations was already done. However, as the referee mentioned, this next step is

beyond the scope of the current publication. Either this observation-based aerosol components maps will "change" or not our way of thinking about aerosol types distribution is highly interesting and desires a more focused effort. Nevertheless, to give a glance on how the retrievals agree with the models, a couple of additional figures are presented below. Figure R1 shows the correlations for monthly averaged dust mass concentrations over the globe for 2008. It shows, for example that the global average coarse dust mass concentration retrieved by GRASP (125.5 mg/m^2) is lower than that simulated by GEOS-5/GOCART (174.7 mg/m^2). Figure R2 shows the map of coarse mode dust distribution in April 2008. The retrievals tend to provide lower coarse dust concentration over the mineral dust region (such as in Northern Africa and Northern China), which is consistent with the previous studies showing that models overestimate mineral dust in dust-dominated places (Jones and Christoper, 2007; Ginoux et al., 2001, Chin et al., 2009). Also, the observations show quite a fine spatial distribution structure.
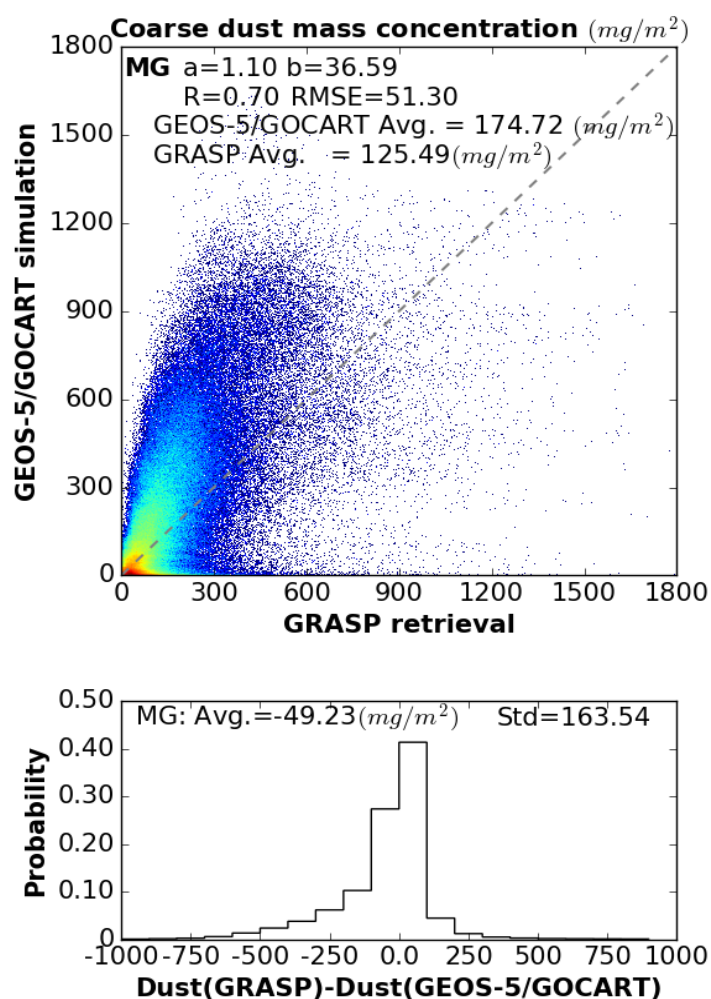
Figure R1. Correlation between the monthly averaged dust mass concentrations of GRASP retrievals and GEOS-5/GOCART model estimations over the globe in 2008.
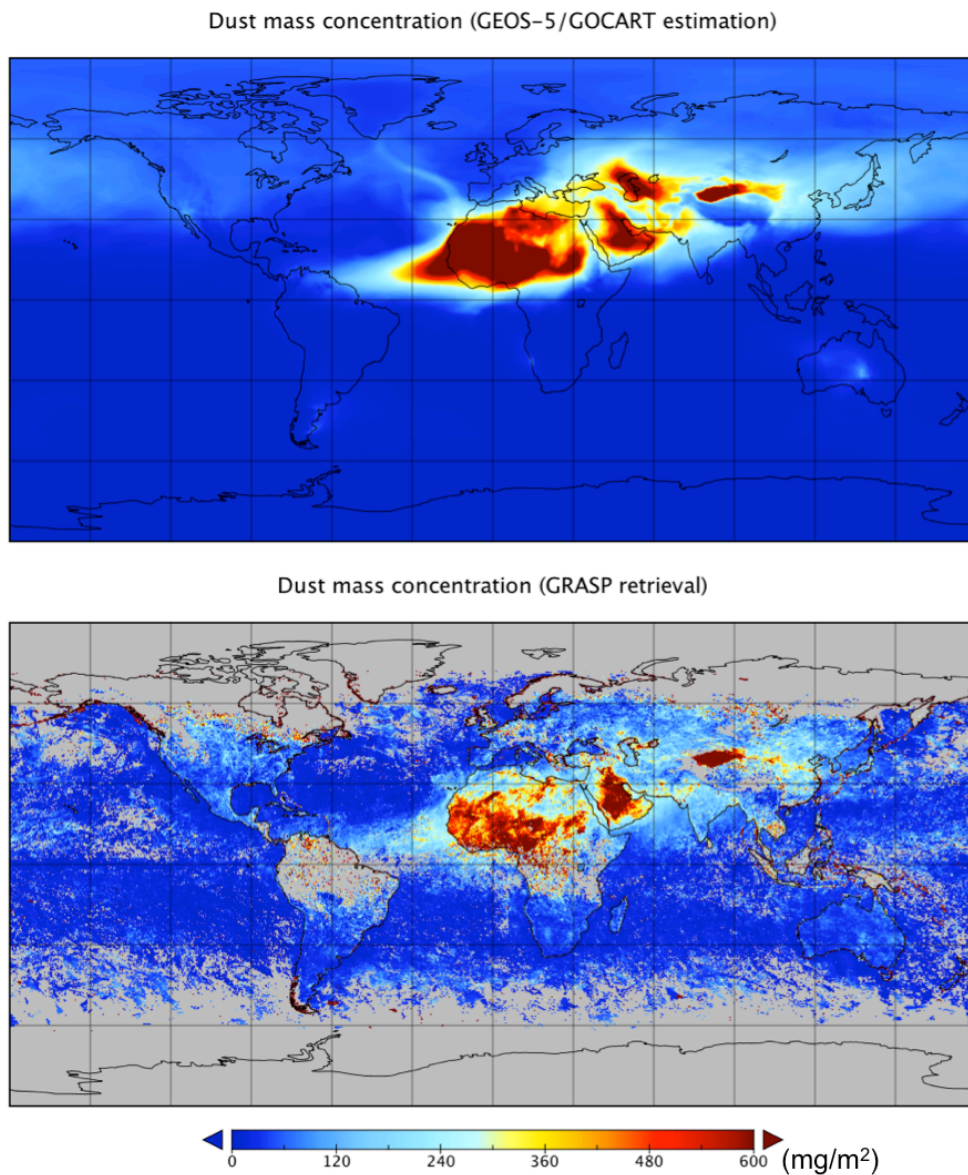
Dust mass concentration (GEOS-5/GOCART estimation)

Dust mass concentration (GRASP retrieval)

Figure R2. Distribution of dust mass concentration estimated by GEOS-5/GOCART model and retrieved by GRASP/POLDER in April 2008.

Chin, M., Diehl, T., Dubovik, O., Eck, T. F., Holben, B. N., Sinyuk, A., and Streets, D. G.: Light absorption by pollution, dust, and biomass burning aerosols: a global model study and evaluation with AERONET measurements, Ann. Geophys., 27, 3439-3464, 2009.

Ginoux, P. Chin, M., Tegen, I., Prospero, J. M., Holben, B., Dubovik, O., and Lin, S.-J.: Sources and distributions of dust aerosols simulated with the GOCART model, 106(D17), 20255-20273, 2001.

Jones, T. A. and Christopher, S. A: MODIS derived fine mode fraction characteristics of marine, dust, and anthropogenic aerosols over the ocean, constrained by GOCART, MOPITT, and TOMS, J. Geophys. Res., 112(D22), 2007.

Specific comments: some small suggestions for improving the paper.

1) Specifically, what are the aerosol type/model components? I feel as if a table could be used to describe each component, its size/shape and refractive index components.

Response: This useful suggestion is addressed by presenting a table summarizing the aerosol components description. The complex refractive indices of each component are presented at 0.440 μm and 0.865 μm.

Table 2. Description of aerosol components and complex refractive indices at 0.440 μm and 0.865 μm employed in the GRASP components retrieval approach, as well as those used in the uncertainty tests.

Abb.	Component	Complex refractive index		Reference
		0.440 μm	0.865 μm	
BC	Black carbon representing wavelength-independent strong absorption	1.95+0.79i	1.95+0.79i	Bond & Bergstrom (2006)
		1.75+0.63i	1.75+0.63i	Bond & Bergstrom (2006)
BrC	Brown carbon representing wavelength-dependent absorption	1.54+0.07i	1.54+0.003i	Sun et al. (2007)
		1.54+0.06i	1.54+0.0005i	Kirchstetter et al. (2004)
FNAI	Fine mode non-absorbing insoluble representing fine non-absorbing dust and organic carbon	1.54+0.0005i	1.52+0.0005i	Ghosh (1999)
		1.53+0.005i	1.53+0.005i	"GKI"[1]
		1.52+0.0006i	1.50+0.0006i	Koepke et al. (1997)
FNAS	Fine mode non-absorbing soluble representing inorganic salts	$1.337+10^{-9}$i	$1.339+10^{-8}$i	Tang et al. (1981); Gosse et al. (1997) for "AN"[2]
		$1.537+10^{-7}$i	$1.517+10^{-7}$i	Toon et al. (1976) for "AS" [3]
FAWC	Fine mode aerosol water content	$1.337+10^{-9}$i	$1.329+10^{-6.5}$i	Hale & Querry (1973)
CAI	Coarse mode absorbing insoluble representing iron oxides	2.90+0.345i	2.75+0.003i	Longtin et al. (1988)
		2.88+0.987i	2.72+0.140i	Triaud (2005)
CNAI	Coarse mode non-absorbing insoluble represented by non-absorbing dust	1.54+0.0005i	1.52+0.0005i	Ghosh (1999)
		1.53+0.005i	1.53+0.005i	"GKI"[1]
CNAI	by Organic Carbon	1.52+0.0006i	1.50+0.0006i	Koepke et al. (1997)
CNAS	Coarse mode non-absorbing soluble represented by an inorganic salt - AN[2]	$1.337+10^{-9}$i	$1.339+10^{-8}$i	Tang et al. (1981); Gosse et al. (1997)
CNAS	by AS[3]	$1.537+10^{-7}$i	$1.517+10^{-7}$i	Toon et al. (1976)
CAWC	Coarse mode aerosol water content	$1.337+10^{-9}$i	$1.329+10^{-6.5}$i	Hale & Querry (1973)

"GKI"[1] denotes dust composed of a mixture of quartz (Ghosh, 1999), kaolinite (Sokolik and Toon, 1999) and illite (Sokolik and Toon, 1999) with the proportions recalculated from Journet et al. (2014).

"AN"[2] denotes ammonium nitrate, which can be used to create a host in aerosols.

"AS"[3] denotes ammonium sulfate, which is an alternative species for the host estimation in aerosols.

2) Around line 290, the terms Frac(i) and dV/dlnr appear without definition. I guess they are in the table 1, but since table 1 (in the PDF) wasn't near the text, one might want to define first time in the text.

Response: Thank you for noticing this. We added the definitions of "$Frac(i)$ and $dV(r_j)/dlnr \ (i = 1, ..., N_r)$" in the text.

3) The stars on equation (1) are confusing. Do the stars represent a priori or solutions?

Response: The term with a star represents satellite measurements. For example, $\boldsymbol{f}_i^*$ denotes a vector of the measurements and $\boldsymbol{f}_i$ denotes a vector of the estimations. It is now clarified in the text.

4) In line 355, Csph appears (see comment #2).

Response: The C_{sph} definition was added in the text.

5) How are the intrinsic aerosol parameters allowed to vary in time and space?

Response: Besides the aerosol component retrieval module, the presented algorithmic developments essentially rely on the available heritage of the previous retrieval developments for POLDER space instrument. Thus, as in the standard GRASP algorithm (Dubovik et al., 2011), the satellite retrieval is designed as a statistically optimized simultaneous fitting of the observations over a group of pixels implemented under additional inter-pixel constraints. Specifically, the variations of the retrieved parameters horizontally from pixel-to-pixel or temporary from day-to-day over the same pixel are limited by the additional a priori constraints, in a similar manner to how it is applied in inverse modeling by Dubovik et al. (2008). The inclusion of these additional constraints is expected to provide retrieval of higher consistency for aerosol retrievals from satellites, because the retrieval over each single pixel will be benefiting from coincident aerosol information from neighboring pixels, in addition to the information about surface reflectance (over land) obtained in preceding and

consequent observations over the same pixel.

Dubovik, O., Herman, M., Holdak, A., Lapyonok, T., Tanré, D., Deuzé, J.L., Ducos, F., Sinyuk, A., Lopatin, A.: Statistically optimized inversion algorithm for enhanced retrieval of aerosol properties from spectral multi-angle polarimetric satellite observations, Atmos. Meas. Tech., 4, 975–1018, https://doi.org/10.5194/amt-4-975-2011, 2011.

Dubovik, O., Lapyonok, T., Kaufman, Y.J., Chin, M., Ginoux, P., Kahn, R.A., Sinyuk, A.: Retrieving global aerosol sources from satellites using inverse modeling, Atmos. Chem. Phys., 8, 209–250, https://doi.org/10.5194/acp-8-209-2008, 2008.

6) For Eq (7), there appear to be a lot of zeros in the matrix. We can assume there is no covariance? For example, I can't see avc (volume size distribution) and av (total volume) as being independent

Response: Zeros in the matrix denote that there are no smoothness constraints for these parameters, such as the spectral smoothness constraint. A clarification sentence is added now in the text.

7) Line 396-397: I guess I am curious, what do you mean by: "choice of mixing rule…significantly affects the results". Can you show something about this?

Response: This statement should be indeed clarified. The meaning is that the different assumptions on mixing rules, which are often used for estimation of aerosol composition, were reported by Xie et al. (2014) as affecting the aerosol composition retrieved by an independent algorithm that uses ground-based AERONET measurements. For instance, the Bruggeman approximation was found as more suitable for the dust case, the Maxwell-Garnett for the haze case, and volume average for the clean case. In our study, the Maxwell-Garnett and volume average mixing rules were employed independently of the aerosol type and the retrieval results are inter-compared (Figure 11). In our approach we have not identified a significant influence of the mixing rule choice on the quality of the retrievals. Moreover, the aerosol optical properties were rather well comparable in both cases. The fractions of the elements present some differences due to the differences in the formulation, but

are still in a reasonable agreement. The text is modified accordingly.

Xie Y., Li Z., Li L. et al.: Study on influence of different mixing rules on the aerosol components retrieval from ground-based remote sensing measurements. Atmospheric Research, 145: 267-278, 2014.

8) It appears that Eq (11) and Eq (12) have the same RHS?

Response: No, please note that there is a difference in the sign before ε_r.

9) Line 448 looks like a formula (11 minus 12) not 11 and 12.

Response: It is corrected.

10) Lines 455-484: See my comment #1.

Response: A table summarizing description of the aerosol components is added (see Table 2 in the revised manuscript and the response to comment #1).

11) I have a few comments regarding figure 5 and paper text. Could Fig 5a be split into two? There is a huge range of real refractive indices for CAI, but not for BrC and NAI. I cannot tell if the differences in assumptions for BrC and NAI around 1.5 are significant.

Response: An axis break is added for the ordinate in Figure 5a to better show the different range of real refractive indices.

12) Line 532-540. These range of values could also be added to a table (e.g. #1)

Response: The values of complex refractive indices at $0.440 \ \mu m$ and $0.865 \ \mu m$, used in the uncertainty test, are added to Table 2 (Please see the response to comment #1).

13) Line 545-546: "Elevated" meaning larger loadings or higher altitudes?

Response: It is reworded to "Therefore, the estimates should be quite reasonable in the cases of large pollution loading."

14) Lines 547-550: Are the fractions of BC and CAI somehow constrained so they can't be "large"? I note that they never approach 0.5 and barely approach 0.1

Response: It is important to say that the maximal retrieved fractions for BC and CAI

(mainly representing iron oxides) do not result from a constrain, despite have a limit due to the range of possible complex refractive indices in the pre-computed kernels of aerosol optical characteristics. That is, the volume fractions of these two highly absorbing species are indeed limited in the algorithm to 10% for BC and 3% for CAI, based on the below listed reasons. However, our analysis showed that these maximal values were never reached in the inversion procedure. Previous in-situ studies (Ganor and Foner, 1996; Guieu et al., 2002; Lafon et al., 2004, 2006, Alfaro et al., 2004; Wagner et al., 2012; Formenti et al., 2014) showed that iron oxides account for 2.8−6.5% of mineral dust by mass. It means approximately 1.4−3.25% by volume, since the density of free iron is much higher than other common minerals (4.28 g cm^{-3} for goethite and 5.25 g cm^{-3} for hematite, as opposed to 2.65 g cm^{-3} for illite, kaolinite, quartz, and calcite; Formenti et al., 2014 The fraction of BC in atmospheric aerosol was generally reported not exceeding 10% (Bond et al., 2013). It is also to note that the retrievals of aerosol composition derived from AERONET measurements by Schuster et al. (2016) demonstrated that the volume fraction of free iron remains relatively constant in West Africa throughout the year (1.4−1.7%) and the volume fraction of black carbon reaches a peak of 1.0% for the fine mode during West African biomass burning season and a peak of 3.0% for the fine mode in southern Africa biomass burning. The corresponding precision is added to the manuscript (lines 590 to 609).

Alfaro, S., Lafon, S., Rajot, J., Formenti, P., Gaudichet, A., and Maille, M.: Iron oxides and light absorption by pure desert dust: an experimental study, J. Geophys. Res., 109, D08208, doi:10.1029/2003JD004374, 2004.

Bond, T.C., Doherty, S.J., Fahey, D.W., Forster, P.M., Berntsen, T., Deangelo, B.J., Flanner, M.G., Ghan, S., Kärcher, B., Koch, D., Kinne, S., Kondo, Y., Quinn, P.K., Sarofim, M.C., Schultz, M.G., Schulz, M., Venkataraman, C., Zhang, H., Zhang, S., Bellouin, N., Guttikunda, S.K., Hopke, P.K., Jacobson, M.Z., Kaiser, J.W., Klimont, Z., Lohmann, U., Schwarz, J.P., Shindell, D., Storelvmo, T., Warren, S.G., Zender, C.S.: Bounding the role of black carbon in the climate system: A scientific assessment, J. Geophys. Res. Atmos., 118, 5380–5552, https://doi.org/10.1002/jgrd.50171, 2013.

Formenti, P., Caquineau, S., Chevaillier, S., Klaver, A., Desboeufs, K., Rajot, J.L., Belin, S., Briois, V.: Dominance of goethite over hematite in iron oxides of mineral dust from Western Africa: Quantitative partitioning by X-ray absorption spectroscopy, J. Geophys. Res. Atmos., 119, 12740-12754, https://doi.org/10.1002/2014JD021668, 2014.

Ganor, E. and Foner, H. A.: The mineralogical and chemical properties and the behavior of aeolian Saharan dust over Israel, in: The Impact of Desert Dust Across the Mediterranean, edited by: Guerzoni, S., and Chester, R., Kluwer Academic Publishers, Printed in the Netherlands, 163-172, 1996.

Guieu, C., Loye-Pilot, M. D., Ridame, C., Thomas, C.: Chemical characterization of the Saharan dust end-member: Some biogeochemical implications for the western Mediterranean Sea, J. Geophys. Res., 107 (D15), 4258, https://doi.org/4210.1029/2001JD000582, 2002.

Lafon, S., Rajot, J. L., Alfaro, S. C., Gaudichet, A.: Quantification of iron oxides in desert aerosol, Atmos. Environ., 38, 1211-1218, 2004.

Lafon, S., Sokolik, I.N., Rajot, J.L., Caquincau, S., Gaudichet, A.: Characterization of iron oxides in mineral dust aerosols: Implications for light absorption, J. Geophys. Res. Atmos., 111, 1–19, https://doi.org/10.1029/2005JD007016, 2006.

Schuster, G.L., Dubovik, O., Arola, A.: Remote sensing of soot carbon - Part 1: Distinguishing different absorbing aerosol species, Atmos. Chem. Phys., 16, 1565–1585, https://doi.org/10.5194/acp-16-1565-2016, 2016.

Wagner, R., Ajtai, T., Kandler, K., Lieke, K., Linke, C., Müller, T., Schnaiter, M., and Vragel, M.: Complex refractive indices of Saharan dust samples at visible and near UV wavelengths: a laboratory study, Atmos. Chem. Phys., 12, 2491–2512, doi:10.5194/acp-12-2491-2012, 2012.

15) For the plots of Figure 6, I am wondering what the "uncertainty" is. Should I read this as uncertainty is fraction (%) of fraction? What if these were presented in same units as x-axis (fraction)? Of course estimates of tiny fractions should have large % uncertainties, (but then that also means that the estimates of the fraction of the other elements will have lower % uncertainties).

Response: Thank you for this comment, it is indeed not sufficiently explained in the text. The uncertainty is defined in percentage as (retrieved_fraction-

assumed_fraction)/assumed_fraction. We would prefer to leave the notation in Figure 6 as it is, however, an explanation is added in the paragraph on uncertainty calculation (lines 646 to 647).

16) Line 581. I don't understand: "The non-absorbing insoluble can stand also for the insoluble organic carbon"

Response: The sentence is reworded. The intention was to be mentioned in the text problematic that the non-absorbing dust and non-absorbing organic carbon have similarity in the complex refractive index and is not distinguishable for the employed type of observations. It is corrected to "The non-absorbing insoluble component can represent not only non-absorbing dust, but also non-absorbing organic carbon, as was mentioned above."

17) Some of the figures have panels with cut-off axes (e.g. Fig 3)

Response: Corrected.

18) Are the units Fig 15-19 correct? (mm^3/m^2)?

Response: It can be confusing, but the units are correct. The units denote the volume concentration in total atmospheric column with unit surface area. We clarified it in the text.

Anonymous Referee #2

General comments:

This paper describes a modification to the GRASP algorithm to generate retrievals of a predefined basis set of aerosol "species." Typically the GRASP and the Dubovik and King (hereafter DK) provide a retrieval of size and real/complex refractive index. This is then used by others to classify species. Here they tie the refractive indices retrieved by GRASP by a basis set aerosol species. Their primary point is that using a predefined basis set of species is more direct than inferring typing from the measured extinction and subsequently derived absorption angstrom exponent method (or in a few cases adding index of refraction) commonly used in the community. As I finished this review, I did do a quick comparison with reviewer 1. I would agree with their point that perhaps the most important aspect of this work is it provides something of a forward operator to perform more apples to apples comparisons between satellite and models to close the radiance fields. I also agree that discussion of this point should be expanded. This discussion needs to cover these points. I think this effort moves the field forward in that they change the basis set as to what the retrieval is producing (BC, BrC, soluble and insoluble). However, these parameters are by no means equivalent to "composition," which is their premise for the entire paper. "Soluble and insoluble fractions" are wholly ill-defined in the context of composition, as they are related really to hygroscopicity. This is also true in part in regard to BC and BrC as they were functionally optical parameters long before we knew much of their true chemical nature. Here they are an indicator of spectral absorption properties. There are a myriad of soluble species with different indices of refraction and hygroscopic properties and likewise spectral dependencies of absorption based on mixtures. Thus, the idea that what is being retrieved as independent information on composition is fundamentally not true. What is a step forward, is they demonstrated that using the GRASP algorithm, you can generate a retrieval of parameters other than the standard size, index of refraction etc. as a basis of some categorization of the optical environment. One could look at this as a complex transform, but really it is simply a way of having an a priori set of basis functions for different aerosol species. But this is sort of what most traditional aerosol retrievals do, provide a best fit on the developers notion of what the aerosol environment looks like. Coarse mode dust, fine mode pollution, absorbing components, etc. So when the authors say they are the first

ones to extract composition directly from satellite, this is not true either, it is just the first time in the GRASP algorithm has taken this approach. Rather, they are taking some liberty with the language. My first major comment is I think the authors need to be very careful about their language here. They should be more up front as to what they are doing, or spend much more time explaining why they think there is something fundamentally different in their approach.

Response: We appreciate this very interesting review and valuable thoughts that pushed us to better communicate the novelty and originality of the proposed approach. First of all, we understand the importance and sensitivity to the semantic and agree that the word "composition" can be more associated with aerosol chemical composition, which does not properly reflect what is retrieved. However, to define as retrieval of aerosol type or classification will be wrong as well, as explained below. We therefore converged to aerosol "component" that will be used hereafter.

We argue here and provide a discussion in the manuscript on why the suggested approach should be distinguished from the traditional aerosol retrievals (LUT approaches) and is fundamentally different to previous approaches. It should be noted that the retrieval of aerosol type has been clearly recognized as an important task by the scientific community and has been addressed in several studies. For example, there are a number of approaches that attempt to identify the type of aerosol through analysis of optical parameters such as single scattering albedo (SSA), Ångström Exponent (AE), AAE (absorption AE), refractive index, etc. Specifically, Russell et al. (2014) relate AERONET- and POLDER-derived optical properties to different aerosol types: urban, dust, marine, biomass burning, etc. Studies by Chung et al. (2010) and Bahadur et al. (2012) use AERONET optical properties like AE and AAE to separate BC, BrC, and dust into species-specific AAOT (absorption AOT). Schuster et al. (2005, 2009, 2016a) and Li et al. (2015) quantify the relative volume fractions of one or more aerosol species (e.g. BC, BrC, iron oxide, water) by adjusting the mixture of several components in an aerosol model to fit AERONET-retrieved refractive indices. However, our new approach differs substantially from all of these methods because it does not use a retrieval of optical parameters as an intermediate step. Thus, we expect the GRASP/Component approach to provide a stronger link to the radiation field than the previous approaches, as well as fundamentally higher retrieval accuracy.

Moreover, some of above methods have additional differences and limitations compared to our proposed approach. For example, the Russell et al. (2014) approach is rather qualitative and does not attempt to quantify the relative volume or mass fractions of different species in an aerosol mixture. Chung et al. (2012) and Bahadur et al. (2012) seem to use a technique for separating carbonaceous aerosols from dust that is not fully consistent with the AERONET retrieval assumptions, as discussed by Schuster et al. (2016b).

Also, the Look-Up Table (LUT) approaches employed in most satellite retrievals (Martonchik et al., 1998; Remer et al., 2005; Kahn and Gaitley, 2015; Popp et al., 2016; Hammer et al., 2018; etc.) are designed to search amongst a preselected set of aerosol models (or their mixtures) for a model that provides the best fit to the observations. Since the models in a LUT are usually associated with a number of aerosol types (e.g. desert dust, smoke, urban aerosol etc.), the identification of the model that provides the best fit is often considered as a retrieval of aerosol type/composition. For observations with enhanced sensitivity, such as the Multi-angle Imaging SpectroRadiometer (MISR), a large number of models can be justified in the LUT and the differentiation of the models described by the ensembles of parameters can indeed be rather robust. However, LUT approaches are fundamentally limited to a discrete set of possible solutions, whereas the GRASP/Component approach searches through a continuous space of solutions; thus, the identification of aerosol components with our new methodology is significantly more detailed and elaborate. The proposed approach also bridges directly to the quantities of aerosol compositions used in the global chemical transport models. Specifically, our aerosol component retrievals can satisfy the requirements of chemical transport models to constrain their aerosol estimations on a large or global scale. However, we note that the GRASP/Component approach is only possible if 1) there is significant instrument sensitivity to the parameters that are related aerosol component (i.e. complex refractive index), and 2) this sensitivity is maintained while other parameters like the size distribution are adjusted.

The retrieval provided in this article is unique because the aerosol component fractions are iterated in the original algorithm until a "best fit" is achieved with the measured radiance field, making it unnecessary to use retrieved optical properties as a constraint. Thus, the aerosol volume fractions determined with this new procedure have a direct link to the measured radiance field, whereas the procedures outlined

above have a direct link to the retrieved aerosol optical properties provided by AERONET or satellite products.

In addition, the sensitivity of aerosol water fraction to the real refractive index is shown in Figure R1 (Schuster et al., 2009). Schuster et al. (2009) illustrated that the soluble aerosol components (sea salt, ammonium sulfate, ammonium nitrate, etc.) indicate similar refractive indices for similar mixing ratios, even though the dry refractive indices can be quite different. Hence, the aerosol water fraction can be derived from the mixture real refractive index if the aerosols are known to be one of the common soluble aerosols (in this study it is assumed as ammonium nitrate). Hygroscopicity, as an indicator of how aerosol growth in size or scattering, is related to relative humidity. However, in this study we are more concerned about how aerosol water content is related to real refractive index, which is much simpler (no hysteresis, no exponential growth, etc.) according to the study of Schuster et al. (2009) shown as Figure R1. These discussions are added to the manuscript.
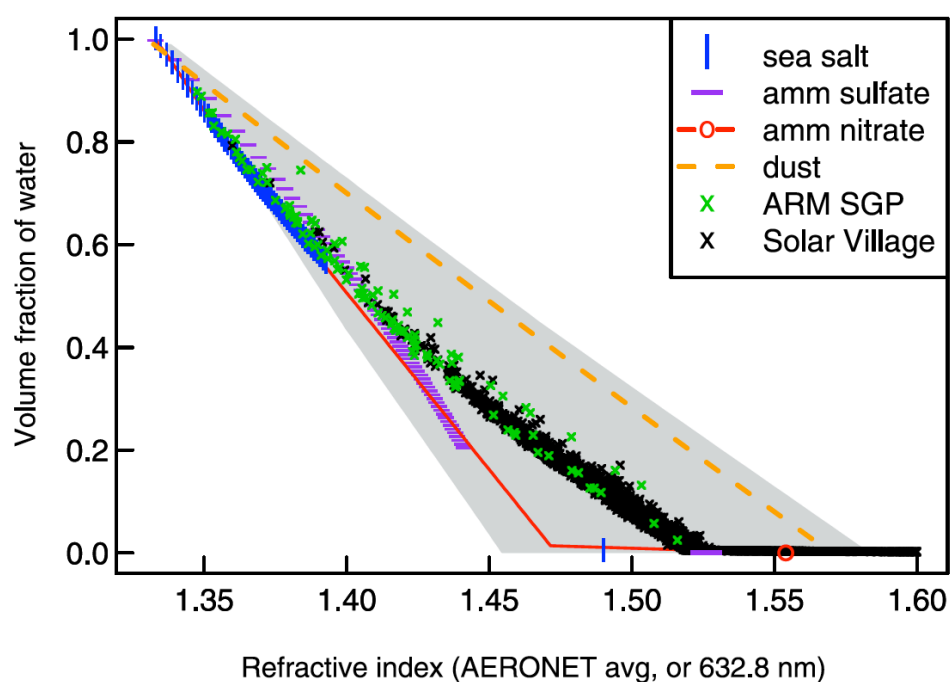

Figure R1. Water fractions for two-component aerosol mixtures as a function of the real refractive index. (Schuster et al., 2009)

We also modified the abstract to better explain the novelty of the approach: "This study presents a novel methodology for remote monitoring of aerosol component over large spatial and temporal domains. The concept is realized within the GRASP

(Generalized Retrieval of Aerosol and Surface Properties) algorithm to directly infer aerosol component from the measured radiances. The observed aerosols are assumed as mixtures of hydrated soluble particles embedded with black carbon, brown carbon, iron oxide, and other (non-absorbing) insoluble inclusions. The complex refractive indices of the dry components are fixed a priori (although the refractive index of the soluble host is allowed to vary with hydration), and the complex refractive index of the mixture is computed using mixing rules. The volume fractions of these components are derived together with the size distribution and the fraction of spherical particles, plus the spectral surface reflectance in cases the satellite data is inverted. The retrieval is implemented as a statistically optimized fit in a continuous space of solutions. This contrasts with most conventional approaches where the type of aerosol is either associated with a pre-assumed aerosol model that is included in a set of Look-Up-Tables, or determined from the analysis of the retrieved aerosol optical parameters (e.g., single scattering albedo, refractive index, etc. provided by the AERONET retrieval algorithm); here, we retrieve the aerosol component explicitly. The approach also bridges directly to the quantities used in the global chemical transport models. We first tested the approach with synthetic data to estimate the uncertainty, and then applied it to real ground-based AERONET and space-borne POLDER/PARASOL observations; thus, the study presents a first attempt to derive aerosol component from satellites. Our results indicate aerosol optical characteristics that are highly consistent with standard products (e.g., R of ~ 0.9 for aerosol optical thickness) and demonstrate an ability to separate intrinsic optical properties of fine- and coarse-sized aerosols. We applied our method to POLDER/PARASOL radiances on the global scale and obtained spatial and temporal patterns of the aerosol component that agree well with the knowledge on aerosol sources and transport features. Finally, we discuss limitations and perspectives of this new technique. ~~This approach is different from the conventional methods that use post-processing of the retrieved aerosol optical properties for aerosol typing. The proposed method assumes observed aerosols as mixtures of particles composed of black carbon, brown carbon, absorbing insoluble, non-absorbing insoluble embedded in a soluble host. The algorithm then derives size distribution and the fractions of these components. The complex refractive index of each component is fixed a priori and the complex refractive index of mixture is computed using mixing rules. The approach is first tested with synthetic data and the uncertainties are estimated. Then, it is applied to the~~

real ground-based AERONET and space-borne POLDER/PARASOL observations, known to be sensitive to aerosol complex refractive index. The study presents a first attempt to derive aerosol component from satellites. The obtained aerosol optical characteristics are highly consistent with the standard products (R of ~ 0.9 for aerosol optical thickness). The approach also presented an ability to separate between aerosol properties in fine and coarse size fractions, in case of POLDER/PARASOL and AERONET. Examples of application to POLDER/PARASOL on the global scale are presented. The obtained spatial and temporal patterns of the aerosol component agree well with our knowledge on aerosol sources and transport features. Finally, limitations and perspectives are discussed."

Bahadur, R., Praveen, P., Xu, Y., and Ramanathan, V.: Solar absorption by elemental and brown carbon determined from spectral observations, P. Natl. Acad. Sci. USA, 109, 17366–17371, https://doi.org/10.1073/pnas.1205910109, 2012.

Chung, C., Ramanathan, V., and Decremer, D.: Observationally constrained estimates of carbonaceous aerosol radiative forcing, P. Natl. Acad. Sci. USA, 109, 11624–11629, https://doi.org/10.1073/pnas.1203707109, 2012.

Hammer, M.S., Martin, R.V., Li, C., Torres, O., Manning, M., Boys, B.L.: Insight into global trends in aerosol composition from 2005 to 2015 inferred from the OMI Ultraviolet Aerosol Index, Atmos. Chem. Phys., 18, 8097–8112, https://doi.org/10.5194/acp-18-8097-2018, 2018.

Kahn, R.A. and Gaitley, B.J.: An analysis of global aerosol type as retrieved by MISR, J. Geophys. Res. Atmos., 120, 4248–4281, https://doi.org/10.1002/2015JD023322, 2015.

Li, Z., Li, L., Zhang, F., Li, D., Xie, Y., Xu, H.: Comparison of aerosol properties over Beijing and Kanpur: Optical, physical properties and aerosol component composition retrieved from 12 years ground-based Sun-sky radiometer remote sensing data, J. Geophys. Res. Atmos., 120, 1520–1535, https://doi.org/10.1002/2014JD022593, 2015.

Martonchik, J., Diner, D., Kahn, R., Verstraete, M., Pinty, B., Gordon, H., Ackerman, T.: Techniques for the retrieval of aerosol properties over land and ocean using multiangle data, IEEE Transactions on Geoscience and Remote Sensing, 36, 1212-1227, 1998.

Popp, T., De Leeuw, G., Bingen, C., Brühl, C., Capelle, V., Chedin, A., Clarisse, L., Dubovik, O., Grainger, R., Griesfeller, J., Heckel, A., Kinne, S., Klüser, L., Kosmale, M., Kolmonen, P., Lelli, L., Litvinov, P., Mei, L., North, P., Pinnock, S., Povey, A., Robert, C., Schulz, M., Sogacheva, L., Stebel, K., Zweers, D.S., Thomas, G., Tilstra, L.G., Vandenbussche, S., Veefkind, P., Vountas, M., Xue, Y.: Development, production and evaluation of aerosol climate data records from European satellite observations (Aerosol_cci), Remote Sens., 8, https://doi.org/10.3390/rs8050421, 2016.

Remer, L., Kaufman, Y., Tanré, D., Mattoo, S., Chu, D., Martins, J., Li, R., Ichoku, C., Levy, R., Kleidman, R., Eck, T., Vermote, E., and Holben, B.: The MODIS aerosol algorithm, products and validation, Journal of the Atmospheric Sciences, 62, 947-973, 2005.

Russell, P., Kacenelenbogen, M., Livingston, J., Hasekamp, O., Burton, S., Schuster, G., Johnson, M., Knobelspiesse, K., Redemann, J., Ramachandran, S., and Holben, B.: A multiparameter aerosol classification method and its application to retrievals from spaceborne polarimetry, J. Geophys. Res., 119, https://doi.org/10.1002/2013JD021411, 2014.

Schuster, G.L., Dubovik, O., Arola, A.: Remote sensing of soot carbon – Part 1: Distinguishing different absorbing aerosol species, Atmos. Chem. Phys., 16, 1565–1585, https://doi.org/10.5194/acp-16-1565-2016, 2016a.

Schuster, G.L., Dubovik, O., Arola, A., Eck, T.F., Holben, B.N.: Remote sensing of soot carbon – Part 2: Understanding the absorption Ångström exponent, Atmos. Chem. Phys., 16, 1587–1602, https://doi.org/10.5194/acp-16-1587-2016, 2016b.

Schuster, G.L., Dubovik, O., Holben, B.N., Clothiaux, E.E.: Inferring black carbon content and specific absorption from Aerosol Robotic Network (AERONET) aerosol retrievals, J. Geophys. Res., 110, D10S17, https://doi.org/10.1029/2004JD004548, 2005.

Schuster, G.L., Lin, B., Dubovik, O.: Remote sensing of aerosol water uptake, Geophys. Res. Lett., 36, https://doi.org/10.1029/2008GL036576, 2009.

My second point is that it is unclear as to what is really going on in the retrieval. If one considers the GRASP algorithm simply has a smoothness of fit contain, but otherwise can pick any refractive index and size it wants, why not just take the

standard GRASP algorithm as it is, and after the fact match the size and refractive index to any basis function they like? Or is that what they are already doing? (it is hard to tell in figure 1 and the associated discussion). Is the goodness of fit always the same from the standard GRASP algorithm, or does your predefinition of species leave a residual? If so, how big is that residual? They also list as an example the refractive index for ammonium nitrate, but what of the other species? We are referred to a GACP dataset, and Figure 3 has such dynamic range between species it is hard to tell even what these values are. I think an appendix needs to be generated that provides details on these key aspects of the retrieval. I think in order for them to prove validity of the algorithm, they should do the retrieval with their basis set, and then as a baseline compare to the standard grasp algorithm, and see to what extent the goodness of fit to the radiance fields changes.

Response:

Regarding the goodness of fit and validity of the new algorithm as compared to the standard GRASP algorithm: we thank for bringing up this point because it is indeed an essential step that was done in early stages of the new algorithm developments, but is not explicitly mentioned in the original manuscript. Figure 11 of the original version, however, already showed an inter-comparison of correlations between optical characteristics derived by the new approach, the standard GRASP and the operational AERONET product, which addresses in a way the raised question. Here, in Figure R2, we present the residuals from different GRASP approaches. The data subset used is the same as for the inter-comparison with the operational AERONET product (Figure 11 and Table 4). Figure R2 shows that the residuals of the GRASP/Component approaches (Maxwell-Garnett (MG) and volume weighted (VW) mixing rules) are almost the same as those of standard GRASP. Although the average residual of aerosol component approach (2.4±0.9% for MG and 2.4±1.0% for VW) is slightly higher than of standard GRASP (2.3±0.9%), the maximum residual of aerosol component approach (5.0% for MG and 5.7% for VW) is somewhat smaller than that of standard GRASP (6.6%). The next sentence is added to the manuscript: "In addition, the GRASP/Component approach produces almost the same average residual (2.4±0.9% for MG and 2.4±1.0% for VW) as that of the standard GRASP algorithm (2.3±0.9%) while the maximum residual for GRASP/Component (5.0% for MG and 5.7% for VW) is smaller than that for standard GRASP (6.6%); ± denotes standard deviation."
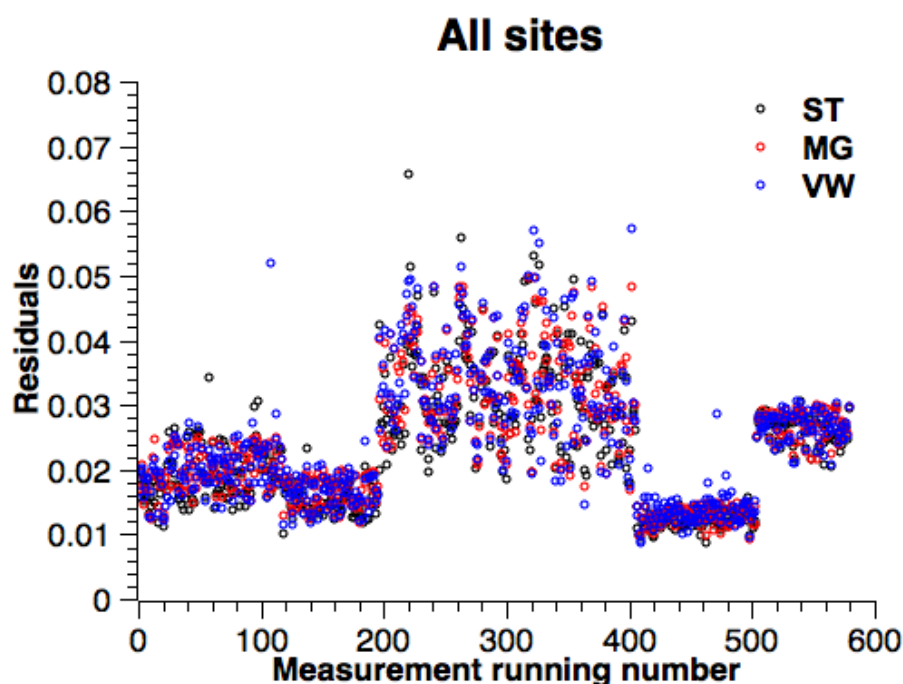
Figure R2. Inter-comparison of retrieval residual among different GRASP approaches. Red color represents the Maxwell-Garnett (MG) mixing model; blue - the volume-weighted (VW) mixing model; and black - the standard (ST) GRASP/PARASOL product that do not employ the aerosol component retrievals. The data subset used is the same as for the inter-comparison with the operational AERONET product (Table 4 and Figure 11 of the manuscript).

Regarding the used refractive indices: while addressing the first specific comment of the first reviewer, we added a table summarizing description of aerosol components and refractive indices (Table 2). In addition, an axis break is added for the ordinate in Figure 5a to better show the different range of real refractive indices. We also modified Figure 1 in the manuscript (see Figure R3 below).
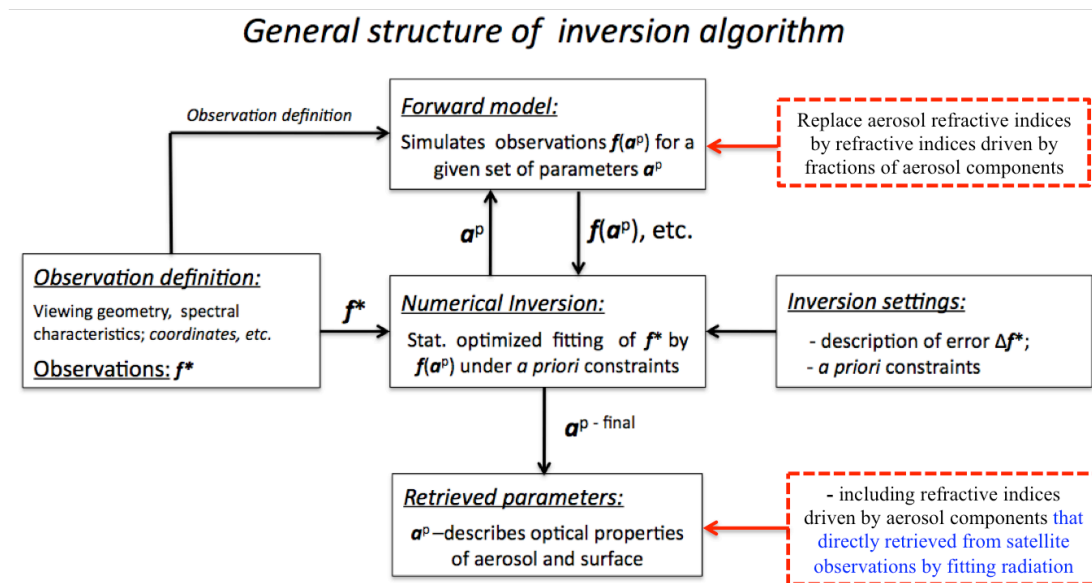
General structure of inversion algorithm

Figure R3. General structure of GRASP algorithm with aerosol component conversion model, courtesy of (Dubovik et al., 2011). The red dashed frames represent modifications for the component inversion approach. f^* represents vector of inverted measurements, a^P represents vector of unknowns at the p-th iteration, $f(a^P)$ represents vector of measurement fit at the p-th iteration.

My final major comment is that there is really very little verification work provide that shows that the results of the retrievals are fundamentally better than other categorization methods (that is getting back to the question in point 2 (if this method leaves a residual from the free running GRASP algorithm). Or can you baseline against a simple AE vs AAE plot for species? One could argue that real verification has always been an issue for retrievals. There are many studies that show that DK retrievals provide reasonable results. But, those studies and here pick sites that are generally single aerosol specie dominated (the once exception is Solar village). This is why at least a self-consistent baseline against the standard GRASP and DK retrievals is so important. The discussions in Section 4 related to Figure 14-20 global maps that provide some truthiness. But close examination (which required me zooming way into the plots) shows many logical inconsistencies, especially around coastlines, where the overall hydration of the particles leads to an increase in the "soluble fraction" Likewise there is a great deal of "insoluble" AOD in Brazil-even though we know smoke organic components do in fact have a hygroscopicity to them, even if it is low), as well as retrieval errors. Are they not really just applying a form Schuster's "water

fraction" algorithm? This then closes the loop with comment 1: are they really doing a soluble and insoluble aerosol specie? In the end, I appreciate what the authors are trying to do, and can see how this will benefit the community. But there are logic issues that need to be wrung out, and some form of baseline verification that shows this method is actually taking us in the right direction.

Response: The first part of this comment is indeed getting back to the question in point 2. Figure R2 and the discussion related to Figure 11 of the manuscript reply to this concern by showing the equivalence of the residuals and consistency of the retrievals between the new and the standard approaches. Regarding global maps, due to overall high complexity of the aimed approach, it is possible that not everywhere the retrieved aerosol components fit perfectly the expectations and a better understanding of what the retrieval represent is desirable. At the same time, not fully logical results are likely caused by a physical reason such as lack of sensitivity to some specific aerosol component, since optical observations in some cases sensitive to certain optical equivalent. This is challenge not only for the proposed methodology and for any other effort aimed to derive aerosol composition from remote sensing observations. In this respect, is can be noted that many known features are correctly represented in our retrievals. Moreover, some not yet known or fully understood phenomena can also be responsible for some "anomalies" and the proposed data set can be very useful basis for formulating new scientific question. Nevertheless, we agree that a more detailed and zoomed analysis should be in scope of future studies. However, due to very large volume of produced data in this publication and limited resources, we made the choice to present an overview of the results. Finally, we believe that the provided above and in the corrected version of the manuscript clarifications explain better the originality of the approach and the sense of the derived aerosol components.